

~~N64-15791~~

9/p.

N64-15791

CODE-1

CR-53069

Space Programs Summary No. 37-24, Volume VI

for the period September 1, 1963 to November 30, 1963.

Space Exploration Programs and Space Sciences

OTS PRICE

XEROX	\$	<u>8.60 pb.</u>
MICROFILM	\$	<u>2.93 mf.</u>

not part of
cost

jpl

JET PROPULSION LABORATORY
CALIFORNIA INSTITUTE OF TECHNOLOGY
PASADENA, CALIFORNIA

December 31, 1963

regs

Space Programs Summary No. 37-24, Volume VI

for the period September 1, 1963 to November 30, 1963

Space Exploration Programs and Space Sciences

**JET PROPULSION LABORATORY
CALIFORNIA INSTITUTE OF TECHNOLOGY
PASADENA CALIFORNIA**

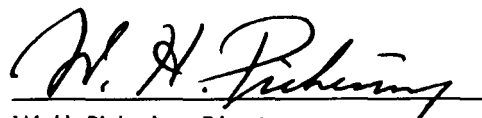
December 31, 1963

Preface

The *Space Programs Summary* is a six volume, bimonthly publication designed to report on JPL space exploration programs, and related supporting research and advanced development projects. The subtitles of all volumes of the *Space Programs Summary* are:

- Vol. I. The Lunar Program (Confidential)
- Vol. II. The Planetary-Interplanetary Program (Confidential)
- Vol. III. The Deep Space Instrumentation Facility (Unclassified)
- Vol. IV. Supporting Research and Advanced Development (Unclassified)
- Vol. V. Supporting Research and Advanced Development (Confidential)
- Vol. VI. Space Exploration Programs and Space Sciences (Unclassified)

The *Space Programs Summary*, Volume VI, is an unclassified digest of appropriate material from Volumes I through V, plus space science instrumentation studies. This instrumentation work is conducted by the JPL Space Sciences Division and also by individuals of various colleges, universities and other organizations. All such projects are supported by the Laboratory and are concerned with the development of instruments for use in the NASA space flight programs.



W. H. Pickering, Director
Jet Propulsion Laboratory

Space Programs Summary No. 37-24, Volume VI

Copyright © 1964, Jet Propulsion Laboratory, California Institute of Technology

Prepared under Contract No. NAS 7-100) National Aeronautics & Space Administration

(NASA

Contents

LUNAR PROGRAM

I. <i>Ranger</i> Project	1
A. Introduction	1
B. Space Flight Operations for <i>Ranger</i> Block III	2
C. Systems Testing	4
D. Midcourse Propulsion System	5
E. Error Analysis	6
II. <i>Surveyor</i> Project	11
A. Introduction	11
B. Space Flight Operations	11

THE PLANETARY-INTERPLANETARY PROGRAM

III. <i>Mariner C</i> Project	13
A. Introduction	13
B. Spacecraft Design and Development	14
IV. <i>Voyager</i> Project	23

THE DEEP SPACE INSTRUMENTATION FACILITY

V. Introduction	25
VI. Communications Research, Development, and Facilities	26

OPERATIONAL AND TEST FACILITIES

VII. Test and Support Equipment	31
A. Environmental Test Laboratory	31
B. Operational Support Equipment	33

SPACE SCIENCES

VIII. Space Instruments Development	51
A. A Capacitor Storage Scheme for Gas Chromatograph Detector Quiescent Current Compensation	51
B. Lightweight Sample Collector for Exobiology Experiments	58
Reference	59
IX. Space Instruments Systems	60
A. An Intermittent Motion Digital Tape Recorder-Reproducer	60
B. Development of a Hysteresis-Induction Motor	67
C. <i>Mariner C</i> Scientific Instrumentation	71

LUNAR PROGRAM

I. *Ranger* Project

A. Introduction

The *Ranger* Project was established to develop a space flight technology for transporting engineering and scientific instruments to the Moon and planets. This technology is then to be utilized for deriving information regarding the nature and history of the Moon. Nine *Ranger* launchings, using *Atlas-Agena B* rockets, are now planned; five of these flights have been made.

Rangers 1 and 2 (Block I) were not lunar-oriented, but were engineering evaluation flights to test the basic systems to be employed in later lunar and planetary missions. Several scientific experiments were carried on a noninterference basis. The *Ranger 3*, 4, and 5 (Block II) spacecraft carried a gamma-ray instrument, a TV camera, and a rough-landing seismometer capsule. All three of these flights experienced failure. As a result, the objectives of future flights have been reviewed, and subsequent design modifications have been accomplished.

Block III. The objective of the *Ranger* Block III (*Rangers 6* through 9) flights is to obtain TV pictures of the lunar surface which will be of benefit to both the scientific program and the U.S. manned lunar flight program. All aspects of the project had been proceeding toward a third quarter launch for *Ranger 6*, which was established in early 1963 as a result of the modified objectives and the outcome of the design review.

In September, information was received that some diodes used in the spacecraft were suspect in that they could be contaminated with gold flakes. Subsequent investigation showed that diodes used for the central computer and sequencer (CC&S) and Earth sensor electronics of the spacecraft were highly contaminated and that some of these would short when subjected to vibration. A decision was made on October 21 to delay the *Ranger 6* launch in order to replace these suspect diodes in the spacecraft. As a result, *Ranger 7* also was rescheduled; *Rangers 8* and 9 remain unchanged.

The proof test model, having completed all of its systems, environmental, and launch vehicle compatibility tests, was shipped to the Goldstone Tracking Station on October 21 for compatibility tests with the Deep Space Instrumentation Facility. Some additional testing is planned on its return from Goldstone.

Ranger 6, which began assembly at the Spacecraft Assembly Facility (SAF) on July 1, 1963, had completed all systems, environmental, launch vehicle compatibility, mission verification, and final preshipment systems tests when the decision was made to delay the launch. The CC&S and Earth sensor electronics were removed for rework, and the spacecraft was placed in controlled storage in the SAF awaiting the reworked assemblies.

Ranger 7, which began assembly on July 17, 1963, had completed systems and launch vehicle compatibility tests and was being prepared for vibration tests when the launch was delayed. It also was placed in controlled storage awaiting reworked assemblies.

The current design weight of the Block III spacecraft is approximately 803 lb, based on the measured weights of *Rangers 6* and *7*. The current launch vehicle capability for injected spacecraft weight is 840 lb.

Analysis of standard and nonstandard flight sequences is continuing, and many of the necessary operational procedures have been developed. Compatibility and initial training tests for the space flight operations have been carried out, and additional tests are scheduled.

Block V. Effort had been initiated toward the extension of the *Ranger* missions for six additional flights under the *Ranger* Block V (*Rangers 10* through *15*) Project. The objectives of the Block V missions were to make hard landings of instrumented capsules on the lunar surface and to make other scientific measurements in the vicinity of the Moon. Specifically, *Rangers 10* and *11* had been designated to: (1) land on the lunar surface a single-axis seismometer which would perform a passive seismic experiment, (2) measure gamma-ray spectra in the vicinity of the Moon, (3) make radar reflectivity measurements of the lunar surface, and (4) transmit TV pictures of the lunar surface. Potential payloads for the subsequent missions of the Block V series had included a photographic capsule which would transmit pictures taken on the lunar surface.

The Northrop Corporation had been placed under contract to JPL to provide the Block V spacecraft, and the Aeronutronic Division of Philco Corporation was under contract to JPL to design the lunar survival capsule for the seismic experiment. However, on December 13 the Block V effort was cancelled.

Lunar facsimile capsule. Aeronutronic Division of Philco Corporation, under JPL contract, has completed Phase I of the lunar facsimile capsule (LFC) development program, and the final report¹ has been published.

During the 8-month program, prototype subassemblies and supporting ground equipment for the LFC were designed and developed. Two prototype capsule assemblies were subjected to severe environmental tests, including impacts at up to 198 ft/sec and 4300 peak *g* followed by long-term functional testing at 10^{-6} mm Hg vacuum. No degradation of any kind due to impact was experienced, and the six 360-deg pictures taken with the Prototype 2 assembly exceeded all design objectives for picture quality. The completed preliminary design of the flight assembly is well within weight and power limits and has a calculated reliability of 96.5%.

Under the contract a small effort is continuing to investigate the problems associated with opening the survival sphere on the lunar surface so that the extension mechanism can be deployed, thus enabling the photographic subsystem to perform its function.

B. Space Flight Operations for *Ranger* Block III

1. Preparation

a. Introduction. The degree of success with which the *Ranger* spacecraft performs its intended mission is dependent upon the facility with which certain tasks are performed in the period between the launching of the

¹Final Technical Report, Lunar Facsimile Capsule, Phase I Development, Publication No. U-2224, JPL Contract No. 950462, Aeronutronic Division, Philco Corporation, September 13, 1963.

spacecraft and completion of the mission. A typical task is monitoring the telemetry data transmitted from the spacecraft.

The operating characteristics of the spacecraft are determined from analysis and interpretation of these data. In addition, the data are monitored to discover any malfunction of the spacecraft and to determine which, if any, commands should be sent to the spacecraft to improve the probability of successfully completing the mission. Preparations for performing this task in the areas of guidance, control, and power are described below.

b. Spacecraft Data Analysis Team (SDAT). Data analysis and interpretation are accomplished during the flight by the SDAT, a functional group within the Space Flight Operations Complex (SFOC). The individuals who make up the SDAT are provided by the various technical JPL Divisions responsible for the design and development of the subsystems onboard the spacecraft.

The Guidance and Control Division at JPL has instituted a training program to enhance the capabilities and usefulness of the personnel it supplies to the SDAT. This program provides the Guidance and Control subsystem representatives with a working knowledge of the entire SFOC. Such knowledge enables each SDAT representative to understand exactly how the data he must evaluate have arrived at the Space Flight Operations Facility (SFOF). Explanations are given of manipulations, conversions to various forms, and delays involved in transmitting the data from the spacecraft to the Earth, through terrestrial communications networks, and finally to the computers which decode and display the data. The limitations, possible errors, validity checks, and decoding algorithms are thus made available to the persons who must finally make decisions based on the data. The possible forms in which the data may appear are demonstrated by samples of test data transmitted through the entire system. Additional items such as trajectory data, tracking station capabilities, and computer capabilities are also presented and explained.

In addition to familiarizing the SDAT representatives with the data system, transmission system, and display system, the Guidance and Control Division is generating

a series of specific procedures to be followed by these persons during flight operations. These procedures will provide the subsystem representatives with a guide for standard missions, i.e., missions in which there are no spacecraft failures. Also, certain other mission sequences in which particular "noncatastrophic" failures occur have been considered. This guide includes a coordinated sequence of events which correlates occurrences in the spacecraft with happenings on the ground in a readily understandable, graphic form. More important, the procedures indicate, as a function of time, the particular telemetry data that are most indicative of the proper operation of the spacecraft. The expected numerical values of these particular measurements, along with corroborative readings from other measurements, are also documented in these procedures. For the case of data which violate the range of expected values, the procedures outline methods for validating the data, troubleshooting techniques for discovering the causes of truly out-of-tolerance readings, and recommendations for corrective action.

2. Compatibility Testing

During this reporting period four compatibility tests were performed. These tests uncovered several computer programming errors which have now been corrected. The next phase of the test schedule will involve personnel training and utilization of the backup computing facility; all operational tests will be carried out in real time (actual mission conditions).

During the third compatibility test, the Deep Space Instrumentation Facility stations sent proof-test-model raw data via telephone line to the Flight Operations Facility. Data received from Woomera and Johannesburg were played through the Telemetry Processing Station's discriminators and were relayed to a strip chart recorder in the Spacecraft Data Analysis Area. Even though the received data were at times very poor due to transmission problems, the Spacecraft Data Analysis Team was able to make a qualitative analysis of three channels. This method of analysis will be used as a backup to the telemetry analysis of teletype data. The higher quality data received from Goldstone was played into a computer system, which includes a discriminator and a decommutator. This method can be used at the

Goldstone Tracking Station and the Atlantic Missile Range for rapid computer reduction of telemetry data.

The spacecraft operated properly and encountered no problems.

C. Systems Testing

1. Ranger Block III Proof Test Model (PTM)

During this reporting period, the *Ranger* Block III PTM spacecraft completed environmental testing. Temperature control tests were conducted in the JPL 25-ft Space Simulator at two levels of simulated solar radiation, 140 and 115 w/ft. During these tests the Earth sensor was difficult to null with the operational support equipment, so the Earth sensor was returned to the laboratory for investigation. Following the tests, a leak was discovered in one of the spacecraft batteries, and the cause of this failure is under investigation. An RF power dropout occurred during full-power operation of the TV subsystem.

The first mission verification test was performed in the JPL 7- × 14-ft horizontal vacuum chamber at low temperature (spacecraft bus at 50°F and TV subsystem at 43°F). The following problems were encountered and are now under investigation: (1) The communications ground receiver lost lock frequently during the test; there were indications that it was an operational support equipment malfunction. (2) An Earth sensor null offset problem occurred during the launch phase of the test; the problem had occurred intermittently in a previous test and was traced to the Earth sensor at this time; as a result, a new unit was installed. (3) One TV battery had a slight electrolyte leak, and one of its cells had no voltage; both batteries were operated below the recommended temperature and voltage limits during the test and were replaced prior to the second mission test.

The second mission test was performed at high temperature (spacecraft bus at 120°F and TV subsystem at 103°F). Problems encountered included an unstable accelerometer, which was not a Block III configuration, and TV picture degradation, which apparently was due to contamination of the collimators and mirrors (operational support equipment) by outgassing products. The third mission test was also performed at high temperature (spacecraft bus at 110°F and TV subsystem at 93°F).

2. Ranger 6

The *Ranger 6* spacecraft has completed Systems Test 3, attitude-control gas system leak check, *Agna* matchmate tests, dummy run, extension system verification, Systems Test 4, weight/center-of-gravity/moment-of-inertia determination, vibration test, vacuum mission tests, postenvironmental inspection, and Systems Test 5 (preshipment).

All spacecraft operations were normal during Systems Test 4, except that low battery voltages on the TV subsystem necessitated an earlier-than-planned turnoff. Subsequent investigation revealed improper charge history on these batteries.

Two battery failures occurred during Mission Test 1 (spacecraft bus at 110°F and TV subsystem at 93°F). One was on the TV subsystem during chamber preparation, and the other, on the spacecraft after installation in the chamber. No damage to the spacecraft bus or TV subsystem structure was incurred. A protective plastic covering was installed around the spacecraft battery to prevent a leakage of KOH from damaging the spacecraft structure. During the terminal phase of Mission Test 1, Camera B of the TV subsystem had extremely low video. After lowering the temperature and opening the chamber, the video reappeared on Camera B. An ambient pressure run at high temperature and a recheck at high temperature in a vacuum failed to make the problem recur. Investigation of the problem will continue.

The scheduled shipment of *Ranger 6* to the Atlantic Missile Range was delayed to allow for rework and requalification of the Earth sensor and the central computer and sequencer.

3. Ranger 7

The *Ranger 7* spacecraft completed an attitude-control gas system leak test, initial power turn-on, Systems Tests 1, 2, and 3, a backup function systems test, *Agna* matchmate tests, dummy run, live pyrotechnic tests, and weight and center-of-gravity measurements. The L-band converter in Communications Case II overloaded shortly after the start of Systems Test 1. Case II was removed and returned to the laboratory for troubleshooting. No

significant problems were encountered during the remaining tests.

D. Midcourse Propulsion System

Successful accomplishment of the *Ranger* mission requires that the spacecraft be capable of undergoing a single midcourse propulsion maneuver to remove or reduce *Agna* injection dispersion errors. This maneuver is accomplished by the use of a small, monopropellant-hydrazine propulsion system delivering 50-lb thrust to the spacecraft. The propulsion system is capable of delivering a variable total impulse in response to signals from an integrating accelerometer circuit.

1. Block III Development Program

SPS 37-23, Vol. VI, described the results of a post-storage firing of the type-approval (TA) 2 propulsion system in which a filter-plugging problem was encountered. During this reporting period the TA 2 system was refueled, pressurized, and placed in storage for a 1-month period in order to repeat this section of the TA test procedure. At the end of this storage period the system was mounted in a test stand and fired for a maximum duration run. A normal ignition and nominal operation were obtained.

An explosive valve squib venting problem was discussed previously (SPS 37-23, Vol. VI). Briefly, the squibs used to actuate the valves on the midcourse propulsion system exhibit an occasional failure mode at initiation wherein the connector assembly is blown off the squib body. During this period fabrication, test, and installation of shields (which will contain the fragments should a failure occur) were accomplished. These shields are aluminum box-like devices that attach to the explosive valves to furnish the required protection to adjacent assemblies in event of squib failure during flight. In order to provide design verification, a typical shield (that for the nitrogen valve) was subjected to a squib failure by utilizing a squib similar to that used for flight and by increasing the severity of operating conditions such that the squib could be predicted to fail. The shield after the test is shown in Fig. 1. The squib failed in the most severe manner; the connector was blown off the body with considerable force. The blast shield design proved capable of containing the connector and protecting the adjacent squib.

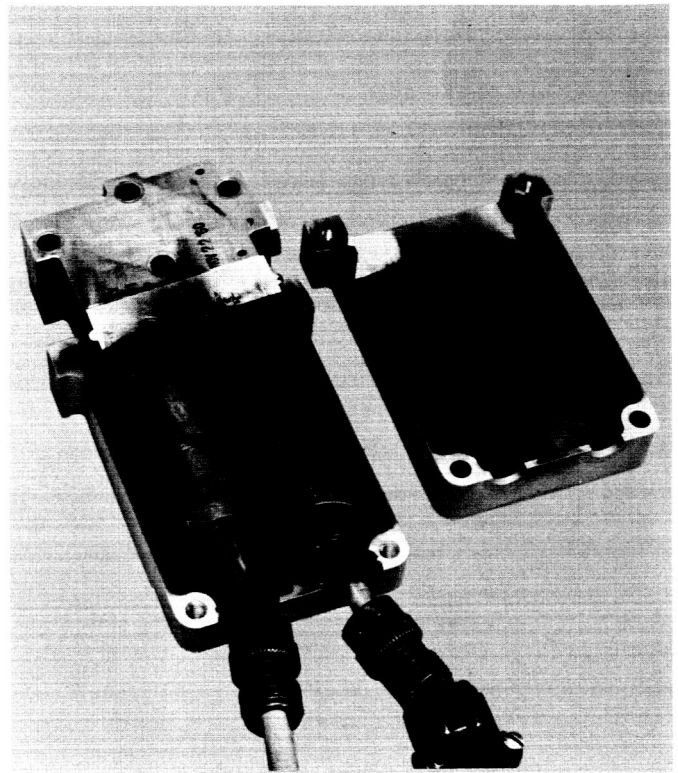


Fig. 1. Nitrogen valve blast shield after squib failure test

In order to ascertain the effect of vibration upon these devices, the system TA vibration test was repeated with blast shields attached. No adverse effects were noted. Upon completion of the vibration test, the system was test-fired with no discrepancies noted.

2. Block V Development Program

The development of the Block V propulsion system is discussed in SPS 37-23, Vol. VI. This system is similar to the Block III system, except that it utilizes an improved propellant. For the *Ranger* application, this propellant furnishes approximately 7% additional impulse. The midcourse propulsion system is functionally a regulated-gas-pressure-fed, constant-thrust rocket. Principal system components include a high-pressure gas reservoir, a gas pressure regulator, a propellant tank and bladder, a rocket engine, and an engine ignition cartridge. The rocket engine contains a quantity of catalyst to accelerate the decomposition of the propellant. Explosively actuated valves are used throughout the system. Normally closed, explosively actuated valves are activated to initiate nitrogen pressurization of the propellant tank, to initiate propellant flow to the rocket engine, and to re-

lease nitrogen tetroxide from the engine ignition cartridge. Normally open, explosively actuated valves are activated to terminate nitrogen pressurization of the propellant tank and propellant flow to the rocket engine. Dual-bridgewire pyrotechnics will be used in each explosively actuated valve to attain a higher degree of reliability. The design and operational philosophy of the subsystem is directed toward maximizing subsystem reliability and reproducibility and minimizing preflight handling and spacecraft interactions, inflight electrical signals, and subsystem components.

The propulsion subsystem can be fueled, pressurized, and monitored for several days prior to emplacement within the spacecraft and the actual launch. The subsystem in the pressurized and fueled condition presents no hazard to personnel within the temperature range of 35 to 125°F. (Burst pressures of the pressure vessels are 2.2 times greater than the maximum working pressures at 125°F.) No spacecraft umbilicals or handlines are required to maintain the propulsion subsystem in the "ready" condition.

In order to avoid electrical or mechanical sequencing, the propellant tank is prepressurized with nitrogen during the preflight operation; therefore, engine ignition and regulated nitrogen pressurization of the propellant tank can occur simultaneously through one signal from the central computer and sequencer (CC&S). Similarly, only one signal is necessary for thrust termination; therefore, a total of two signals is required by the midcourse propulsion subsystem for impulse initiation and termination.

The firing of the midcourse propulsion subsystem is controlled by the CC&S, which receives the time, direction, and magnitude of the midcourse firing through the ground communication link. After the spacecraft has assumed the correct firing attitude (maneuver being executed 16 hr after launch), the midcourse propulsion subsystem is ignited, at the prescribed time, through an electrical signal from the spacecraft's squib firing assembly, which has been initiated by the CC&S. Since the propellant tank is prepressurized, the rocket engine ignition can occur simultaneously with the release of the high-pressure nitrogen to the regulator without allowing time for the propellant tank pressures to build up to the normal operating level. Thrust termination is controlled by the CC&S by means of an electrical signal through the squib firing assembly once the specified velocity increment has been realized, as computed by the spacecraft integrating accelerometer. During the rocket engine fir-

ing, spacecraft attitude is maintained by the autopilot-controlled jet vane actuators.

E. Error Analysis

1. Analysis of Ranger Block III Midcourse Execution Errors

a. Introduction. The nominal trajectory of each *Ranger* Block III spacecraft is designed to impact the Moon at a particular point. Errors normally occurring during injection guidance will cause the actual trajectory to differ from the nominal. The differences may be large enough that a midcourse maneuver is required to correct the impact location. After execution of the maneuver, a residual error remains that is caused by performance variations in the components of the spacecraft guidance subsystem. An analysis of these midcourse maneuver execution errors is reported here.

b. Maneuver sequence. Several steps are necessary to perform the midcourse maneuver, including: determination of the spacecraft trajectory; determination of the components of the maneuver velocity increment; computation of commands for the spacecraft transmission, verification, and storage of the commands; turning of the spacecraft from its cruise attitude to the maneuver attitude in order to point the body-fixed rocket motor in the desired direction; firing of the rocket motor; and reacquisition of the cruise attitude. The errors discussed here occur during the turning of the spacecraft to its maneuver attitude and during the rocket firing.

Prior to execution of the turns, commands for controlling the maneuver are sent to the spacecraft and stored in the central computer and sequencer (CC&S), which directs the spacecraft maneuver sequence. The commands received by the spacecraft are telemetered back to the Earth for verification. When it has been established that the correct commands were received by the spacecraft, a command is transmitted to start the maneuver sequence.

Before the maneuver begins, the spacecraft is in its optically controlled cruise attitude. The spacecraft orientation is controlled by sensing the directions of celestial reference bodies. Motion about the pitch and yaw axes is controlled by Sun sensors to point the roll axis at the Sun. Motion about the roll axis is controlled by an Earth sensor to cause the spacecraft yaw-roll plane to contain the Earth.

The command to begin the maneuver initiates a fixed sequence directed by the CC&S. The roll axis is switched from optical to inertial (gyro) control, while the pitch and yaw axes remain optically controlled to reduce drift. The spacecraft rolls at a constant rate ω_R through an angle θ_R and then remains at rest for the remainder of the roll turn period T_R , which is a fixed interval sufficiently long to allow the maximum roll turn of 90 deg. At the end of the roll turn period, the pitch and yaw axes are switched to inertial control, and the pitch turn is performed in a manner identical to that of the roll turn just described. The pitch rate, turn angle, and turn period are denoted by ω_P , θ_P , and T_P , respectively. When the pitch turn has been completed, the nominal motor thrust line (parallel to the negative roll axis) is pointed in the correct direction. The spacecraft remains at rest in this attitude with all axes under inertial control until the end of the pitch turn period, at which time the rocket motor is ignited. Shutoff occurs when an integrating accelerometer which is sensitive along the roll axis indicates that the commanded velocity has been added.

Table 1 lists the nominal values or limits of the turn rates, angles, and periods, as well as additional parameters not previously mentioned. The actual values of some of the parameters listed vary slightly between different pieces of equipment and with changes in the environment (e.g., temperature). However, the nominal values shown are sufficiently accurate for the error analysis reported here.

c. Relationship of error sources to maneuver errors. Table 2 lists the error sources contributing to the pointing errors, together with the coefficients relating the error source magnitudes to the final pointing errors. Because the velocity vector is added along the roll axis, only pointing errors about the pitch and yaw axes need to be considered. In the present analysis, the pointing errors are assumed to be small angles.

The error sources which contribute to shutoff errors in the maneuver magnitude are the accelerometer scale factor and the accelerometer null offset, with coefficients of 1 and $1/V$, respectively. The shutoff errors are proportional to the maneuver magnitude.

The error sources which contribute to velocity resolution errors in the maneuver magnitude are the velocity increment resolution (computation and measurement) and the velocity tailoff error. Both have coefficients of 1. The resolution errors are independent of the maneuver magnitude.

Table 1. Maneuver parameters

Parameter	Value or limits
Roll turn angle θ_R , deg	$-90 \leq \theta_R \leq 90$
Pitch turn angle θ_P , deg	$-180 \leq \theta_P \leq 180$
Roll turn rate ω_R , mrad/sec	± 3.5
Pitch turn rate ω_P , mrad/sec	± 3.5
Roll turn period T_R , sec	570
Pitch turn period T_P , sec	1020
Earth-probe-Sun angle β , deg	$45 \leq \beta \leq 135$
Feedback gain in the pitch gyro-autopilot-jet vane loop, G_{FBP}	4
Feedback gain in the yaw gyro-autopilot-jet vane loop, G_{FBY}	4
Average acceleration of spacecraft during motor burn, V , m/sec ²	0.615

d. Limiting assumptions and conclusions. To calculate the actual errors, the coefficients must be evaluated. This is a straightforward procedure, except for the coefficients containing the turns θ_R or θ_P , or the Earth-probe-Sun angle β . Since these angles vary for different trajectories and maneuvers, values that maximize each coefficient are used. For this reason the pointing error estimate may be somewhat pessimistic. Nevertheless, this technique is useful in determining the contribution of the individual errors to the total pointing error and gives a reasonable estimate of the pointing accuracy.

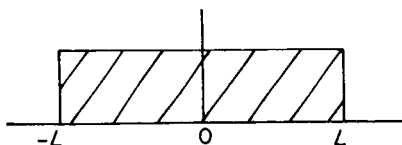
The method for estimating pitch and yaw pointing errors and the shutoff and resolution magnitude errors is described next. Each of the error sources is assumed to: (1) have a zero mean value, and (2) be statistically independent of all other sources. As a result of the first assumption, the variance of each individual error source is equal to the mean value of the squared error, and the standard deviation (1σ value) is equal to the rms value. As a result of the second assumption, the variance of the final pointing, resolution, or shutoff error is the sum of the products formed when the square of each individual error standard deviation is multiplied by the square of its coefficient. When each individual product is divided by the sum of the squares and multiplied by 100, the percentage contribution of the individual error source to the variance of the final error under consideration is obtained. If 3σ values are used instead of the 1σ standard deviations, the square root of the sum of the squares is the 3σ value of the final error. The use of individually maximized coefficients tends to yield an upper bound on the 3σ value if the individual errors are indeed statistically independent.

Table 2. Pointing error sources and coefficients

Error source	Pitch coefficient	Yaw coefficient	Error source	Pitch coefficient	Yaw coefficient
Pitch sensor electrical null offset	-1	0	Roll gyro drift	0	$-T_R \sin \theta_P - \frac{(1 - \cos \theta_P)}{\omega_P}$
Pitch sensor mechanical null offset	-1	0	Roll turn calibration	0	$\theta_R \sin \theta_P$
Initial pitch dead zone position	1	0	Roll capacitor leakage	0	$-\sin \theta_P$
Pitch switching amplifier null offset	-2	0	Roll turn time resolution	0	$\omega_R \sin \theta_P$
Yaw sensor electrical null offset	0	$-\cos \theta_P - \cot \beta \sin \theta_P$	Pitch turn calibration	θ_P	0
Yaw sensor mechanical null offset	0	$-\cos \theta_P - \cot \beta \sin \theta_P$	Pitch capacitor leakage	-1	0
Initial yaw dead zone position	0	$(\cos^2 \theta_P + \cot^2 \beta \sin^2 \theta_P)^{1/2}$	Pitch turn time resolution	ω_P	0
Yaw switching amplifier null offset	0	$-2 \cos \theta_P - \cot \beta \sin \theta_P$	Yaw gyro misalignment in roll	0	$\sin \theta_P$
Roll sensor electrical null offset	0	$-\frac{\sin \theta_P}{\sin \beta}$	Roll gyro misalignment in yaw	0	$-(1 - \cos \theta_P)$
Roll sensor mechanical null offset	0	$-\frac{\sin \theta_P}{\sin \beta}$	Roll sensor hinge misalignment in yaw	0	$\cot \beta \sin \theta_P$
Initial roll dead zone position	0	$\frac{\sin \theta_P}{\sin \beta}$	Roll sensor hinge misalignment in roll	0	$-\sin \theta_P$
Roll switching amplifier null offset	0	$-\frac{2 \sin \theta_P}{\sin \beta}$	Location of cg, angular error in pitch	$1 + \frac{1}{G_{FBP}}$	0
Pitch gyro drift	$-T_P$	0	Thrust vector angular error in pitch	$-\frac{1}{G_{FBP}}$	0
Yaw gyro drift	0	$\frac{-\sin \theta_P}{\omega_P} - \left(T_P - \frac{\theta_P}{\omega_P}\right)$	Location of cg, angular error in yaw	0	$1 + \frac{1}{G_{FBY}}$
			Thrust vector angular error in yaw	0	$-\frac{1}{G_{FBY}}$
			Roll sensor albedo asymmetry	0	$-\frac{\sin \theta_P}{\sin \beta}$

Tables 3, 4, and 5 list the error sources, maximum values of the error coefficients, 3σ values of the individual errors, and the percent of total variance contributed by each error for the pointing, shutoff, and resolution errors, respectively. The numerical values should be considered as typical of *Ranger* Block III performance, but not as final estimates of expected performance.

The error sources listed in the tables are assumed to have Gaussian distributions except where indicated otherwise (in which case, the errors are assumed to be uniformly distributed, as illustrated below).



For a zero mean uniformly distributed random variable, the 3σ standard deviation is $3^{1/2}L$.

It is possible that, as a result of solar or other extraneous torques, the limit cycle errors (initial pitch, roll, and yaw dead zone positions) would be forced to one or the other of their extreme values. Thus, they might approach a discrete distribution, as shown below.



If this were the case, the 3σ standard deviation for these errors would be $3L$ or $3^{1/2}$ times their present tabulated values.

Table 3. Pointing error values

Error source	3 σ source error	Maximized coefficient	3 σ pointing error ^a , mrad	Percent of total variance
Pitch sensor electrical null offset	0.5 mrad	1	0.50	<0.1
Pitch sensor mechanical null offset	2.2 mrad	1	2.20	0.4
Initial pitch dead zone position	5.0 mrad ^b	1	5.00	2.1
Pitch switching amplifier null offset	1.0 mrad	2	2.00	0.3
Yaw sensor electrical null offset	0.5 mrad	2 ^{1/2}	0.71	<0.1
Yaw sensor mechanical null offset	2.2 mrad	2 ^{1/2}	3.11	0.8
Initial yaw dead zone position	5.0 mrad ^b	1	5.00	2.1
Yaw switching amplifier null offset	1.0 mrad	5 ^{1/2}	2.24	0.4
Roll sensor electrical null offset	8.0 mrad	2 ^{1/2}	11.31	10.6
Roll sensor mechanical null offset	1.73 mrad	2 ^{1/2}	2.45	0.5
Initial roll dead zone position	15.0 mrad ^{b,c}	2 ^{1/2}	21.21	37.4
Roll switching amplifier null offset	1.0 mrad	2 (2 ^{1/2})	2.83	0.7
Pitch gyro drift	$4.85 \times 10^{-3} \frac{\text{mrad}}{\text{sec}}$	1020 sec	4.95	2.0
Yaw gyro drift	$4.85 \times 10^{-3} \frac{\text{mrad}}{\text{sec}}$	1020 sec	4.95	2.0
Roll gyro drift	$4.85 \times 10^{-3} \frac{\text{mrad}}{\text{sec}}$	925 sec	4.49	1.7
Roll turn calibration	$3.0 \frac{\text{mrad}}{\text{rad}}$	1.57 rad	4.71	1.9
Roll capacitor leakage	5.0 mrad	1	5.00	2.1
Roll turn time resolution	0.867 sec ^b	$3.5 \frac{\text{mrad}}{\text{sec}}$	3.03	0.8
Pitch turn calibration	$3.0 \frac{\text{mrad}}{\text{rad}}$	3.14 rad	9.42	7.4
Pitch capacitor leakage	5.0 mrad	1	5.00	2.1
Pitch turn time resolution	0.867 sec ^b	$3.5 \frac{\text{mrad}}{\text{sec}}$	3.03	0.8
Yaw gyro misalignment in roll	1.53 mrad	1	1.53	0.2
Roll gyro misalignment in yaw	1.53 mrad	2	3.06	0.8
Roll sensor hinge misalignment in yaw	2.6 mrad	1	2.60	0.6
Roll sensor hinge misalignment in roll	2.6 mrad	1	2.60	0.6
Location of cg, angular error in pitch	5.0 mrad	1.25	6.25	3.2
Thrust vector angular error in pitch	2.8 mrad	0.25	0.70	<0.1
Location of cg, angular error in yaw	5.0 mrad	1.25	6.25	3.2
Thrust vector angular error in yaw	2.8 mrad	0.25	0.70	<0.1
Roll sensor albedo asymmetry	9.6 mrad ^c	2 ^{1/2}	13.57	15.3

^aTotal 3 σ pointing error = 34.68 mrad.^bThese errors have been taken as uniform distributions.^cThese errors depend on angular diameter and were calculated for a range of approximately 160,000 km.

Table 4. Shutoff error values

Error source	3 σ source error	Maximized coefficient	3 σ shutoff error ^a , m/sec	Percent of total variance
Accelerometer scale factor	2.5×10^{-3}	V	$2.5 \times 10^{-3}V$	4
Accelerometer null offset	$7.5 \times 10^{-3} \text{ m/sec}^2$	$1.63V \text{ sec}^2/\text{m}$	$12.2 \times 10^{-3}V$	96

^aTotal 3 σ shutoff error = $12.45 \times 10^{-3} V \text{ m/sec}$. For the rms maneuver of 20 m/sec, the 3 σ shutoff error = 0.249 m/sec.

Table 5. Resolution error values

Error source	3σ source error, m/sec	Maximized coefficient	3σ resolution error ^a , m/sec	Percent of total variance
Velocity increment resolution	$(37.3 \times 10^{-3})^b$	1	37.3×10^{-3}	50.5
Velocity tailoff error	37×10^{-3}	1	37×10^{-3}	49.5
^a Total 3σ resolution error = 52.5×10^{-3} m/sec. ^b These errors have been taken as uniform distributions.				

II. *Surveyor* Project

A. Introduction

The *Surveyor* Project will take the next step in advancing lunar technology by making soft landings on the Moon, beginning in 1965 with a group of four test missions whose objective is to demonstrate successful soft landing by post-landing spacecraft operation. An engineering payload including elements of redundancy, increased diagnostic telemetry, touchdown instrumentation, and survey TV will be used.

The general objective after 1965 is to perform operations on the Moon contributing new scientific knowledge and basic data in support of manned lunar landings. A group of four flights planned for 1966 will carry a scientific payload selected from the following experiments: two-camera TV, micrometeorite ejecta, single-axis seismometer, alpha-particle scattering, soil properties (surface sampler), and touchdown dynamics.

In 1965 and 1966, the 2150-lb (separated weight) spacecraft will be injected into the lunar trajectory by direct ascent, using single-burn *Atlas-Centaur* vehicles. The midcourse correction capability will be 50 m/sec in 1965 and 30 m/sec in 1966.

Hughes Aircraft Company is under contract to develop and manufacture the first seven spacecraft. Studies are under way at the Bendix Corporation, Systems Division, and the General Motors Defense Research Laboratories on the feasibility and design of lightweight lunar roving vehicles as possible later payloads for *Surveyor*.

B. Space Flight Operations

Surveyor space flight operations (SFO) activity during this reporting period has involved the production and publication of the preliminary SFO Plan for the *Surveyor* P-42 mission and preparation of the P-42 SFO Test Plan and the *Surveyor* Space Flight Operations System (SFOS) Design Specifications Book.

THE PLANETARY — INTERPLANETARY PROGRAM

III. *Mariner C* Project

A. Introduction

The over-all objective of the *Mariner C* Project is to perform a successful mission to Mars during the 1964 period of availability.

The primary objective of the *Mariner C* Project is to conduct close-up (flyby) scientific observations of the planet Mars during the 1964–1965 opportunity and to transmit the results of these observations back to Earth. The planetary observations should, to the greatest practical extent, provide maximum information about Mars. A TV system and a reasonable complement of fields and particles experiments will be carried. An effort will be made to identify organics in the atmosphere and on the surface of the planet.

A secondary objective is to provide experience and knowledge about the performance of the basic engineering equipment of an attitude-stabilized flyby spacecraft during a long-duration flight in space farther away from the Sun than the Earth. An additional secondary objective is to perform certain field and/or particle measurements in interplanetary space during the trip and in the vicinity of Mars.

The *Atlas-Agena D* launch vehicle to be used in this project will provide a minimum separated spacecraft weight of 570 lb.

It is planned to conduct two launchings of *Mariner C* missions from two separate launch pads. All activities will be planned to exploit the limited launch period to the maximum extent. To accomplish this, spacecraft and launch vehicles will be processed in parallel, so that following the launching of the first space vehicle the second vehicle may be launched without delay; however, no earlier than two days after the first launch.

Final assembly of the spacecraft proof test model has begun in the Spacecraft Assembly Facility.

Three test spacecraft structures have been assembled and individual testing programs have commenced. The structural test model has successfully completed the static test and Phase I of the modal vibration surveys. The temperature control model has undergone a series of tests in the 25-ft Space Simulator. The developmental test model is being prepared for the simulated mid-course interaction test.

Mariner C shroud development is currently being re-directed. Either a mechanically separated “clam shell” or an “over the nose” shroud will be developed.

B. Spacecraft Design and Development

1. Structural and Thermal Testing

The structural test model (STM), minus solar panels, omni-antenna and dampers, was mounted on the Lockheed Missiles and Space Company (LMSC) adapter and subjected to a series of modal surveys (Fig. 1). These tests consisted of exciting the various resonant frequencies or modes of the structure using low-level vibration shakers. The data from this test were used to determine the behavior of the linear portions of the spacecraft structure. The tests indicate that the basic spacecraft structure should successfully complete the high-level vibration qualification tests.

Results of the static test on the STM indicate that the separation V-band loads (and their effects on the spacecraft lower ring) and the maximum shear and overturning moment loads are within the design capability of the structure.

The temperature control model (TCM) is being tested in the JPL 25-ft Space Simulator (Fig. 2). Because of high losses through the thermal shields, the TCM ran colder than anticipated at Mars solar intensity. New shields have been designed which should reduce the expected temperature drop between Earth and Mars to approximately 20°F.

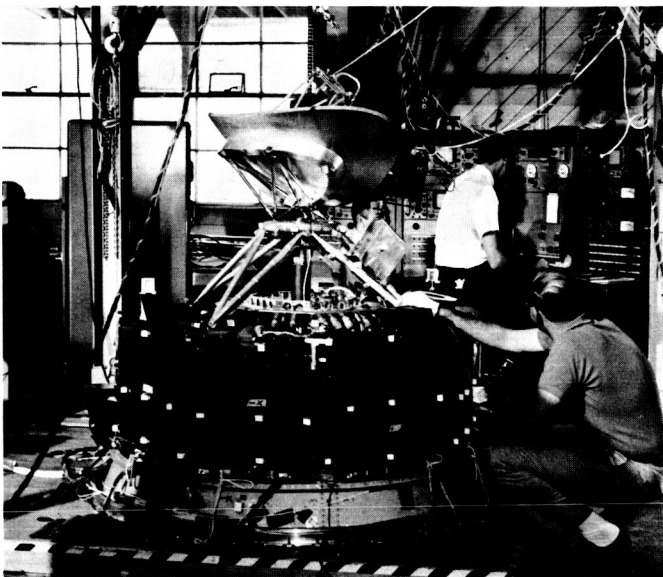


Fig. 1. Structural test model

2. Packaging

The basic subchassis profile of *Mariner C* is the same as that used in *Ranger* and *Mariner 2*; however, there are new developments in the electronic packaging area. New designs have been made in: (1) detailed electronics layout; (2) the electronics chassis; (3) component handling, shipping, and storage; and (4) the scientific instrument package.

Electronics assemblies within the octagonal equipment compartment are located as shown in Fig. 3.

The electronics assemblies occupy seven bays of the octagonal instrument compartment; the eighth bay is occupied by the midcourse motor. Because the midcourse motor was difficult to relocate, it was used as a reference point about which the assemblies were arranged.

Clockwise from the midcourse motor is Assembly III, which contains the electronics for the scientific instruments together with the data automation subsystem. Fig. 4 shows the layout of Assembly III, which illustrates the following examples of six packaging techniques used on the *Mariner C* spacecraft:

- (1) Two-dimensional component layout on printed wiring boards using bifurcated terminals [TV electronics, scan electronics, and data automation system (DAS) power supply].
- (2) Welded three-dimensional cordwood modules connected to printed wiring boards by means of bifurcated terminals (magnetometer electronics and TV electronics).
- (3) Soldered three-dimensional modules (cosmic ray telescope).
- (4) Component parts with formed leads, soldered in plated-through holes on a printed wiring board (plasma electronics).
- (5) Miniature component leads soldered directly to a printed conductor (buffer memory).
- (6) Pellet component parts interconnected with vacuum-deposited and dip-soldered conductors, potted in modules, welded into groups of modules, and finally cabled with soldered wires (DAS logic).

A typical *Mariner C* electronics chassis is shown in Fig. 5. The chassis is machined from ZK 60 magnesium forgings to a minimum thickness of 0.050 in. for the bottom surface. The average weight of each chassis is about 4.5 lb, which is approximately the same weight as the

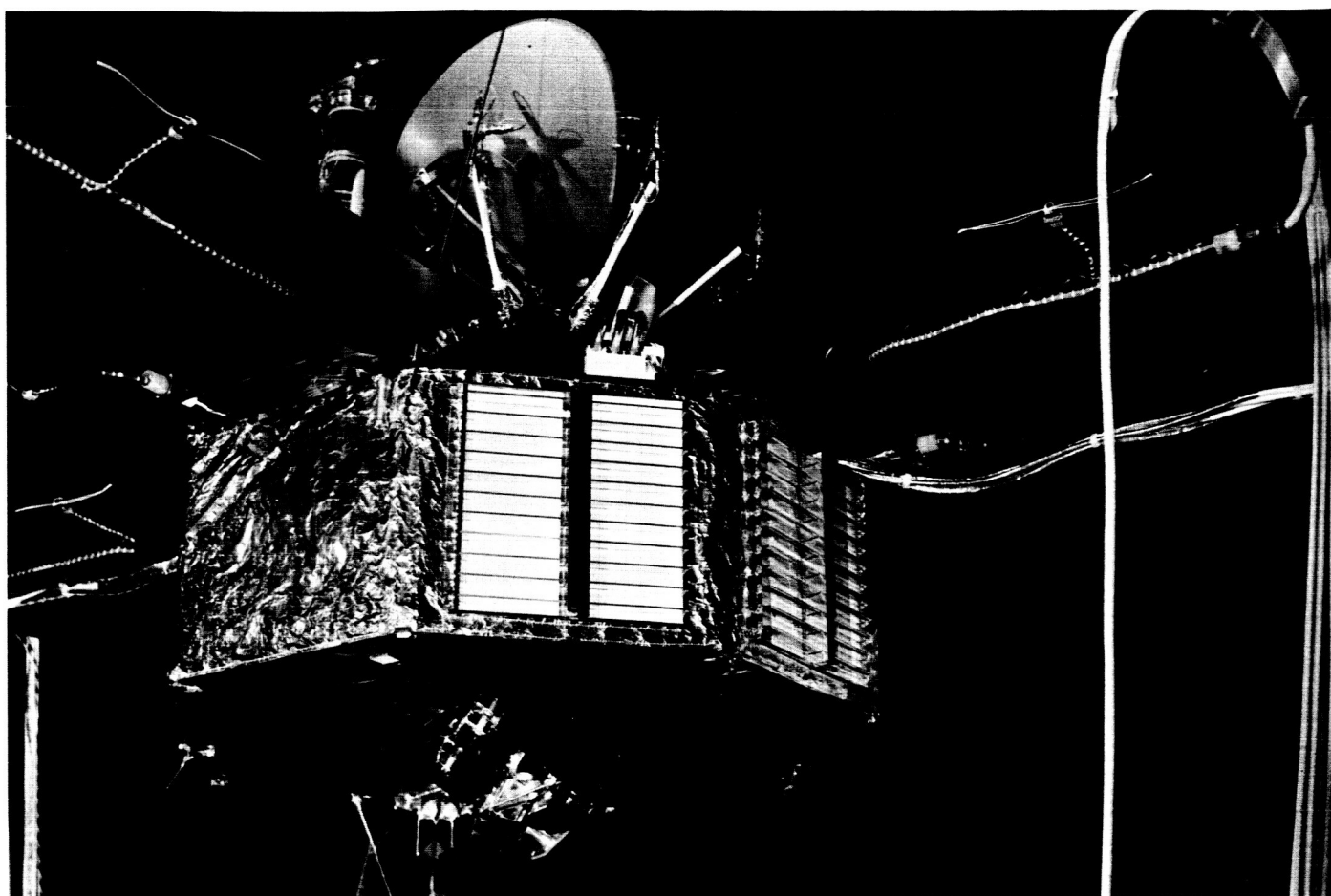


Fig. 2. Temperature control model

Mariner 2 chassis. However, the larger *Mariner C* chassis is capable of holding 25% more equipment and, in addition, is performing a greater structural function, which makes it possible to reduce the weight of structural members.

Two primary considerations influenced packaging and geometry of the scientific instruments: (1) the sensing element, its size and direction of sensitivity; and (2) attachment to the spacecraft—direction, alignment, geometry, and clearances.

A brief description of packaging considerations for each instrument follows:

The magnetometer requires a location as far away from the spacecraft magnetic fields as possible. Such a location is available on the low-gain antenna. The most efficient instrument geometry results in a sphere which

contains the optics, the magnetic coils, and other elements of the magnetometer.

The ion chamber is located on the low-gain antenna to provide the ion chamber and 10311 detector tube a maximum possible field-of-view, since both sensors have omnidirectional sensitivity. An I-section, U-shaped chassis was designed to house the electronics on printed wiring boards. This chassis is used to hold the two sensors in optimum orientation and to distribute the instrument weight equally around the cylindrical antenna mast. Fig. 6 shows the general instrument configuration.

The cosmic dust detector required 50 in.² of sensor plate in the plane of the ecliptic; both sides of the plate were exposed to unobstructed space. A location was selected which is above the superstructure holding the high-gain antenna.

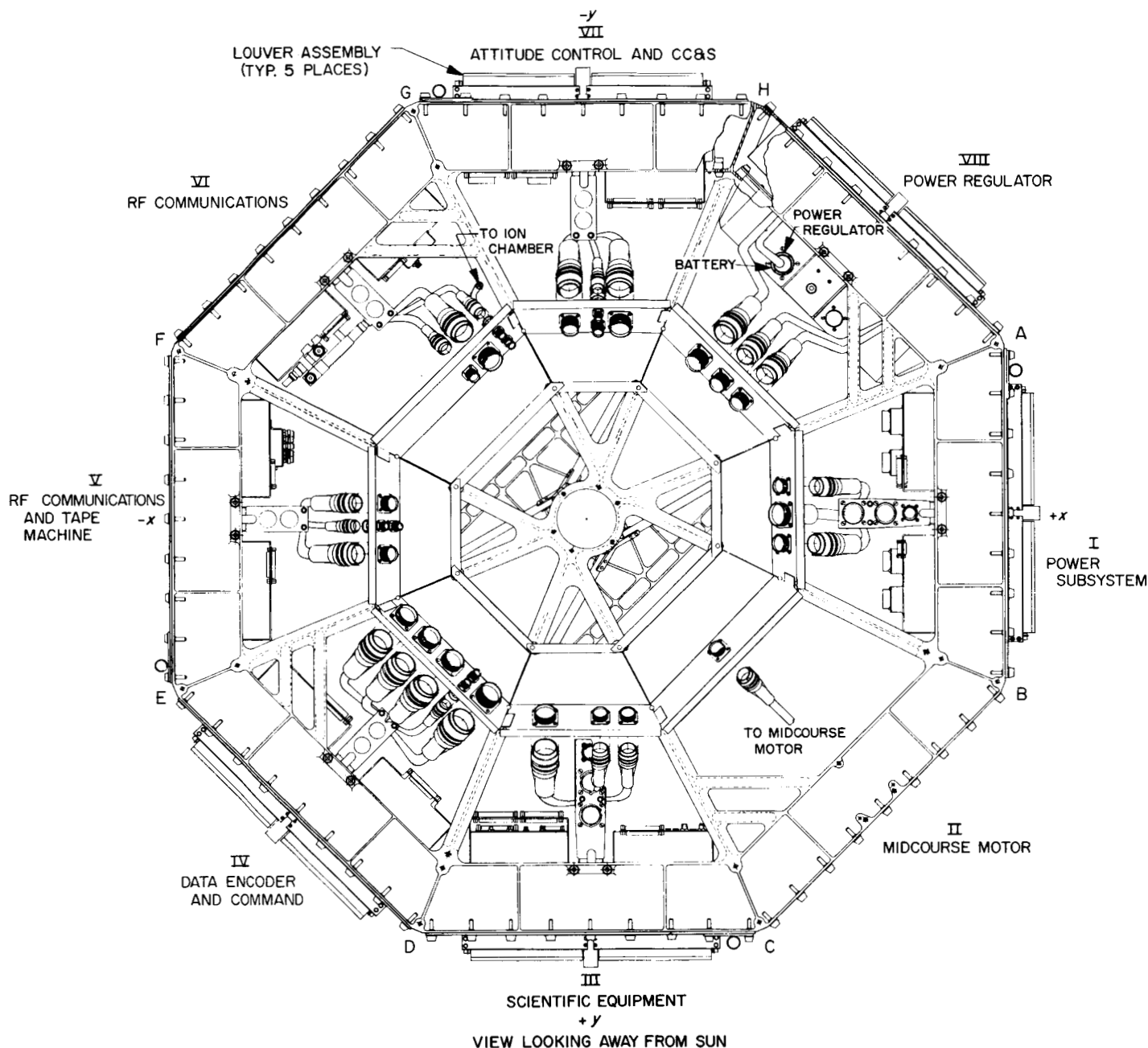


Fig. 3. Mariner C electronics compartment

The trapped radiation detector sensors are directional, and are pointed at various angles away from the spacecraft-Sun line. A location which satisfied the detector requirements was on top of the octagon between the solar panels. A box-shaped chassis provided support for sensors and the electronics.

The solar plasma probe is a simple cup with screens at various voltages. The probe is located above Assembly III to provide an unobstructed view of the Sun.

The planetary sensor, TV, and ultraviolet photometer are mounted on a scanning platform below the octagon.

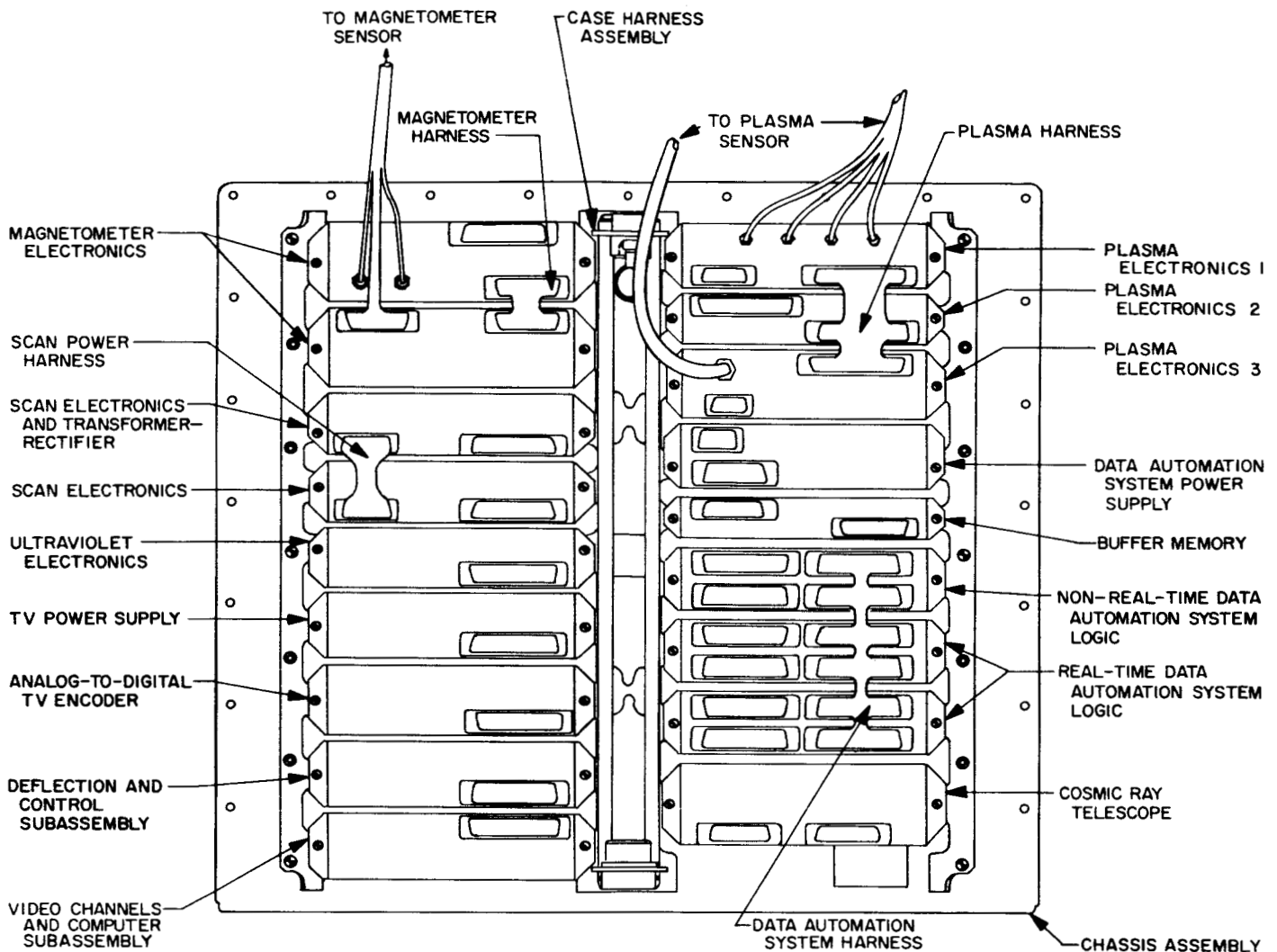


Fig. 4. Layout of Assembly III (scientific equipment electronics)

The planetary sensor consists of a lens and optical sensor joined to a small preamplifier chassis at the mounting flange to the scanning platform. The preamplifier electronics are packaged using printed wiring boards.

Television camera packaging is shown in a sectional view layout (Fig. 7). The vidicon tube is completely surrounded by electronic printed wiring board assemblies on the four surfaces. The instrument is covered with a highly polished aluminum shield for temperature control.

The ultraviolet photometer chassis is shown in Fig. 8. Three sensor tubes are located inside the basic housing; the electronics are mounted around the chassis internal surfaces.

3. Gyro Control Assembly

The purpose of the gyro control assembly (GCA; Fig. 9) is to provide inertial rate and position information to the spacecraft attitude control system. This information is used in damping the spacecraft motion during acquisition or for steering during the midcourse-maneuver motor burn period.

Three modes of operation are possible within the GCA. The first is a conventional rate mode. Rebalance currents to the three gyro torquers are used to develop voltages which are proportional to spacecraft turning rates. This rate mode is used to damp out spacecraft turns during the acquisition of the Sun or Canopus.

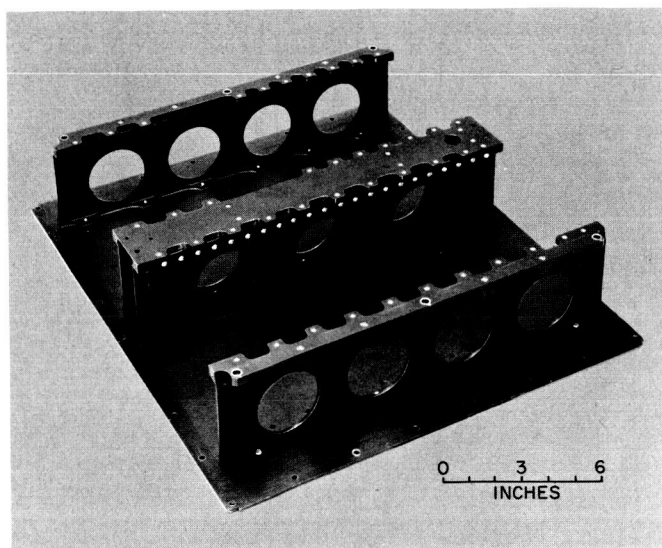


Fig. 5. Mariner C assembly chassis

In the second mode the gyro gimbal is torqued by a precision current for a controlled length of time. Motion

of the gyro gimbal produces an error signal to the switching amplifier in the attitude control system. Gas is then vented through the appropriate jets, causing the spacecraft to follow the gyro gimbal motion. To allow a wider range of motion for the gyro input axis, a large integrating capacitor is inserted into the rebalance loop during this mode. This capacitor stores a voltage proportional to the gimbal motion and allows greater input range to be obtained.

The third mode of operation is used in steering the spacecraft. The rebalance loop is the same as that of the second mode, but the precision command current is removed. Gyro signals are then fed to the autopilot and jet vane actuators to keep the spacecraft on the correct heading during the midcourse motor burn period.

A new concept in functional and life testing of the gyro control assembly is being investigated for use on this program. A fully automatic test set is being designed to supplement the normal functional electronic tests. This automatic unit will proceed through 10 operations or

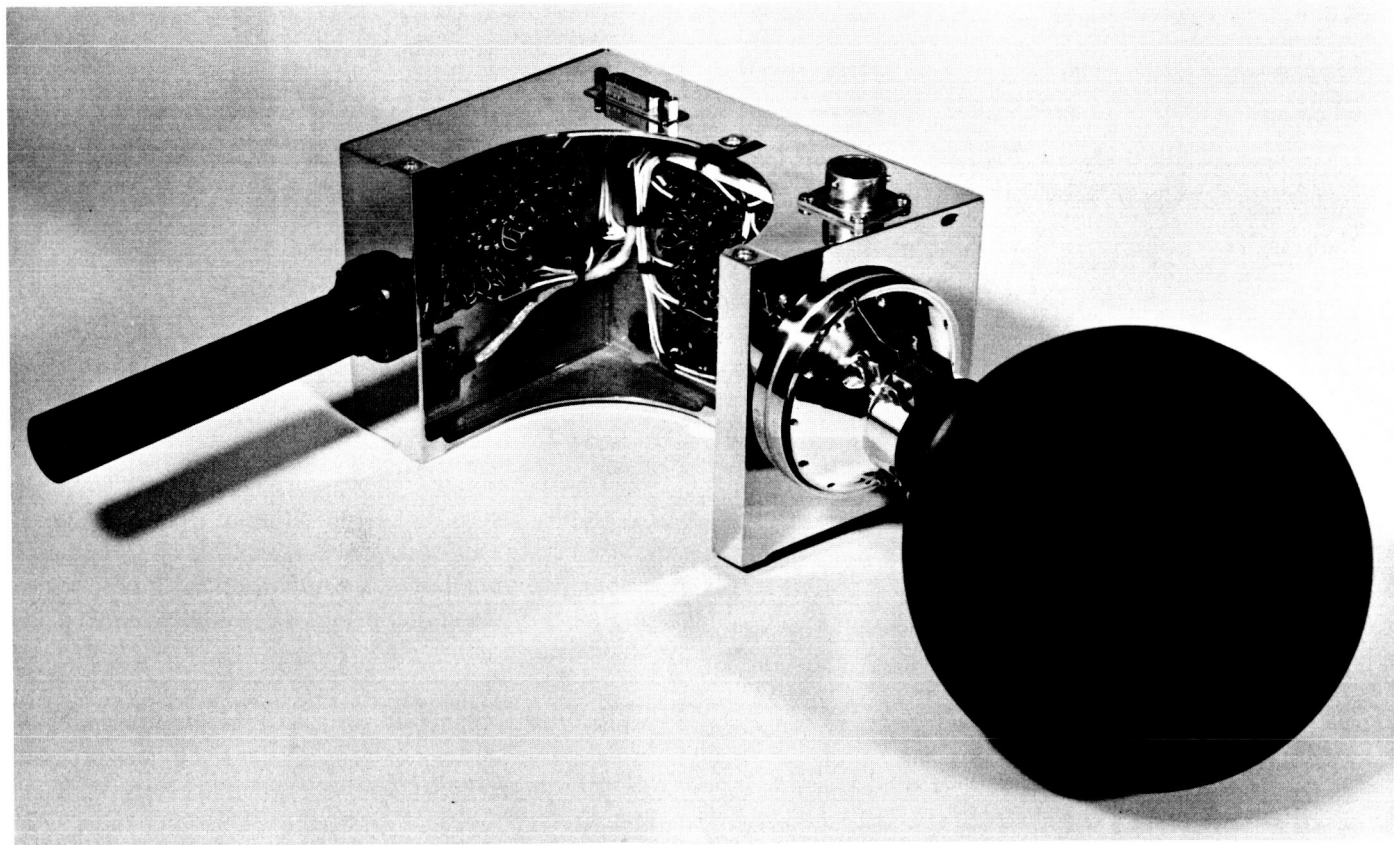


Fig. 6. Ion chamber configuration

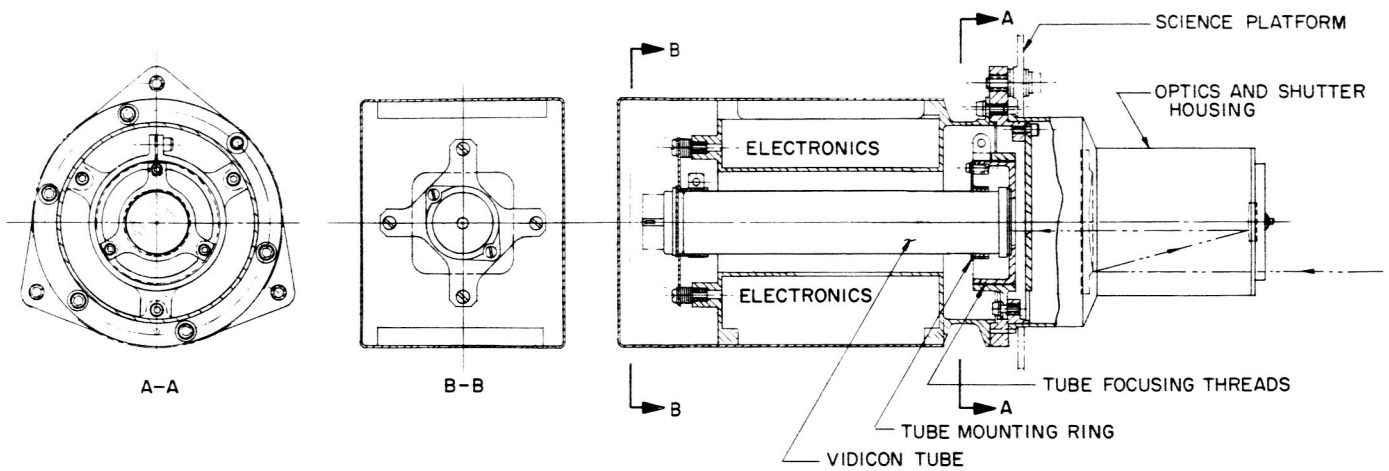


Fig. 7. TV instrument—section view

measurements and record the results as *go*, *no-go* on decimal counters. In the past, functional testing was performed three or four times during the normal sequence of calibration and performance and environmental testing. With the automatic test set, the total number of times that any individual parameter can be measured can be increased several hundred times. It is felt that a higher level of confidence in the ability of the gyro control assembly to function for 6000 hr in space can be obtained if the unit will correctly function through several hundred cycles on the ground.

Construction and evaluation of the automatic test set is now proceeding on such a schedule that the next GCA (the type approval unit) will be put through the automatic test procedure from the beginning of laboratory bench testing. This test method does not replace the normal manual method of testing, which actually covers

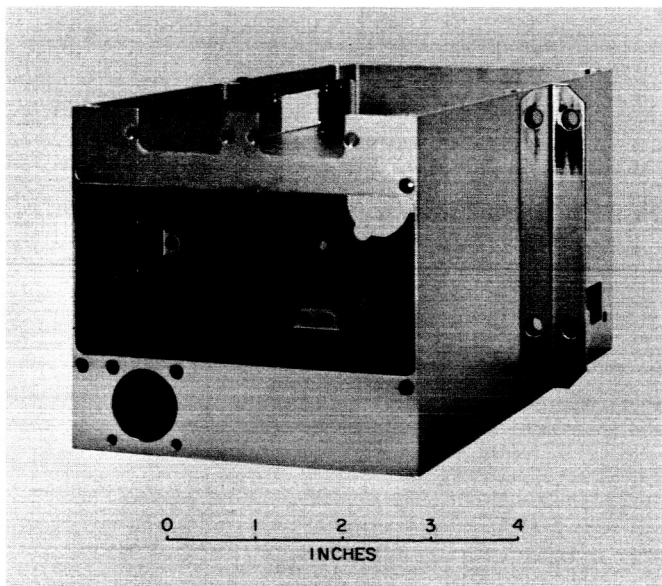


Fig. 8. Ultraviolet photometer chassis

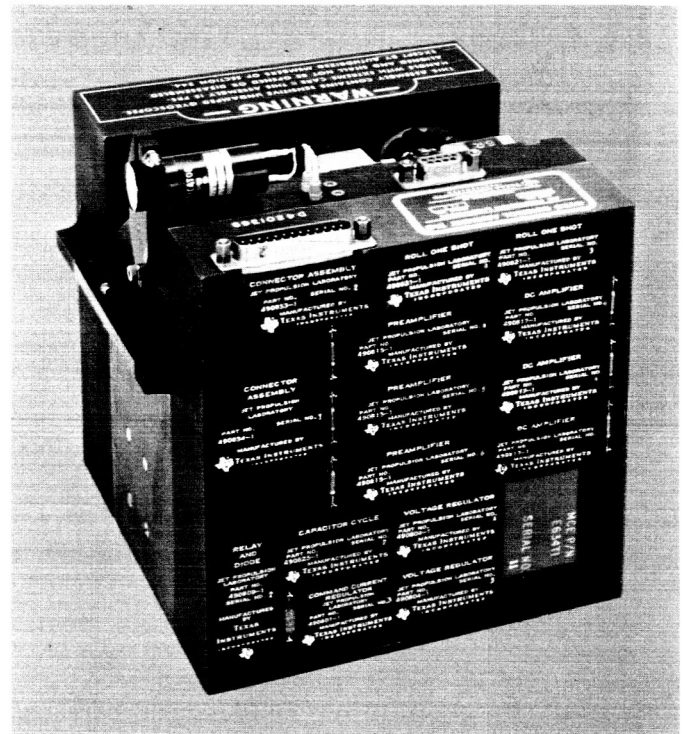


Fig. 9. Gyro control assembly proof test model

considerably more than 10 items, but is intended to supplement the method now used.

4. Electrical Conversion

A full set of prototype electrical conversion equipment was built at JPL to permit electrical testing before the proof test model and type approval sets were fabricated. A second set of prototype equipment was built by Space Technology Laboratories to checkout fabrication, quality control, and testing procedures and fixtures. This prototype set is now being used for the simulated midcourse interaction test power equipment.

The prototype power regulator assembly is shown in Fig. 10. This assembly is equivalent to three of the *Mariner 2* modules and contains the power switch and logic, power telemetering transducers, and two booster regulators. The one-piece case is a full-flight assembly and is mounted directly to the spacecraft frame.

The other electrical conversion equipment is designed into 6- × 6-in. subassemblies and is mounted in a standard flight case assembly. Circuit boards and larger components are mounted directly to the module web in the standard JPL design.

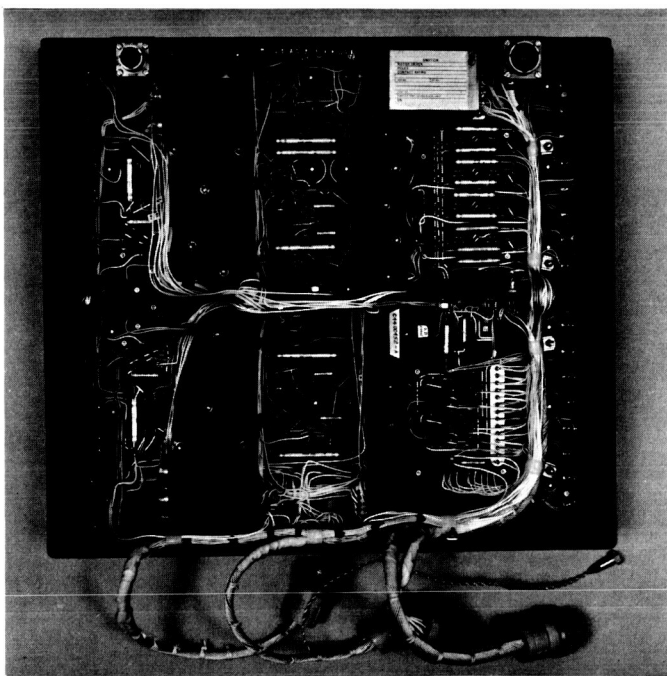


Fig. 10. Prototype power regulator assembly

The power distribution subassembly controls power to several of the spacecraft users. Commands are received from the central computer and sequencer and command subsystems to switch latching relays at certain times during flight. The command and power interfaces into the subassembly are shown in Fig. 11.

5. Batteries

Four prototype Mark VI *Mariner C* batteries are being flight acceptance tested. This includes a bench test for electrical and physical characteristics, a vibration test in three planes while the battery is under load, a discharge-charge cycle under vacuum at room temperature, and another bench test. The batteries have satisfactorily passed the first bench test and the vibration test.

6. Solar Panels

The solar cells (Heliotek) are boron, shallow-diffused P on N devices (1×2 cm). Electroless nickel plating is used to obtain an ohmic contact to the silicon.

The solar cells are required to produce a mean power output of 22.4 mw at 28°C when tested under a tungsten source adjusted to have an equivalent sunlight intensity of 100 mw/cm^2 . In addition, the cells are required to produce a mean power output of 22.4 mw at 28°C when measured in sunlight at Table Mountain with a solar irradiance of 100 mw/cm^2 at an air mass between 1.5 and 1.8.

The conversion efficiency of the solar cell varies widely depending upon the wavelength of the incident radiation. This dependence can be measured in terms of relative spectral response and is slightly different for each solar cell. As a result of the difference in spectral response (Fig. 12), cells can produce a different output when measured using a tungsten source and when measured in sunlight. The loss usually results in less power output in sunlight than would be expected, based on measurements using the tungsten source.

Calibration procedures have been used to assure that the tungsten/Table Mountain power output ratio would be maintained at unity.

A solar cell submodule design was selected as the basic building block for the prototype solar panel MC-P-1. The submodule design consisted of seven P/N silicon solar cells (1×2 cm) electrically connected in parallel with a 3-mil-thick copper N bus bar and a 16-mil-D copper P bus wire.

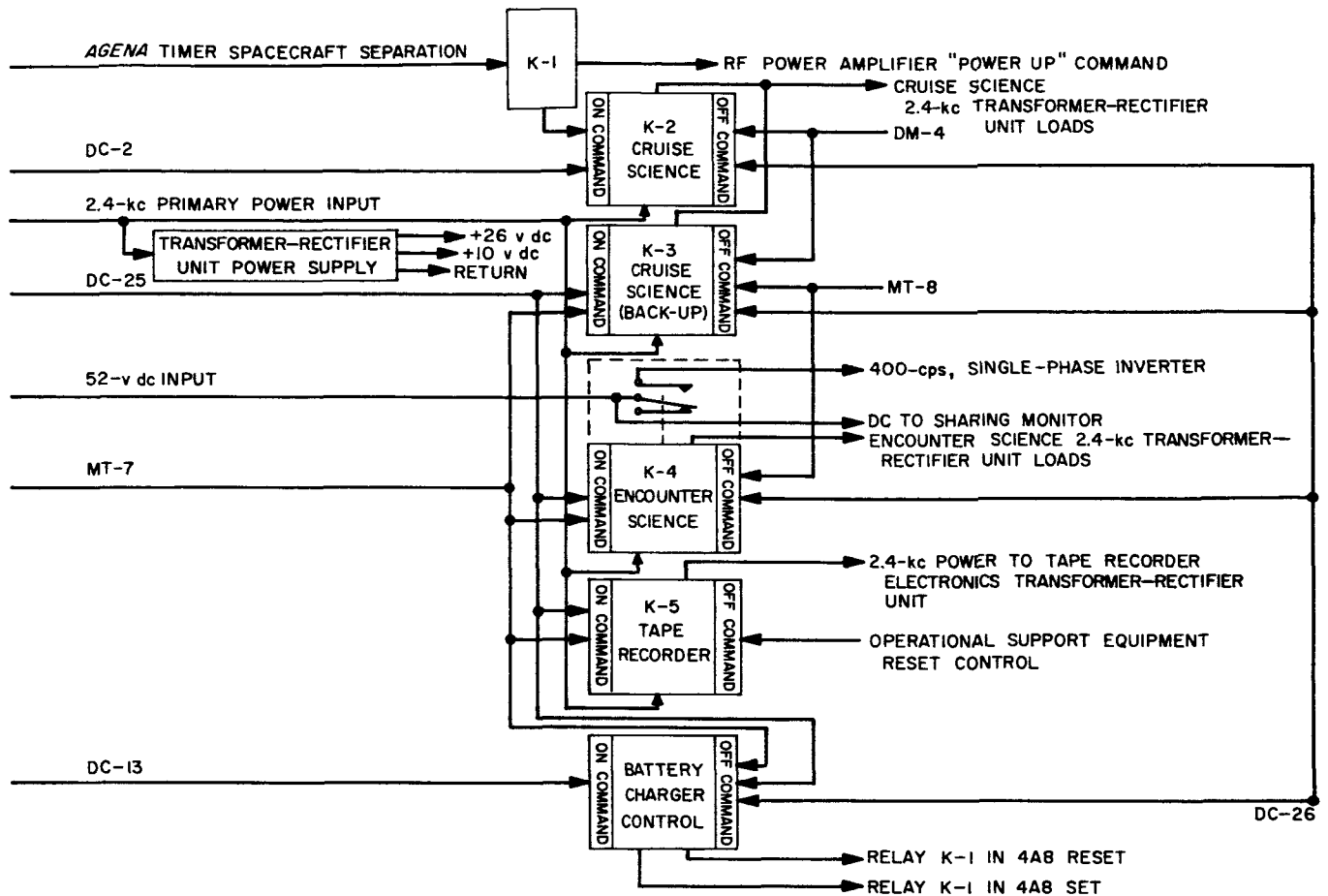


Fig. 11. Power distribution subassembly block diagram

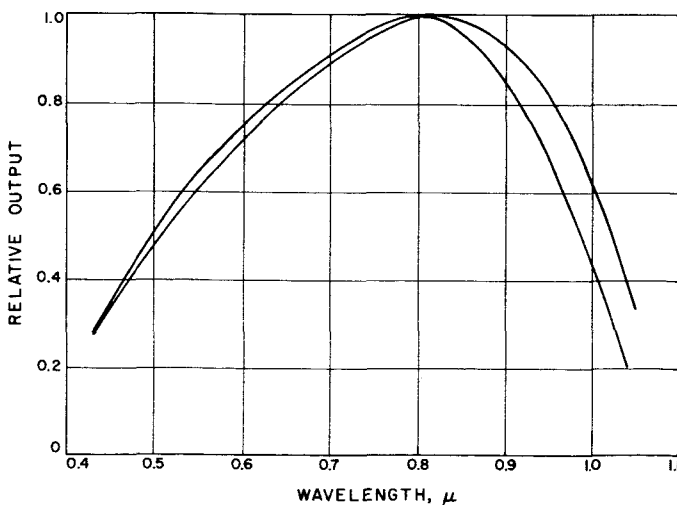


Fig. 12. Relative spectral response of typical solar cell

Tooling design, fabrication, and assembly of 1008 sub-modules, and submodule installation onto the structure have been completed.

Pre-environmental electrical tests were performed on the prototype solar panel. All four electrical sections of the panel were acceptable.

Cell efficiency with a glass cover attached and connected in 21-parallel \times 84-series cell sections was 8.38% at Earth-space conditions and 8.96% at Mars encounter conditions. The efficiency of the projected panel area was 6.91% at Earth-space conditions and 7.33% at Mars encounter conditions. The 151.6 w achieved with the first prototype panel represents a 27% improvement over the minimum requirement. The increased efficiency was due to a more accurate control of cell performance and a reduction in assembly degradation.

Prototype MC-P-1 was also subjected to the following type approval tests: (1) acoustic noise, (2) high-frequency vibration, (3) humidity, and (4) thermal vacuum.

The solar panel was inspected and electrically tested after each of the tests. The results revealed no measurable electrical degradation; however, a significant number of broken glass covers and possible cell fractures were noted after the acoustic noise test.

The design of the type approval solar panels was modified to incorporate tunnel oven soldered submodules using Kovar bus bars. Lockheed Electronics will assemble two type approval panels utilizing submodules fabricated by a conveyor belt or tunnel oven process. Space Technology Laboratories will assemble two additional type approval solar panels, one of which will use submodules fabricated by a static oven soldering process.

7. Postinjection Propulsion System

The primary function of the *Mariner C* postinjection propulsion system is to remove, or reduce, boost vehicle injection dispersion errors so that a Mars flyby with a sufficiently small miss distance can be reasonably assured. This function is performed during the two possible spacecraft midcourse maneuvers when the spacecraft is directed to turn to a prescribed position in space and impart a corrective impulse via the postinjection propulsion system.

Assembly of the propulsion systems for the structural test model and developmental test model spacecraft was completed and the systems were delivered for incorporation into their respective spacecraft.

Component flight-acceptance testing for the proof test model (PTM) propulsion system was completed without incident. The system has been assembled and delivered to the Spacecraft Assembly Facility for incorporation into the PTM spacecraft.

Components were qualified for two type-approval systems, designated TA-1 and TA-2. Assembly of the TA-1 system has been completed and testing will begin immediately. Assembly of the TA-2 system is following approximately one week behind the TA-1 system.

Type-approval testing of the rocket engine was completed. An attempt was made to fire the engine at 1.5 times nominal chamber pressure for 300-sec duration. A failure of the chamber wall occurred at the end of

71 sec of operating time. However, when the chamber wall thickness was changed from 0.031 to 0.045 in., the engine was successfully fired twice at 1.25 times nominal chamber pressure, each test being 200-sec duration. Two tests were then made, each of 100-sec duration, with the engine installed in an inverted position. The purpose of these tests was to demonstrate that the holdup propellant at engine shutdown will vaporize off without detonating from heat soak back from the catalyst bed. All tests were successful using the increased chamber wall thickness.

The start cartridge, similar to that being used on the *Ranger* Block III propulsion system, has been modified to provide a two-start capability. It consists of two metallic bellows welded into a single housing. Normally closed explosive valves are connected to the outlet of the bellows with a check valve between them to prevent backflow of oxidizer into the other bellows during the second engine firing. Approximately 15 cm³ of oxidizer are filled into the internal volume of each bellows. The exterior of the bellows is pressurized with gaseous nitrogen. When the explosive valve is fired, the nitrogen gas compresses the bellows and injects the oxidizer into the engine for ignition.

The pneumatic regulator is similar to that used on the *Ranger* Block III systems, the main modification being that electron beam welding of a diaphragm is employed to assure better seal characteristics.

To eliminate the fuel tank pressure rise noted during the *Mariner 2* flight, the fuel tank bladder material has been changed from Fargo Rubber Company compound FR-6-50-3 to compound FR-6-60-26. Another compound (EX-9835-75), made by Stillman Rubber Co., appears to be superior to the Fargo FR-6-60-26 compound and is being pursued on a backup basis.

Evaluation tests have demonstrated that the Hi-Shear gas generating squib is superior to the Pyronetics squib. A slight pin leakage at the one and one-third, and one and two-thirds, nominal charge can be eliminated by improvements in the quality control procedures used in brazing the pins into the squib header. On the basis of these tests the Hi-Shear squib has been selected to be used for valve actuation.

The propellant and nitrogen tanks on the propulsion system are made of 6 Al-4V titanium alloy. Two each of the tanks have been burst to prove their design adequacy. In all cases the burst pressure was slightly above the minimum design value.

IV. *Voyager* Project

The primary objective of the *Voyager* Project is the scientific exploration of Mars and Venus by means of spacecraft designed for use with *Saturn* boost vehicles. Secondary objectives are the scientific exploration of interplanetary space in the Mars-Venus region, and the determination of the feasibility of, the development of technology for, and the collection of scientific data necessary to successful manned flights to these planets.

Studies of Stage S-VI for use on a *Saturn* I-B vehicle are continuing at Marshall Space Flight Center. The tentative payload capability of such a launch vehicle is currently estimated to be in the range of 6,000 to 7,000 lb.

The JPL Advanced Planetary Spacecraft Study Committee completed the mission analyses. Results indicate

that the optimum mission for the *Voyager* class of spacecraft is probably a combination orbiter/lander. Studies were carried to the point of the generation of typical design concepts and a listing of design or feasibility problems which should be resolved before the *Voyager* is authorized as a project.

Voyager studies conducted by General Electric and Avco have been completed and final reports have been submitted to NASA. Several other companies operating on their own company support have also turned in *Voyager* reports.

The results of JPL and industry studies are now being reviewed by NASA Headquarters.

THE DEEP SPACE INSTRUMENTATION FACILITY

V. Introduction

The DSIF is a precision tracking and data acquisition network which is designed to track, command, and receive data from deep space probes. It utilizes large antennas, low-noise, phase-lock receiving systems, and high-power transmitters at stations positioned approximately 120 deg around the Earth. Its policy is to continuously conduct research and development of new components and systems and to engineer them into the DSIF so as to continually maintain a state-of-the-art capability.

The DSIF is comprised of three permanent deep space stations, one mobile station, and one launch station. The three permanent stations are located to provide continuous coverage of a deep space vehicle. Their locations are Goldstone (Pioneer and Echo), California; Woomera, Australia; and Johannesburg, South Africa. The Mobile Tracking Station (MTS) is presently located near the permanent station in South Africa and is used mainly for

early acquisition, and tracking and communications with spacecraft from injection into orbit to an altitude of about 10,000 mi. The Launch Station is used to provide real-time telemetry during the spacecraft prelaunch tests and to record spacecraft transmitted telemetry data from launch to the end of the visibility period.

The testing and development engineering of new equipment for the DSIF are performed at the Goldstone Space Communications Stations. In most cases new equipment is installed and tested at Goldstone before it is integrated into the system. An 85- and a 30-ft Az-El antenna are installed at the Goldstone Venus site for primary use in research and development.

Section VI of this Report, regarding the DSIF Program, is abstracted from SPS 37-24, Vol. III.

VI. Communications Research, Development, and Facilities

Goldstone operations. A 50-w backup transmitter, a command system, and a Beckman decommutator have been installed and tested at the Echo site in preparation for *Ranger 6*. Compatibility tests with the RCA video equipment also have been completed successfully. The hydromechanical building at the Pioneer site has been completed and all equipment has been reinstalled.

Mark I ranging subsystem. The Mark I ranging subsystem is designed for use by the DSIF with "turnaround" spacecraft transponders for ranges up to 800,000 km. Its test panel includes an internal read-out pulse generator and a variable frequency generator to simulate doppler, and "shift and decision" switches so that the ranging equipment can be tested prior to operation.

Systems engineering. Project engineering for the DSIF included tests plans and information for the *Surveyor*,

Ranger Blocks III and V, *Pioneer*, *Lunar Orbiter*, *Mariner C* (Mars mission 1964), *Mariner B* (Centaur-based entry capsule mission) and *Apollo* Projects. The problems of Sun and Moon noise temperature contributions and signal acquisition are also being studied.

Antenna engineering. Extensive tests indicate that thermal loads on a parabolic antenna materially affect the quadripod and mechanical axes pointing errors. To help prevent this, the antenna is painted with a specially developed white paint with a spectral gloss of the order of 2%. Special hoisting slings and service trailers have been developed to handle the Cassegrain cones at each station. The cones are built of 0.080-in. 7178-T6 aluminum to ensure survival in severe hailstorms, and are drilled from JPL-owned templates to assure interchangeability. The Cassegrain hyperbola is built with a new lamination process which provides a five-fold increase in tolerances

and uses a stronger aluminum alloy (6061-T6) to provide hailstone resistance. The positioning hardware has been designed to be less expensive, less complicated, and more reliable.

Ground antennas. After the new surface on the 85-ft antenna at the Goldstone Venus site had been aligned, accurate gain measurements showed a gain improvement of 0.4 db to a new value of 54.4 ± 0.15 db. Pattern measurements indicate that the quadripod shadow causes a gain loss of 0.7 db and a zenith noise temperature contribution of 5°K .

A radiometer and gas tube noise generator were used at X-band (8448 Mc) to measure the antenna noise temperature of the 30-ft antenna at the Venus site. Preliminary calculations indicate a noise temperature of $18.4 \pm 2.7^\circ\text{K}$.

The astronomical techniques which have been developed to calibrate 85-ft antennas were used to boresight the 85-ft Az-El antenna at the Venus site and its optical tracker. A continuous tracking method was used with corrective angular offsets used to determine the amount of boresight error. Boresight corrections of -0.061 deg in azimuth and $+0.021$ deg in elevation were made. A systematic elevation error read-out also was found.

The mobile antenna test instrumentation system was used to measure wind and thermal loads on the 85-ft Az-El antenna at the Venus site following the installation of the new surface. Wind velocity and direction, temperatures at 24 different locations on the antenna, and ten deformation measurements were made simultaneously and automatically recorded. The deformations were smaller than expected.

Planetary Radar Project. The recently designed water rotary joint was installed on the Az-El 85-ft antenna at the Venus site and placed in operational use. The final installation of the rotary joint is shown in Fig. 1. A few days after installation, the leaks amounted to 1 gal every 2 hr, but are now less than 1 gal/day. This indicates the seals are wearing in.

The 100-kw S-band transmitter has been completely documented and some design improvements to the crowbar circuitry have been completed. The filament of a power klystron was damaged by an arc-over and is being replaced. A silicon rectifier for the power supply unit is being investigated for possible replacement of the tube rectifiers. It will deliver 0 to 33 kv dc at 30 amp and

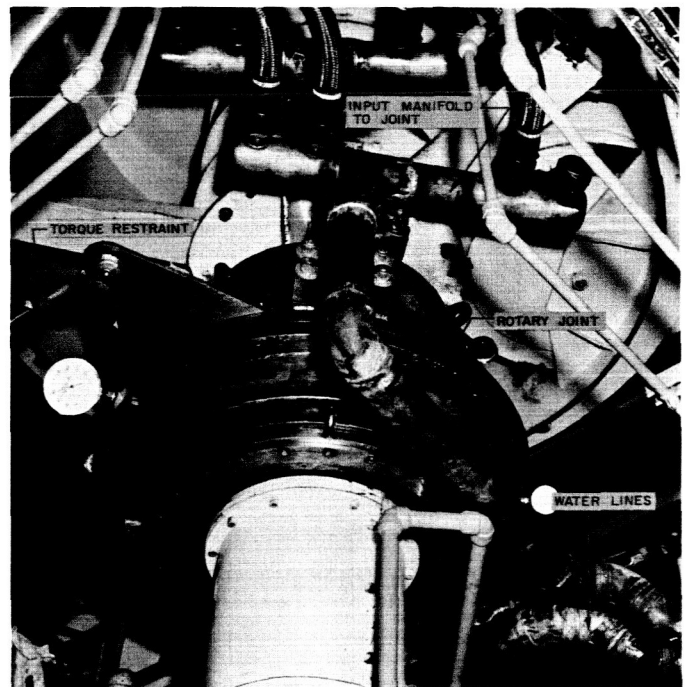


Fig. 1. Rotary joint final installation

33 to 55 kv at 1 Mw over a temperature range from -25 to $+135^\circ\text{F}$.

The Mod IV ranging equipment has a wired program special purpose computer with six available programs, five of which are selectable. These programs will:

- (1) Provide ephemeris programmed signals.
- (2) Make a closed-loop range measurement.
- (3) Make a closed-loop range measurement plus a measurement of the signal delay in the range system.
- (4) Perform a closed-loop calibration measurement.
- (5) Provide transmit-receive keying signals.
- (6) Synchronize the ephemeris tape with station time.

The ephemeris programmed signals are used for spectrum analysis, radiometer analysis, and multiple range-gate analysis of radar echoes. The transmit-receive keying signals control the alternate connection of transmitter and receiver to a single antenna.

Using the same techniques used on Venus in 1962, radar measurements were made on Mercury in May 1963. These measurements were:

- (1) Total echo power.

- (2) Analysis of the radar echo into frequency components.
- (3) Analysis of range-gated radar echo into frequency components.

The radar cross-section of Mercury was found to be 5% of its geometric cross-section compared to 10% for Venus and 3% for Mars. The measurement of the speed of rotation of Mercury agreed with its known period, and thus corroborates the measurements made on Venus. It was found that residuals in the doppler and range measurements could be essentially eliminated by correcting the argument of the ephemeris by 6 sec and the astronomical unit (AU) by 10^5 m. This data provides striking confirmation of the accuracy of the radar measurements of Venus made in 1961 and 1962.

Lunar Radar Project. Additional tests on klystron noise power, for 100 kw at 2388 Mc, show that when the tube is tuned broad-band, the noise power per cycle decreases as the bandwidth increases, while for either high efficiency or synchronous tuning, there is little change in the noise power per cycle as the bandwidth is increased.

Because of the short round-trip time for a radar echo to the Moon it has been decided to use the 85-ft reflector for transmitting and a 6-ft diameter dish, with a shielding tunnel 20 in. deep mounted to its periphery, for receiving. The 6-ft antenna will be mounted at the apex of the 85-ft quadripod. System noise temperatures as a function of klystron beam voltage and antenna elevation were measured. A figure of merit was defined as the ratio of the transmitted power to the system noise temperature measured with the same klystron beam voltage but with no excitation. The figure of merit is presented as a function of transmitted power. Noise stability measurements indicate it may be desirable to sacrifice a db or so of figure of merit to improve the accuracy of the power measurements.

Ranging and tracking system development. To establish operating parameters for a satellite radar at S-band, a preliminary analysis of expected worst case target dynamics has been made. Using a worst case doppler requirement of ± 120 kc, it was found that an additional $\times 20$ in dc loop gain is required to meet the VCO constant of 4330 cps/v. A feedback limited amplifier with sufficient short- and long-term stability has been found to be satisfactory to furnish this gain. For unaided tracking of a satellite at 250-mi altitude, the maximum doppler rate requires a loop bandwidth $2\beta_{L_0} = 100$ cps. Since this is 13 db worse than the goal of 5 cps, either a programmed

change in frequency or a variable bandwidth will be required. These constraints require operation, at least temporarily, between 20- and 63-cps bandwidths and have the effect of increasing the keying rates in order to reduce the effects of poor phase integrity and degradation of performance of the anti/sideband system. Typically this would be 300 to 900 cps for satellites.

The monostatic keyed radar is intended to provide a model for a DSIF S-band tracking system for use during initial passes of a spacecraft. The system design has been influenced by the problems which have been encountered and, in its present state, it consists of a ranging system only. Ultimately the capability will be extended to include the tracking of doppler and angles. Using a rubidium vapor standard frequency oscillator and counting RF as well as clock frequencies, a range resolution of 1.25 m is obtained. The ranging code has the interesting property of possessing a two-level autocorrelation function whose value at any displacement is equal to the ratio of the number of agreements minus the number of disagreements to the number of agreements plus the number of disagreements. The transmitter has a second phase modulator for the range-gating subsystem. An additional 3-db improvement in signal-to-noise ratio is obtained by keying the receiver in opposition to the transmitter. An anti-sideband lock system is used. Digital control equipment generates the ranging code and provides a stored program computer to automatically acquire and make range measurements. Fig. 2 illustrates the basic principle of operation.

A digital system for performing RF acquisition, including anti-sideband lock, has been tested and proved to be successful. It was also made capable of controlling the transmitter to achieve acquisition of the ground-to-spacecraft link. With the addition of a small amount of RF and signal conditioning equipment, the digital computer which controls the pointing of the antenna can be used.

S-band implementation for the DSIF. Traveling wave masers with closed cycle helium refrigerators are planned for operational use at DSIF Stations. The prototype unit, complete with performance measuring equipment, operated successfully at the Venus site for 600 hr before condensation of impurities in the gas supply line forced a shutdown for repairs. This unit has a net gain of 40 db, a bandwidth of 12 Mc, and a noise temperature of 9°K .

The design of the S-band acquisition aid system has been completed. It consists primarily of the basic 85-ft antenna feed horn and a separate receiver system. The

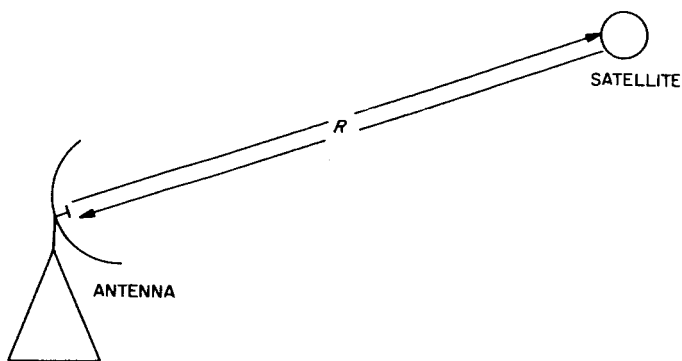


Fig. 2. Method of operation

use of a separate receiver system allows smooth transition from acquisition aid antenna to the 85-ft antenna. The acquisition aid receiver is also used to control the automatic gain control of the 85-ft antenna receiver system until successful switchover is achieved. This prevents acquisition on a side lobe of the large antenna.

Telemetry system development. A large number of trial runs was made on a biorthogonal telemetry system which was described in SPS 37-18. Using a 4-kc square wave biphasic modulated subcarrier and sampling it at a rate of 8000 samples per second, the bit error rate was measured with various signal-to-noise ratios. The results were within 0.3 db of theoretical even when the noise power was 15 times greater than the signal.

It has been found desirable to design a set of logic modules which can be used in the development of all types of JPL digital systems. As the result of a comprehensive study, including market survey, it was decided

to standardize on a printed circuit card 4.75 by 3.18 in. with each card holding four separate identical circuits and with cards that use pin connectors for wiring. There are four basic logic circuits, which use highly reliable parts such as epitaxial silicon semiconductors. They are connected together using synchronous logic. The basic concept and design are now undergoing tests following the receipt of sample products from two separate manufacturers.

RF signal generation and control. Both the receiver and transmitter systems usually require frequency control over the local oscillator in small steps over a large range. To replace the free running voltage controlled oscillators which are normally used, it has been proposed that a pseudonoise generator be used with a frequency synthesizer and a phase-lock loop circuit to generate a very stable variable frequency. An experimental test showed virtually no degradation in phase noise.

Mesa Antenna Range. In order to improve the capability of the Mesa Antenna Range, two RF anechoic rooms will be built and a $\frac{3}{4}$ -mi range will be added. The building housing the two anechoic chambers is under design and the new range is about 60% complete.

Advanced Antenna System. A master summary schedule for the installation of the 210-ft antenna at Goldstone has been approved and work is generally proceeding on schedule. Site clearing and antenna foundation construction has begun, and the access road is virtually complete. A 200-ton, 180-ft tall, grey derrick mounted on a 135-ft tower has been procured for use in installation work. Design and analysis work is continuing on various component parts of the antenna structure.

OPERATIONAL AND TEST FACILITIES

VII. Test and Support Equipment

A. Environmental Test Laboratory

1. 25-ft Space Simulator Modifications

A new virtual source for producing a 6-ft (across the flats) hexagonal light beam was fabricated and installed. The maximum intensity in the 6-ft beam during the initial test was 120 w/ft². The intensity variation in a horizontal plane was $\pm 3\%$ while the axial intensity gradient was negligible. Several steps are planned for increasing the intensity in the 6-ft beam to 130 w/ft² for extended test periods. An 8-ft (across the corners) hexagonal beam is available for an intensity variation of $\pm 10\%$ (due to fall-off at the edge of the light beam).

2. Contamination Investigation

A test was conducted to develop an operating procedure which would minimize spacecraft contamination caused by the simulator. The "dirt" which the simulator deposits on a test vehicle, independent of the vehicle's contribution, comes from the simulator wall and consists mainly of material which has outgassed from previous test vehicles. A clean stainless steel plate was placed in the simulator, and several modes of simulator operation

were executed for different model or plate temperatures. Following each mode of operation, the "dirt" deposited on the plate was qualitatively analyzed in order to determine the best operating procedure.

The procedure which adds the least amount of "simulator" contamination to a test vehicle consists of these steps:

- (1) Prior to installation of the test vehicle and after removal of the obvious "dirt," the simulator should be evacuated to less than 10^{-5} torr for 12 hr with a wall temperature of 100°F (maximum practical).
- (2) During a test the vehicle temperature should be kept above the wall temperature whenever possible. This procedure, presently in force, may be supplemented by chemically cleaning the simulator wall prior to installation of the test vehicle.

Test vehicle contaminants resulting from the use of outgassing material in support equipment (e.g., cables and tape) will be reduced as better material becomes available and through improvements in the design of such equipment.

3. Vacuum-Temperature Testing

Vacuum-temperature testing of spacecraft assemblies requires some means of insuring a known, uniform temperature on the assembly surfaces. Fluid-type heat exchangers have been developed for testing *Ranger* Block III assemblies that mount in cases on the spacecraft bus; two of these are shown in Figs. 1 and 2. Hot and cold gaseous nitrogen may be alternately circulated through copper tubing, attached to the bottom plate and top frame, to attain temperature control at desired levels.

The heat exchanger test assemblies are compatible with the 18-in. bell jars that have been used for vacuum-temperature testing.

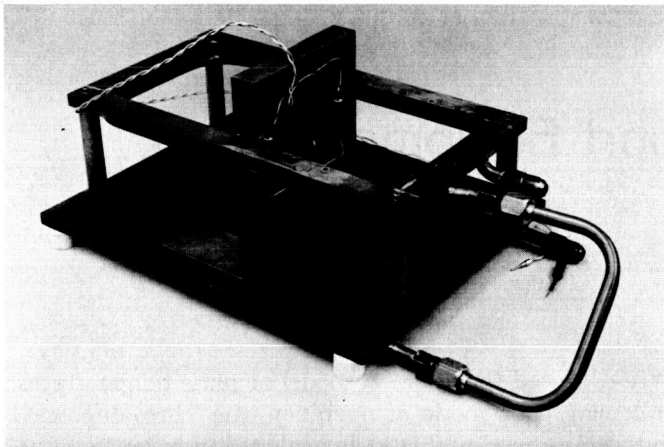


Fig. 1. Heat exchanger for the squib firing box assembly

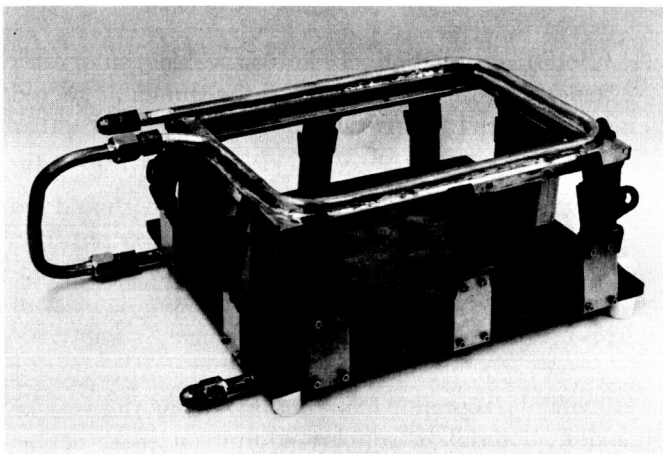


Fig. 2. Module heat exchanger with mockup specimen installed

4. Acoustic Testing

A series of high-intensity acoustic tests was performed on the *Ranger* structural test model (STM), shroud, and forward equipment rack (Fig. 3). The acoustic energy was supplied by two of the Ling electropneumatic transducers purchased for the acoustic test facility. A special horn was designed to deliver acoustic energy to the shroud, with the enclosed spacecraft, and the forward equipment rack. The intensity variation of the incident energy was within ± 3 db (measured in a plane tangent to the shroud and normal to the direction of flow of sound energy). A mobile air compressor supplied the required airflow to the transducers at a pressure of 40 psi. With the horn-spacecraft test setup shown in Fig. 3, three tests were made utilizing: (1) normal hard-mounting between all units (spacecraft, adapter, shroud, and forward equipment rack), (2) soft-mounting between the adapter and the forward equipment rack, and (3) soft-mounting between the shroud and the adapter.

During all phases of these tests, a broad-band spectrum of random noise was applied to the test specimen. Twenty-three microphones, located inside the shroud around the spacecraft and around the outside of the shroud, were used to determine the sound field, measur-

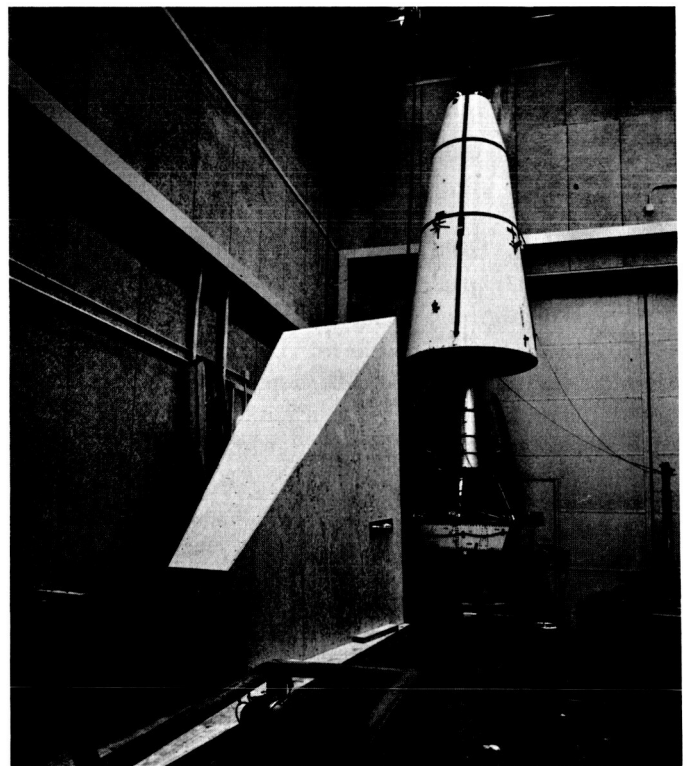


Fig. 3. Acoustic test on *Ranger* STM

ing both over-all sound pressure level and spectral distribution.

Accelerometers were also placed on the spacecraft, shroud, and forward equipment rack. A reference microphone was located on the outside of the shroud, about 3 in. from its surface, and directly in line with the center of the incident sound field. During all three phases of these tests, this microphone indicated a sound pressure level of 141 db (ref 0.0002 μ bar)

B. Operational Support Equipment

1. Central Computer and Sequencer Operational Support Equipment

The following is a description of the central computer and sequencer (CC&S) operational support equipment (OSE) developed for use in the *Ranger* Block III spacecraft test program. The equipment is basically the same as that used for Block II; however, modifications have been made to satisfy altered functional requirements and to include product improvement changes. These modifications are described in the functional description of each OSE panel.

The CC&S OSE consists of three basic categories of equipment:

Blockhouse (launch test set). The blockhouse panel, operating in conjunction with the blockhouse power supply, contains the controls and circuitry required to perform all CC&S launch countdown operations. The following functions are always performed from ground support equipment (GSE) power prior to applying spacecraft power in order to insure that no false commands are generated upon power application:

- (1) Electrically hold all CC&S relays in the reset or safe state.
- (2) Reset the CC&S counter back to its zero state.

- (3) Inhibit the CC&S counter operation.

- (4) Provide a composite indication showing that all CC&S relays and flip-flops are in the proper pre-launch state.

After application of spacecraft power, the blockhouse GSE must, in addition to the functions above, supply a go, no-go indication that the first stages of the CC&S counter are functioning properly by sensing a CC&S relay closure during prescribed time limits.

Systems test set. In addition to the blockhouse functions described above, the systems test set has the capability to exercise the CC&S through its entire flight program, either automatically or manually, and record its performance in either mode of operation.

Automatic subsystem checkout. An automatic checkout system has been developed to obviate the difficulties of testing the CC&S manually and to provide the required permanent record of test results. This equipment generates a printed paper record of the state of all event commands and the times of their occurrence. The contacts and electronic switches representing CC&S outputs to other systems in the spacecraft are energized and monitored by the checkout equipment. A printout cycle is initiated by any relay or electronic switch change-of-state, resulting in a readout whenever a command is set or reset. The automatic checkout equipment is presently used primarily in the laboratory and for initial checkout of the CC&S in the spacecraft assembly area. In case of suspected trouble, the automatic checkout equipment is connected and a complete CC&S test cycle is made. The resulting printed tape is then compared to a standard tape to pinpoint problem areas.

Fig. 4 shows a complete set of equipment as used in the laboratory or in the spacecraft assembly area. This set contains all equipment described above, and, with proper cabling, will operate and check the CC&S in any of the test areas.

2. Scientific Instruments Subsystem Test Complex

A test complex (Fig. 5) has been assembled for operational verification of the *Mariner C* (Mars mission, 1964) scientific instrument subsystem prior to delivery of the subsystem to the Spacecraft Assembly Facility (SAF). This complex utilizes the same type of equipment that will be used in the *Mariner C* systems test complex in the SAF and at the Atlantic Missile Range.

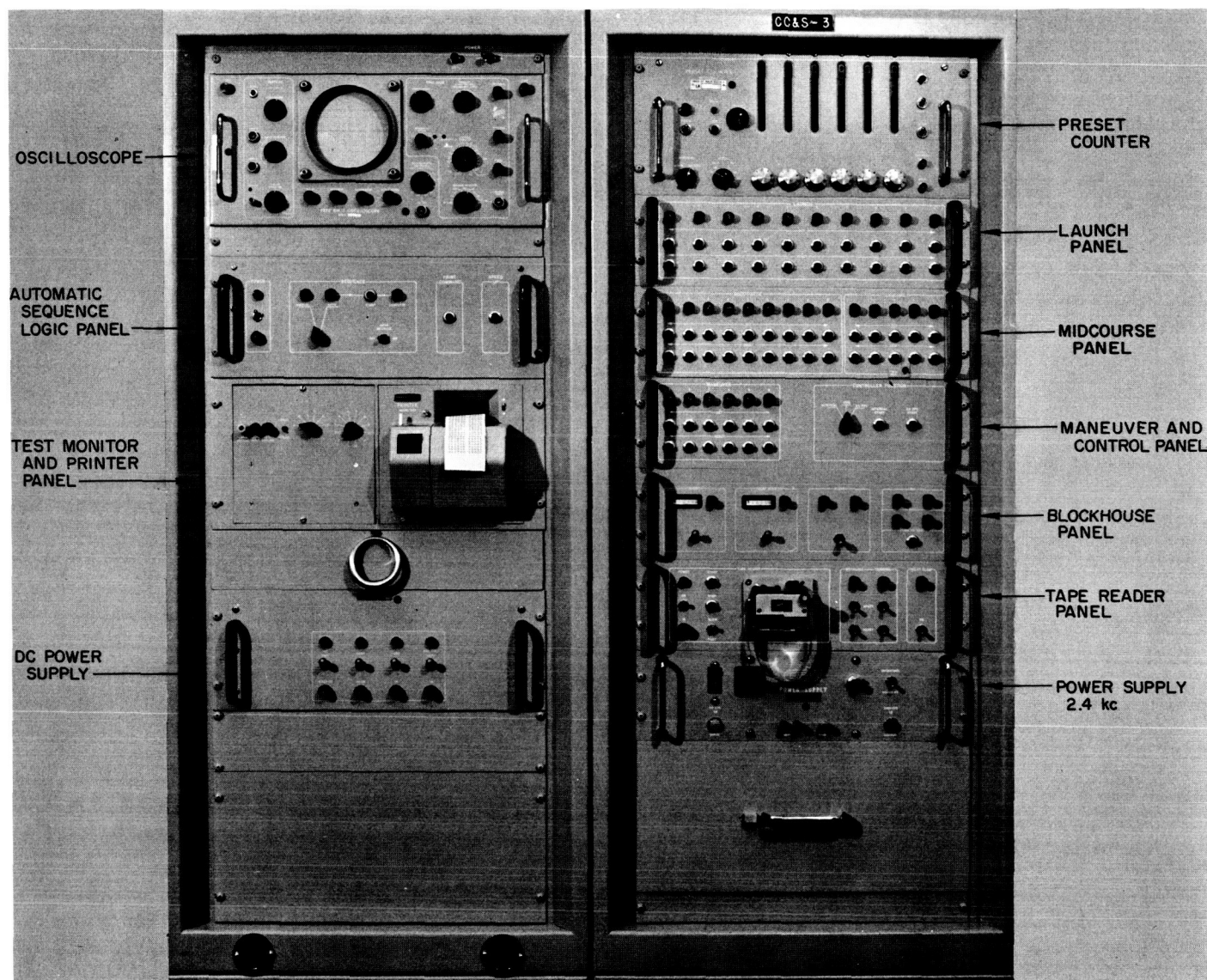


Fig. 4. CC&S operational support equipment

During assembly operations the instruments and the operational support equipment (OSE, Fig. 6) are mated into a science flight configuration, and the instrument interfaces are verified for compatibility with the cabling and the OSE. The system test complex cables and a mockup (Fig. 7) of the spacecraft are provided for the test.

The assembly and testing of the subsystem is accomplished instrument by instrument. Each instrument is mounted on the spacecraft and verified for correct operation with the OSE. After all the instruments are tested, a complete subsystem test is performed using the subsystem test procedures. Both the subsystem test procedure

and instrument performance are verified by this test. In the testing of the spacecraft, the subsystem test procedure is used to provide the basis for the system test procedure to be used at SAF and AMR. During the tests in the subsystem test complex, each instrument cognizant engineer verifies the correctness of the test procedure and the data that is obtained from his instrument through the OSE.

Upon completion of the subsystem test, special tests and calibrations are conducted. Interface tests with other subsystems, such as the data encoder and power subsystem, are also performed. Due to the large number of

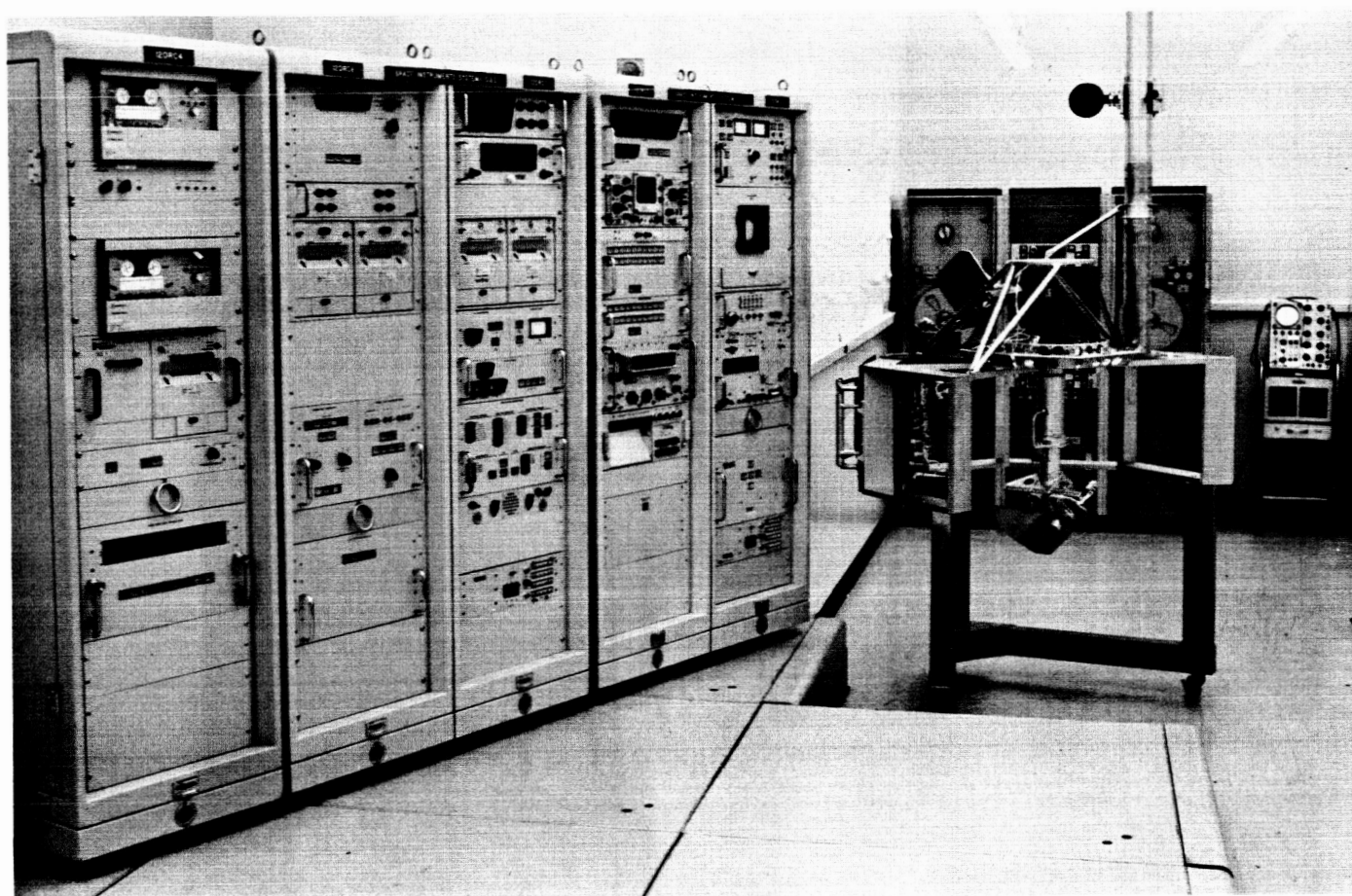


Fig. 5. *Mariner C* scientific instrument subsystem test complex

instruments which comprise the science subsystem, it is mandatory that the instruments be tested with the data automation system (DAS) and the OSE prior to delivery to SAF. By satisfactorily accomplishing this pre-SAF testing, interactions within the science subsystem are detected and eliminated and with a certain degree of confidence the testing at SAF can be limited to an investigation of the interaction of the scientific subsystem with the other spacecraft subsystems.

Considerable progress has been made to date in the testing of the *Mariner C* scientific instruments. A number of problems have been uncovered and eliminated. This method of verifying the science subsystem, OSE, and test procedures greatly reduces the number of science subsystem problems occurring on the spacecraft. Furthermore, it facilitates the early investigation of incompatibilities and malfunctions.

Fabrication and initial checkout of OSE No. 1 is complete. Checkout of the complex is underway; the

ionization chamber and trapped radiation detector have been satisfactorily mated with the OSE and mockup, initially checked out, and are ready for the over-all subsystem test. The TV is partially checked out and is undergoing further tests before being mated to the DAS.

3. TV Operational Support Equipment

Operational support equipment (OSE) has been developed to monitor the performance of the *Mariner C* spacecraft television system. Although the signal from the spacecraft communications systems is digital, the OSE monitoring equipment is required to compare the analog video with the digital video signal to insure that reliable conversion is being accomplished. The OSE is also required to strip the TV data from the data automation system format.

a. TV OSE monitoring system. The following equipment is being used in the testing of the *Mariner C* television system:

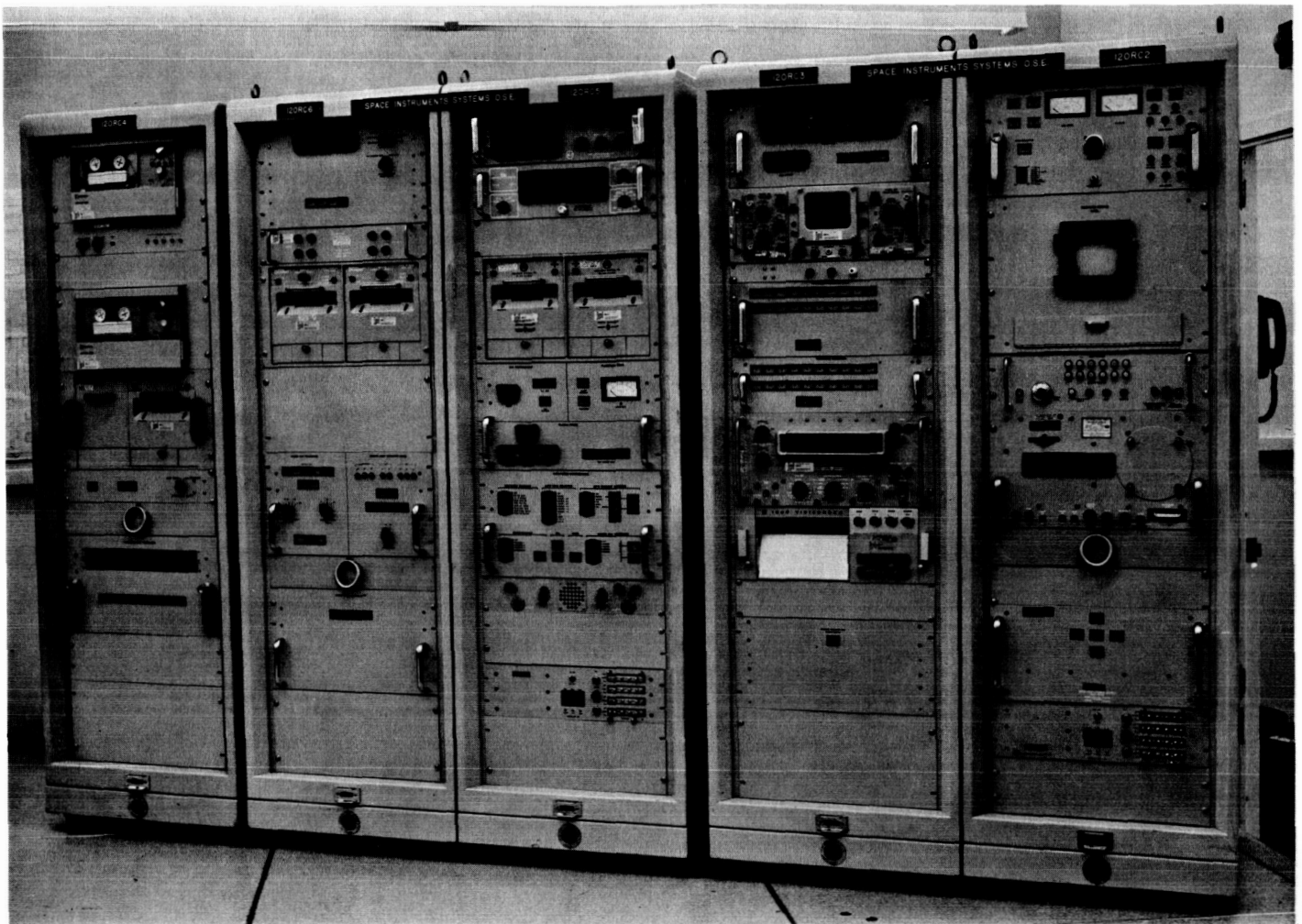


Fig. 6. Mariner C scientific instruments operational support equipment

- (1) TV control panel, which consists of:
 - (a) Switching functions.
 - (b) Video simulate.
 - (c) Data stripper.
 - (d) Video reconstruct.
 - (e) Collimator control.
- (2) Conrac slow-scan TV monitor and polaroid camera.
- (3) Adcom—digital-to-analog converter.
- (4) Kinescope 35-mm recorder.

Fig. 8 shows the monitoring equipment mounted in the OSE console.

b. TV control panel. The TV control panel is shown in Fig. 9. A description of the switch functions and operation is listed below.

Video simulate switch. The video simulate switch disconnects all video input signals and provides internal calibration video signals to the monitoring system.

Analog video spacecraft switch. The analog video spacecraft switch disconnects all video input signals and provides spacecraft camera analog video directly to the monitoring system.

Digital video spacecraft switch. The digital video spacecraft switch provides spacecraft camera digital video to the Adcom unit for conversion to analog video and then applies the analog video signal to the monitoring system. All other video inputs are disconnected during this mode.

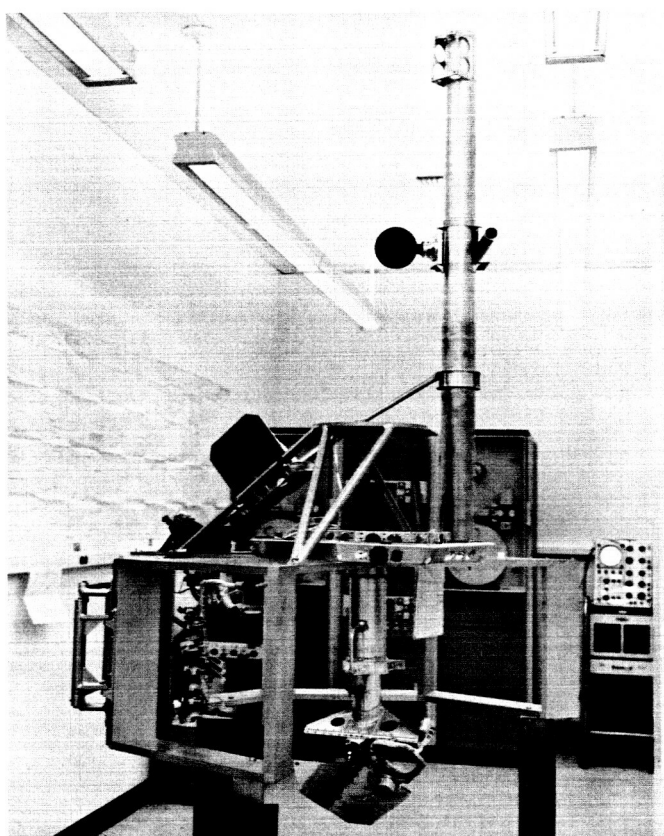


Fig. 7. Mariner C scientific instruments mockup

Systems/subsystems switch. When this switch is in the systems position, the video data presented to the monitoring system is from the DAS through the TV control panel data stripper. When this switch is in the subsystems position, the video data presented to the monitors is hard line from the spacecraft camera and the buffer outputs are disconnected from the circuit.

Split screen switch. The split screen switch activates a circuit comprised of a delay multivibrator, a flip-flop, and a transistor switch. The input to one side of the transistor switch is analog video direct from the camera.

The second switch input is the converted digital-to-analog output from the Adcom unit. The switch timing is such that after line start direct analog video is displayed for a horizontal sweep time of 7 msec, or approximately half of the monitor-viewing screen area. The next 7 msec of the sweep display is converted digital data.

Video level pot. By connecting an oscilloscope to the external video coax connector, the video level input to the monitor may be adjusted with the video level pot.

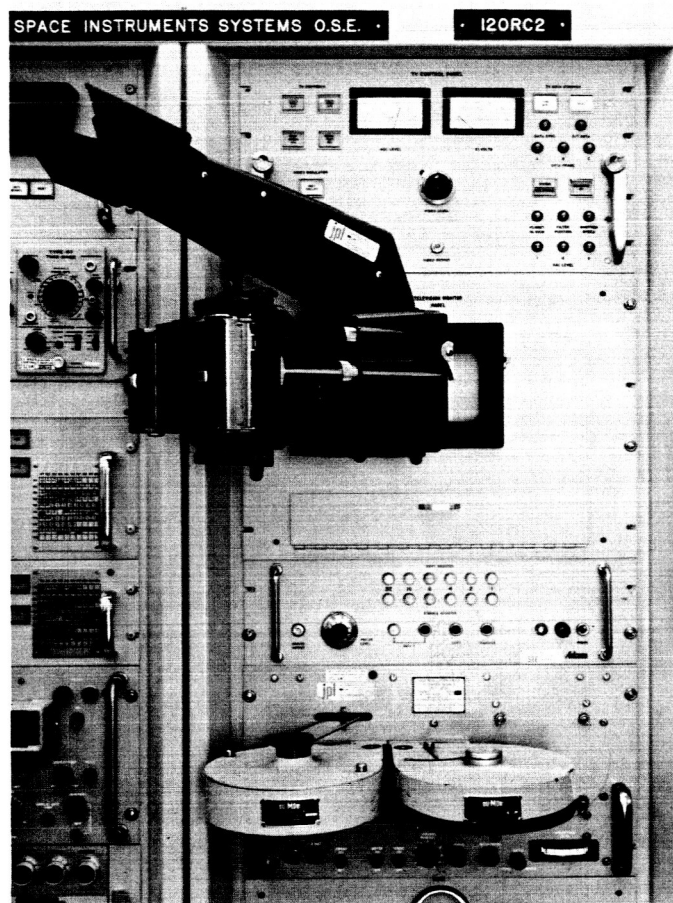


Fig. 8. Mariner C TV operational support equipment

Planet-in-view light. Whenever the TV camera is energized with light or by the collimator, a 12-kc signal is generated and this signal turns on the planet-in-view indicator at the OSE.

Automatic aperture control logic lights. The automatic aperture control (AAC) circuit in the TV camera controls the camera aperture electronically. Depending on the amount of light entering the vidicon, various combinations of AAC lights will be turned on.

Signal level and G1 meters. The automatic gain control signal level meter displays the dc voltage which indicates the peak-to-peak output video voltage and provides the vidicon gain. The G1 voltage meter displays the dc voltage applied to the vidicon control grid.

Video reconstruct. Since the digital data input is comprised of two separate lines, one line carrying 0's and the other 1's, a circuit termed video reconstruct, consisting of a gate, a flip-flop, and a power amplifier, is used

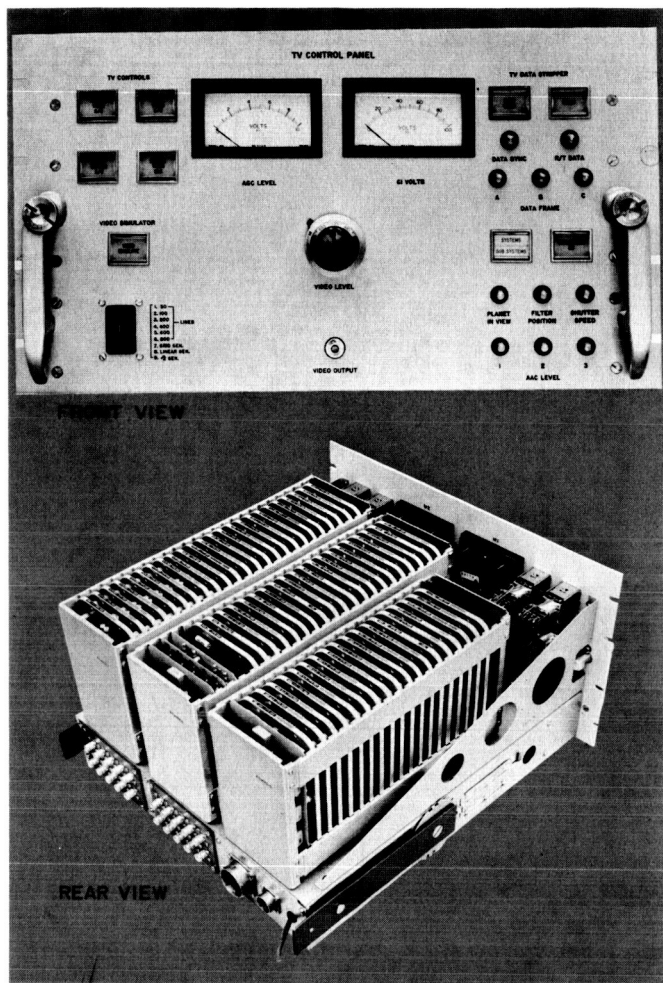


Fig. 9. TV control panel

to combine the 1's and 0's into a single line leading to the TV monitor.

Video simulate. The video simulate circuit is comprised of a vertical line generator, a grid generator, and a shades-of-grey generator. These internally generated video calibrate signals provide the means for adjusting and evaluating the Conrac and Kinescope monitors. Basically, the circuit consists of an 80-kc oscillator working into a countdown chain of flip-flops. Timing pulses are derived from an additional counting chain and gates. The output is a pulse of 0 to -2 v. When viewed on a TV monitor, the 0 level is white video and the -2 -v level is black. The position of the thumb switch selector determines the frequency, or that portion of the countdown chain circuit to be applied to the monitor input to produce the desired number of vertical black bars from 50 to, and including, 800. Additional timing and blanking pulses are applied to produce the shades-of-grey and grid pattern.

Data stripper. The data stripper contains an input register sync detector, bit counters, and appropriate timing gates.

In the reset condition, all the data flows through the input register. When the pseudonoise (PN) sequence is present in the register the sync detector enables a 30-bit counter. At the end of 30 bits a flip-flop is commutated, which causes the input register to stop shifting data, allows data and bit sync to be directed to the video monitoring equipment, activates a one-shot which is used as a TV line start, and activates a 1200-bit counter.

During the period between flip-flop commutation and the end of a TV line, data is stripped out of the 30 bits which remained in the input register. This data contains TV analog data, TV line number, DAS real-time data, and DAS frame identification (A, B, or C).

At the end of 1200 bits, a one-shot is activated which causes all counters, flip-flops, and register to return to a reset condition.

c. Conrac slow-scan video monitor. The Conrac CSS-5 is a direct-view slow-scan video monitor. A 4-in.² raster is displayed on a 14-in. picture tube with a long persistence phosphor (P7) and optical filter. It operates from a dc-restored video signal and separate vertical and horizontal drive pulse-signals. The monitor is transistorized except for the high voltage and regulator tubes. In addition to the usual TV monitor controls, a switch is provided on the front panel enabling the selection of a horizontal sweep time of 14.4 or 105.6 msec. A Tektronic C2 oscilloscope camera is adapted to the front panel to provide permanent records of the video display.

d. Adcom digital-to-analog converter. The Adcom converter is a commercial high-speed digital-to-analog converter capable of accepting a serial 6-bit input and providing a 0 to -5 v output. The full-scale output is variable from the front panel over the range of 0 to -5 v. The necessary time delays and sequencing are supplied by an internal timing card which is controlled by internal pulses. Manual input functions are provided for internal checkout and front panel lamps provide a visual check of some of the digital functions. The unit requires three input signals for proper operation. The signals are data, bit sync, and word sync.

e. Kinescope recorder. The Fairchild video recorder, with a resolution of from 800 to 1000 TV lines, records slow-scan video information on 35-mm film. Plug-in scan

rate generators and a variable-speed recording camera combine to provide an extremely versatile device. The camera is equipped with 400-ft quick-detachable film magazines, a controlled selective speed film drive mechanism with an electrical brake, and a timing marker.

f. General. The system which has been described has been thoroughly tested and provides excellent monitoring of the *Mariner C* television data. The internal pattern generation provides a very simple method for establishing the control settings for the monitors prior to the initiation of any test. It is anticipated that this type of system will be usable for not only the *Mariner C* system but also for other systems on future projects.

4. High-Speed Printer and Ground Tape Recorder Evaluation

A General Dynamics 3070 high-speed printer and tape recorder have been tested in a system closely simulating actual spacecraft operating conditions. Both the printer and tape recorder operated as per manufacturers specifications; however, extensive testing has shown that an improvement in these specifications would be desirable for increased reliability.

a. Objective. As spacecraft checkout becomes more sophisticated more output data is produced at higher readout rates and it becomes evident that readout devices with more capability than those now in use must be made available. The objectives of the tests performed were to determine if the 3070 printer and tape recorder would meet the projected as well as the present needs of spacecraft checkout equipment and also to become more aware of the limitations of the equipment.

b. Equipment description.

General Dynamics 3070 printer (Fig. 10). The S-C 3070 is an asynchronous printer capable of printing at a rate up to 300 characters/sec. The S-C 3070 combines a *charactron*-shaped beam tube with an electrostatic paper to provide rapid output of hard copy. Character generation (Fig. 11) is accomplished by logic circuits that convert the six-line teletype (TTY) code into weighted digital voltages. The circuits apply these voltages to the *charactron*-shaped beam tube in such a manner that the symbols corresponding to the particular input codes are selected, deflected, and brightly displayed at the proper positions on the face of the tube. The images of the displayed symbols are optically projected onto a charged

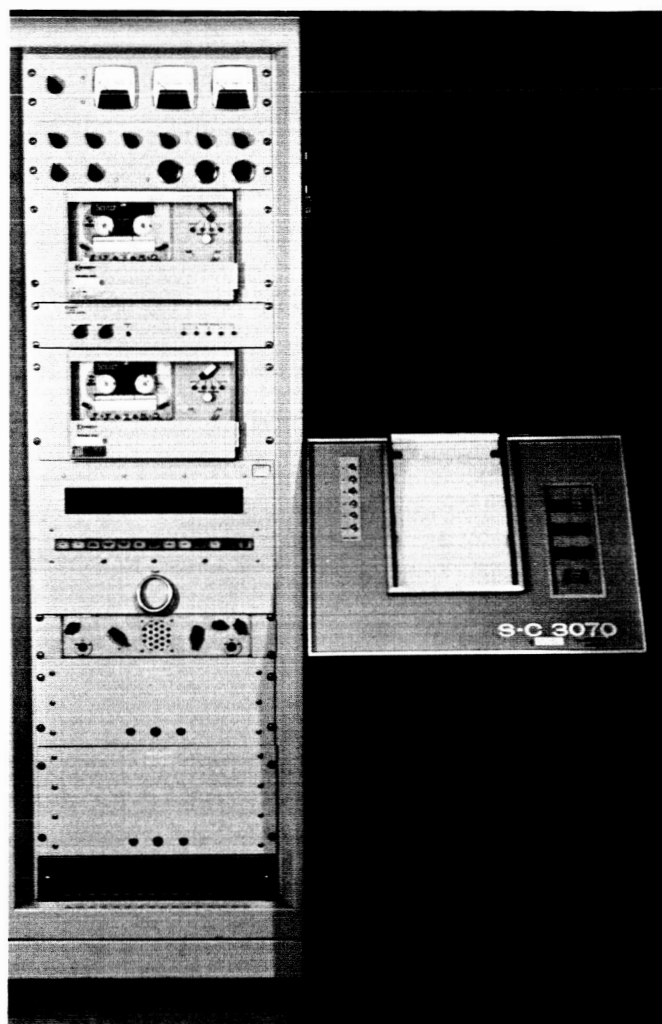


Fig. 10. General Dynamics 3070 printer

sensitized paper. Photon bombardment discharges the paper in the exposed areas, forming latent electrostatic images. Development of these electrostatic images is accomplished by brushing the exposed surface of the paper with a toner consisting of small black particles of thermo-setting plastic. These particles adhere to the latent electrostatic images and thereby develop legible printed copy. The developed paper is then subjected to sufficient heat to fuse the toner particles to the paper, which results in permanent copy that can be handled without smudging and subsequent loss of information.

Kennedy tape recorder (Fig. 12). The input requirements for this unit are the same as those for the S-C 3070 printer. The TTY input information (Fig. 13) is parallel-dumped into the input shift register and then serially stored on magnetic tape as either a "1" or "0" at a max-

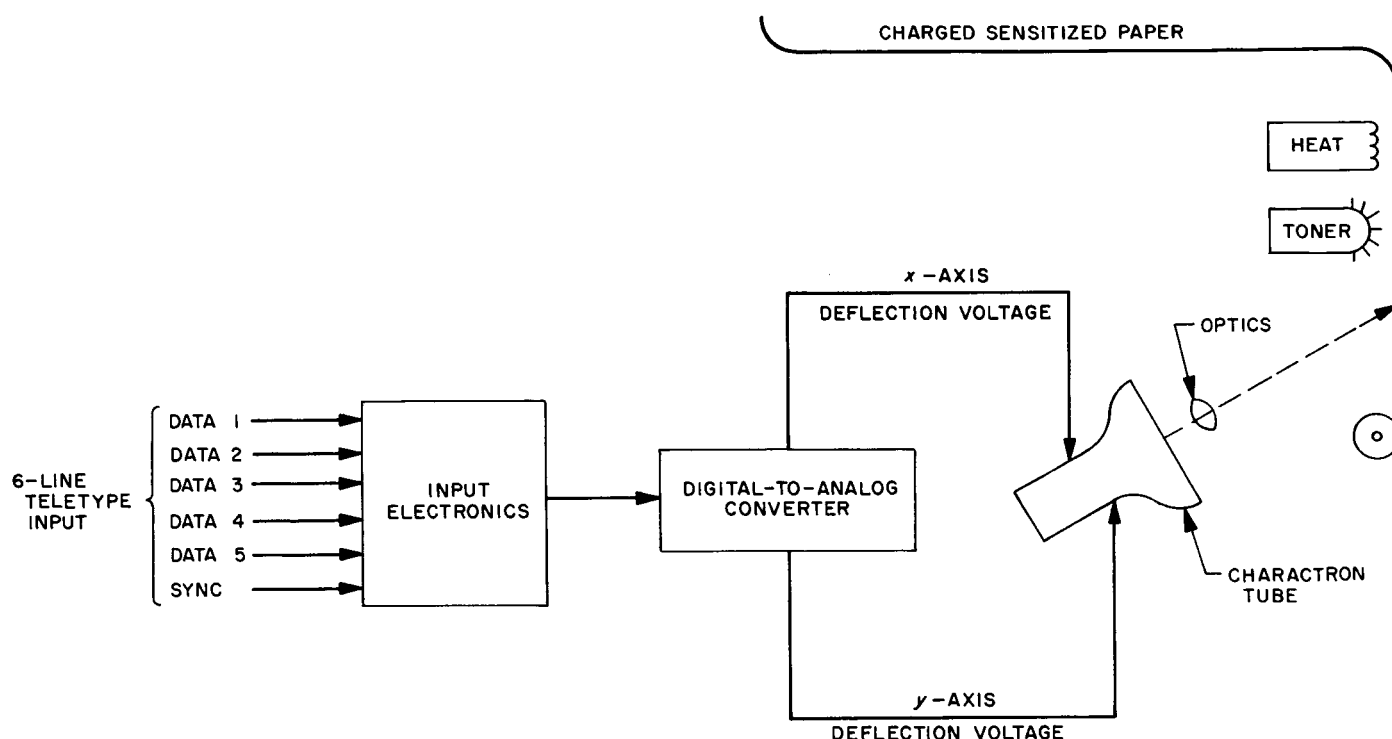


Fig. 11. S-C 3070 printer block diagram

imum bit rate of 50 characters/sec. The magnetic tape is contained in a quick-load plastic cartridge holding 600 ft of 1.0-mil tape and is capable of storing approximately two million bits of information.

Kennedy TTY adapter Model TA-21 (Fig. 12). This adapter was designed to operate with the Kennedy tape recorder and is used to read out the information contained on the magnetic tape (Fig. 13). The magnetic tape data is parallel-transferred from the tape recorder input shift register to the adapter output shift register and also to the output connector for Flexowriter operation. Information in the output shift register is shifted serially at 45 bits/sec, and actuates an output relay for direct teletype transmission.

Ranger follow-on operational support equipment (Fig. 14). An operational *Ranger* scientific follow-on operational support equipment and spacecraft mockup, which included all of the proposed scientific experiments and data automation system, was used for a system simulation. This system was used to provide known and controlled outputs to the printer and tape recorder. A more complete description of this system can be found in JPL TM 33-127.

c. Test conditions. A minimum amount of test equipment was used to reduce the possibilities of external interference and, therefore, establish the most ideal testing conditions practical (Fig. 15). The TTY outputs from the science data translator (SDT) were connected to the inputs of the unit being tested and to a Tally tape perforator. The perforator tape was printed out by a Flexowriter when the input data to the unit being tested required verification. A H-P 562 digital recorder was also used to monitor the output of the SDT as a further check of the data presented to the unit being tested. Several types of data were supplied to the recording equipment. The data inputs that were used are:

- (1) Subsystem test data from the *Ranger* follow-on scientific instruments.
- (2) A sync word which was circulated in the SDT at 25 bits/sec.
- (3) A sync word which was circulated in the SDT and increased in 25-bit/sec increments from 25 to 150 bits/sec.

The Tally tape punch and H-P 562 printer were removed from the system at 50 bits/sec and the tape recorder was removed at 70 bits/sec.

Readout of the tape recorder was accomplished by connecting the tape recorder output to the TTY adapter, which operated the Flexowriter to display the recorded data. This same tape recorder information was also supplied to the communication system link to Goldstone from the serial TTY output from the adapter. Information was transmitted to Goldstone and looped back to the JPL communication center where it was printed on a teletype recorder for comparison with the original information.

d. Test results.

Printer checkout results.

- (1) Accuracy in recording presented data was excellent. No discrepancies were found when a comparison was made of the printer recording with the information received from the H-P 562 and the Tally which was read out through a Flexowriter.
- (2) Noise transients under all operating conditions created no problem. It was found that a minimum of 4 v was required to trigger the printer electronics.
- (3) Recording readability was good above 100 bits/sec but at the slower rates the printed copy began to fade after prolonged use. This problem was partially corrected by aperture adjustment and controlling toner feed.
- (4) Printer cleanliness was poor. This situation was improved by reducing the toner feed.

Tape recorder results.

- (1) In general the recording accuracy was good with the one-bit dropout/1000 bits attributed to tape head misalignment and/or false triggering. Above 60 bits/sec (10 bits/sec greater than manufacturer's specifications) the information recorded on tape became unintelligible.
- (2) Noise transients less than 1 μ sec affected the recorder. This problem was corrected by a slight integration of the input signal.
- (3) The TTY adapter Flexowriter outputs functioned properly but the teletype transmission output relay required an inductance-resistance-capacitance (LRC) network across its contacts for arc suppression before proper operation was realized.
- (4) Minor kinks in the 1-mil magnetic tape caused the tape recorder to stop operating. No problem was encountered with the use of the 1½-mil magnetic tape.

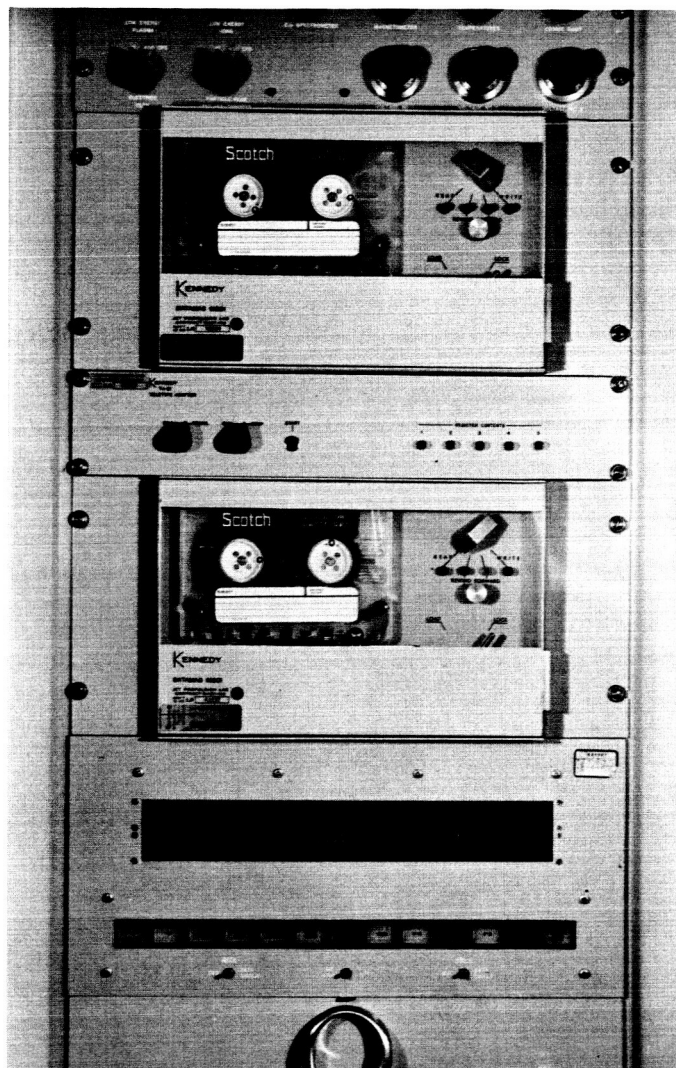


Fig. 12. Kennedy tape recorder and teletype adapter unit

The S-C 3070 printer and tape recorder functioned together with no apparent interactions or other problems except those noted for the individual units.

e. Summary. The printer operated per manufacturer's specifications for the most part; however, the printer used for these tests requires some adjustment to produce a consistent legible copy. A modification in the toner system is necessary to improve the cleanliness of the printer. The S-C 3070 printer offers many advantages over mechanical printers; however, the unit would benefit by an increase in the printout rate and a change from a fixed to an adjustable internal self-check bit rate. A reduction in the physical size of the printer is also extremely desirable.

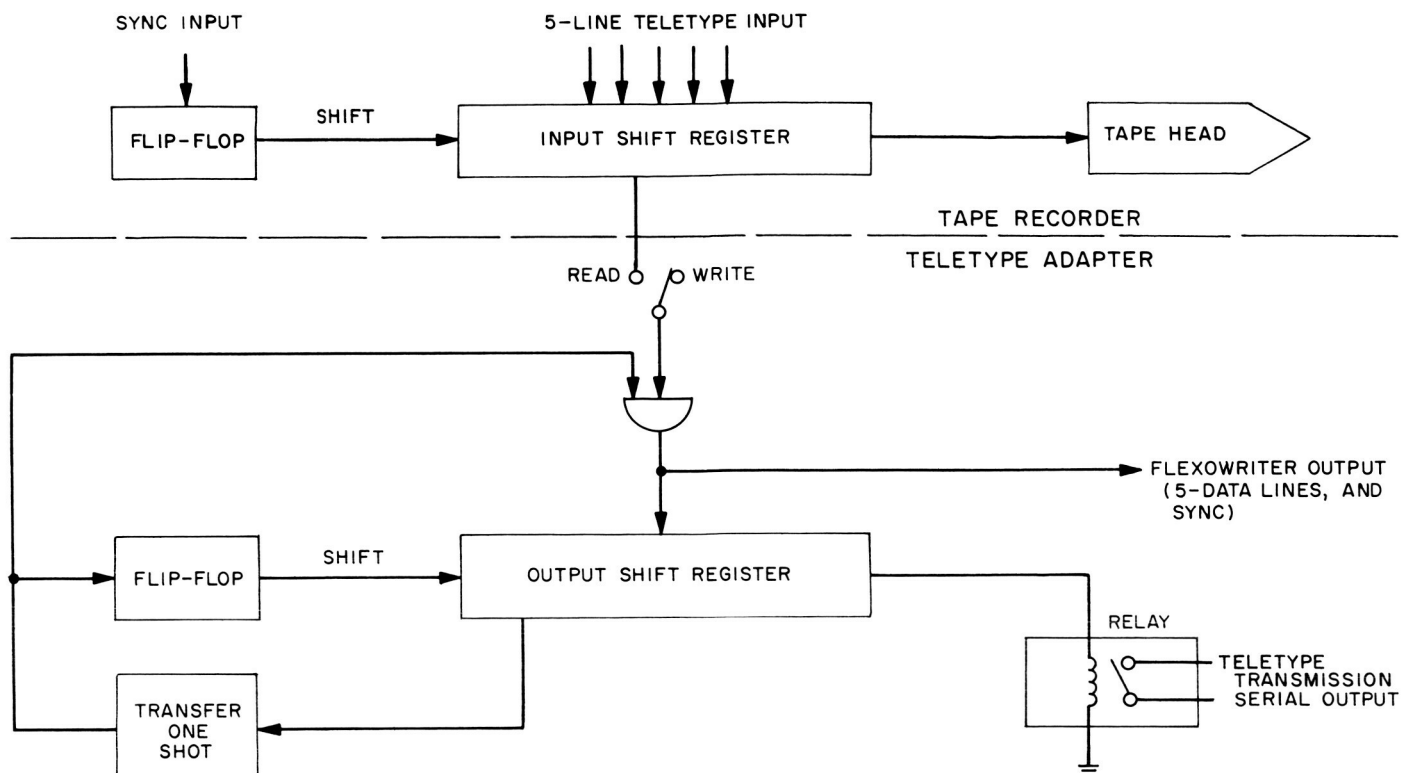


Fig. 13. Kennedy tape recorder/adaptor block diagram

The one advantage the Tally tape punch has over the tape recorder is that the punch tape can be converted directly into IBM computer magnetic tape. The Kennedy

tape recorder 1/4-in. tape at present has to be converted into punch tape if it is to be used as an input to a computer. It is anticipated, however, that in the immediate future the 1/4-in. tape will be converted directly into IBM computer magnetic tape.

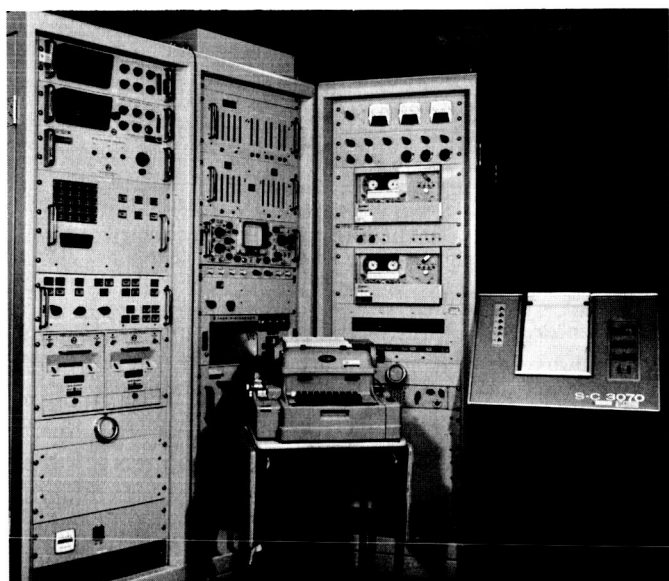


Fig. 14. Ranger follow-on operational support equipment system

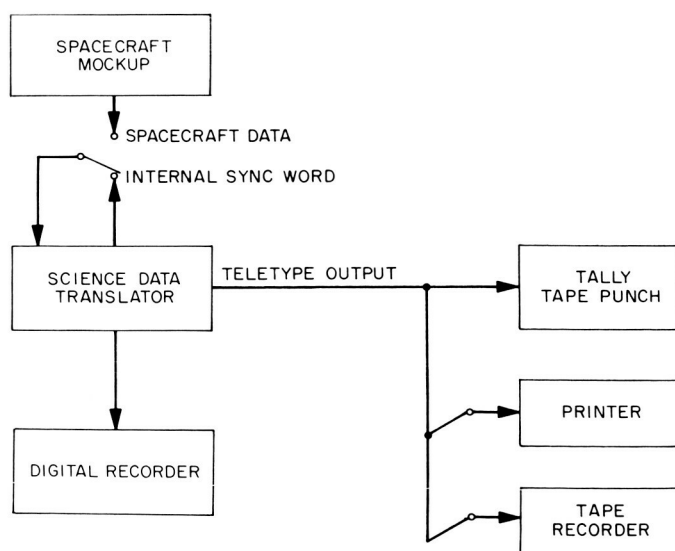


Fig. 15. Testing system block diagram

The tape recorder enjoys many advantages over the tape punch. A greater amount of data can be stored on magnetic tape, it is much quieter acoustically than the tape punch, and it is capable of producing the proper output for direct teletype transmission. Improvements recommended for the tape recorder would include the addition of electrical noise rejection circuitry, increased component quality, the addition of a self-check capability and more accessible servicing of components. The two areas which limit the usefulness of this tape recorder are its speed and channel capabilities, both of which must be increased to keep pace with future requirements. The advantages and dependability of this tape recorder are enough to warrant its use on present systems with a relatively high degree of confidence; however, it is recommended that its low speed and limited channel capabilities be considered before it is integrated into any future system.

5. OSE Digital Incremental/Continuous Magnetic Tape Recorder

A digital tape recorder is being developed for the scientific operational support equipment (OSE) to be used in the *Mariner C* program. Kinellogic Corporation, Pasadena, California, is presently completing the final phases of the program. This recorder is being designed to bridge the gap between low-speed paper tape punch devices and costly high-speed magnetic tape recorders.

a. Objective. The objective of the recorder is to provide a versatile data storage device for handling spacecraft scientific data obtained during subsystem and systems test. With the higher data rates being used on *Mariner C* and those anticipated on future programs a high-density storage device is mandatory. Furthermore, fast playback of data into a computer or high-speed printer for rapid data analysis is also a necessity. This recorder is designed to meet these needs.

b. Requirements. Briefly, the requirements set forth for the recorder are:

- (1) Record and reproduce.
 - (a) Incrementally—six data channels at 1000 bits/sec each; or
 - (b) Incrementally—one data channel at 5000 bits/sec; or
 - (c) Continuously at rates up to 30,000 bits/sec.

- (2) Tape.
 - (a) Tape width— $\frac{1}{2}$ in.
 - (b) Recording format—IBM format.
 - (c) Bit packing density—556 bits/in.
 - (d) Bit dropout rate—not to exceed one bit in 10,000 bits.
- (3) Inputs and outputs.
 - (a) Positive or negative polarity.
- (4) Dimensions.
 - (a) Height—24½ in.
 - (b) Width—19 in.
 - (c) Depth—17 in.
- (5) Special features.
 - (a) Teletype (TTY) serial output.
 - (b) Incremental readout rate—variable between 7 and 5000 bits/sec.
 - (c) Environment—operation between 50 and 120°F.
 - (d) Fast wind and rewind capability.

The design, development and fabrication of this recorder originally was specified to be 90 days; however, due to some modifications to the recorder options, delivery has been delayed 30 days.

c. Basic operation. The recorder is designed for two modes of operation; an incremental mode and a continuous mode. To achieve very high packing density the recorder, in the incremental mode, only records when data is present. During the continuous mode, digital data is recorded at a preselected tape speed. Playback may be either continuous or incremental. Although data that is continuously recorded must be played back continuously, incrementally recorded data may be played back either incrementally or continuously.

The flexibility of the recorder is further enhanced through the use of IBM reels and IBM track spacing to make it compatible with computer tape units. Another auxiliary feature is a serial teletype (TTY) output which produces data that is capable of being transmitted via a TTY line.

d. Input-output operation. The tape recorder can record six data channels incrementally up to 1000 bits/sec or one data channel up to 5000 bits/sec. It can also record six data channels continuously up to 30,000 bits/sec. During the incremental playback mode, the data output can be varied to play back between 7 and 1000 bits/sec

for six data channels or between 7 and 5000 bits/sec for one data channel. In the continuous playback mode, the data, either continuously or incrementally recorded, may be played back continuously at either $7\frac{1}{2}$, 15, 30, or 60 in./sec.

To illustrate the potential of this recorder, the present *Mariner C* science OSE system will be used as an example. This system records digital data from the data automation system as shown in Fig. 16. The data rate may be as high as $33\frac{1}{3}$ bits/sec. After the OSE scientific data translator has formatted and converted the data to 5-line TTY code, the data is recorded. The packing density is 556 bits/in. Assuming an 8-hr test, the entire test, at a $33\frac{1}{3}$ -bit/sec output rate, could be recorded on 160 ft of tape. Using the maximum playback speed, 60 in./sec, this same 8-hr test could be played back in 32 sec.

At the present time a S-C 3070 high-speed printer is being used to read out the recorder. The maximum read-out rate of this printer is approximately 300 characters/sec. Each line consists of a maximum of 120 characters. It will take approximately 1 hr to read out the 8-hr test. Fig. 17 illustrates this mode of operation.

Another output mode provides serial TTY data (7-bit/sec rate) which can be transmitted via commercial teletype lines. This output is extremely useful for transmit-

ting information from the Atlantic Missile Range to JPL or from remote facilities at JPL to the central computer facility. Fig. 17b illustrates the TTY mode of operation.

e. Tape recorder design. The tape recorder utilizes a buffer storage system which operates in conjunction with a relatively fast-acting tape transport of special mechanical characteristics. The buffer storage element provides the bit-rate response range required while the fast start-stop transport keeps the buffer at a reasonable size. In the incremental mode, after the buffer is filled, the tape motion is started and when the tape reaches its nominal speed, data from the buffer is recorded on the tape. After the buffer has been read out, a special signal called a block marker is recorded on the tape and the tape motion is stopped. The tape is then automatically reversed and backed to a point on the tape where data has just been recorded. During the next incremental record operation, the tape is started and brought up to speed. When the block marker is encountered, the readout of the next segment of buffer data is initiated. A second buffer is used to record data while the first buffer is being read out. Fig. 18 shows the sequence of operation. The playback mode operates in much the same manner. Forty bit buffers are used for storage.

During the continuous record and playback modes the buffers are bypassed.

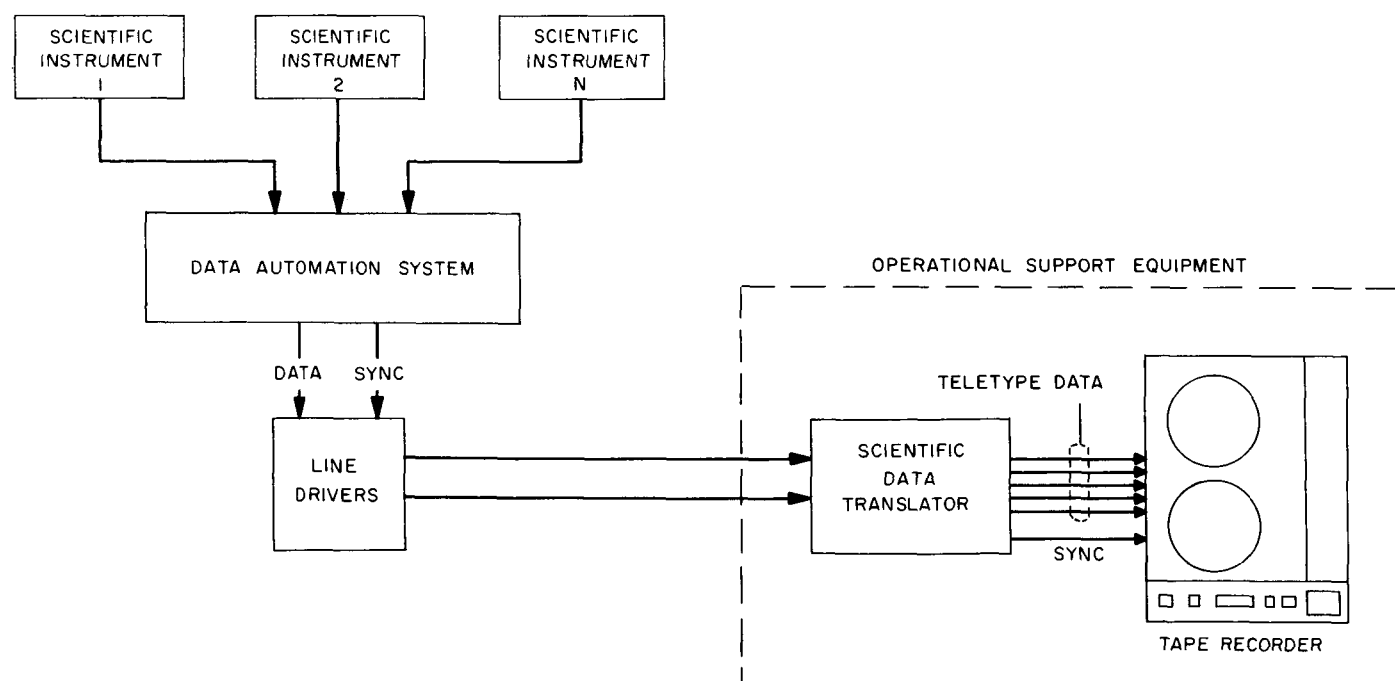
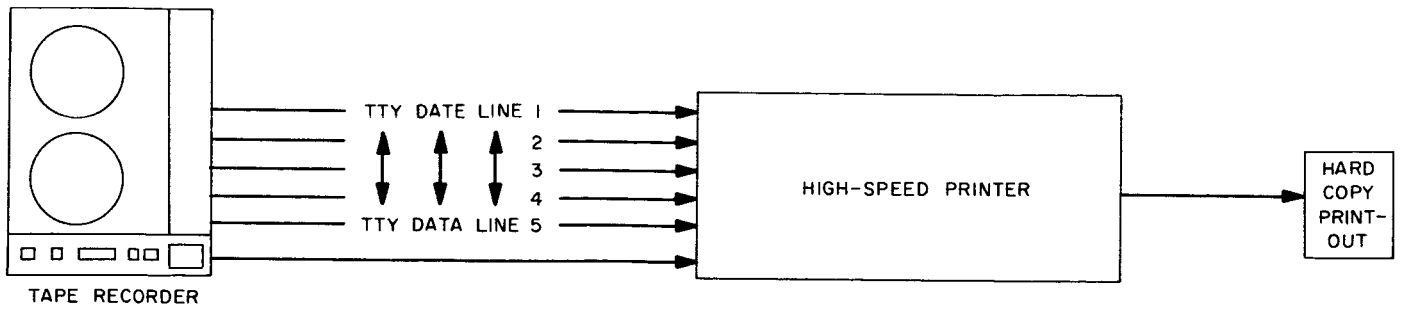
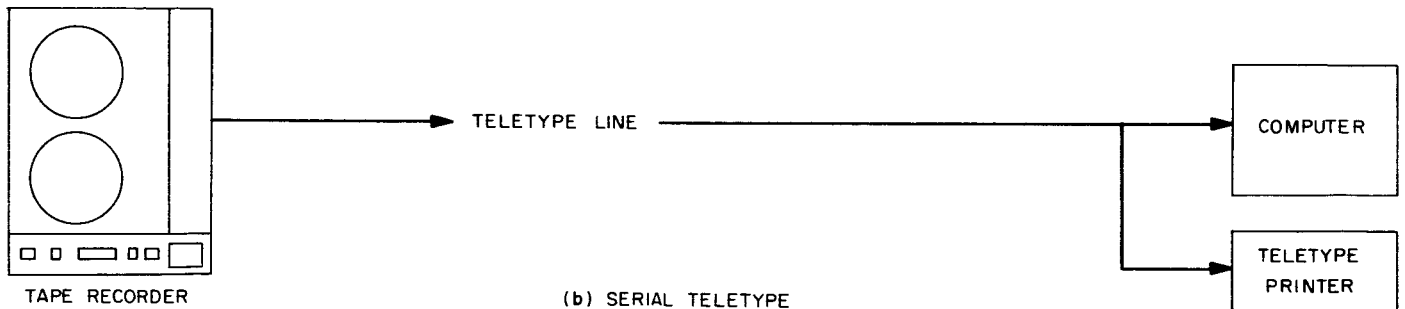


Fig. 16. Science operational support equipment data storage system

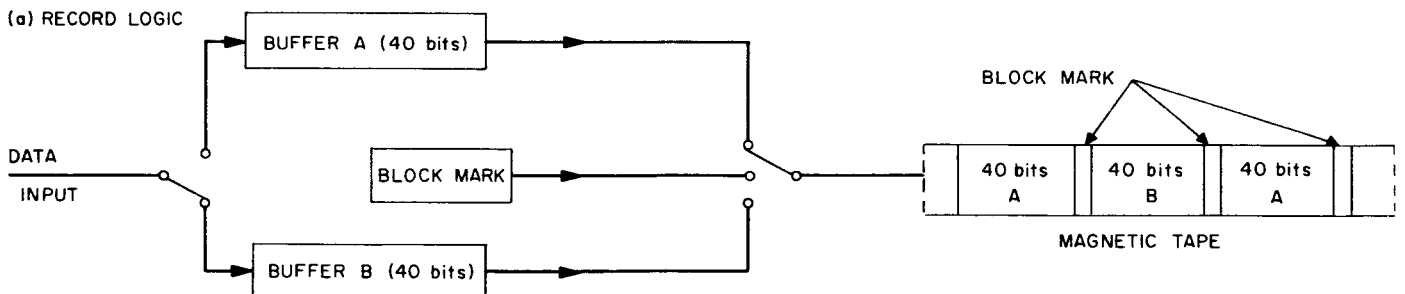


(a) PARALLEL TELETYPE



(b) SERIAL TELETYPE

Fig. 17. Readout modes



(b) RECORD CYCLE

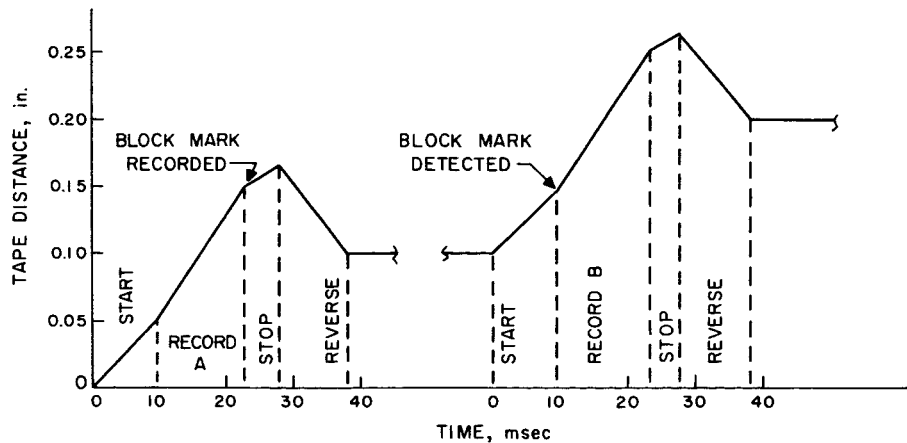


Fig. 18. Recording mode

The general approach in incremental recorders is to use a stepper motor which transmits incremental motion to the tape through a pressure roller-capstan drive system. This method is limited because of the high tape accelerations required and the mechanical impacting involved. The recorder being developed uses an electrostatic tape drive system (Fig. 19). Tape is started by applying an ac voltage between the forward running capstans which causes each drive belt to be attracted to its running capstan. At the same time sections of the drive belts sandwiching the magnetic tape are attracted to each other, causing the tape to be clamped between them; hence the tape moves with the belts. The belts have extremely low mass and the forces developed are substantial, making it possible for the tape to be accelerated with great speed. The magnetic tape is clamped over a wide area which results in extremely gentle tape handling compared to the forces to which the tape is subjected with conventional pinch roller digital drive systems. Removing the ac voltage from the forward capstans and placing the voltage on the fixed stopped electrodes causes the tape to be stopped. By applying the ac voltage momentarily to the reverse capstans and removing the voltage from the stop electrodes, the tape can be backed up a fixed amount. This action provides extremely high packing density of data on the tape.

f. General. The tape recorder being developed is extremely versatile and uses very simple design concepts. It is anticipated that the reliability of the recorder will

be enhanced through this simplicity. For the *Mariner C* program the recorder will be used to incrementally record data from the data automation system at 8½ and 33½ bits/sec. Data from the television instrument at 10.7 kc will be continuously recorded. This tape will be processed through the IBM 7090 computer to provide the necessary data reduction. Immediate data processing of the tape will be accomplished through the use of the high-speed S-C 3070 printer. This recorder is expected to provide the necessary data handling required of the scientific OSE systems for both present and future programs during the next few years.

6. Operational Support Equipment Junction Box

One of the major problems in operational support equipment (OSE) systems is the interconnection of the checkout equipment to the spacecraft electronics. Normally, the OSE cabling system is an integral part of the checkout console. A junction box has been developed for the *Mariner C* scientific OSE which is completely removable from the OSE console. This junction box incorporates an interconnection method which utilizes patch board blocks.

a. General description. Fig. 20 shows the junction box assembly. The junction box is completely fabricated and wired external to the OSE console in the same manner as any other chassis. It is then mounted on slides and installed at the bottom of the OSE console from the rear. Internal OSE cables are separate items which are fabricated external to the console, installed, and then connected to the junction box. Functions from the spacecraft are routed through the connectors at the rear of the junction box to feed-through patch boards. OSE internal functions are routed through the connectors at the top of the box to other patch board blocks. Jumpers are then added to the patch boards to connect the spacecraft with the OSE electronics. To allow access to the patch boards, the junction box may be extended out of the console after removing the internal cables. These cables can then be reconnected as required.

Connectors on the rear of the junction box are mounted at a 45-deg angle to prevent the heavy external cables from being stressed at the connector. In the past when external cables have been mounted perpendicular to the OSE console, the weight of the cable has been great enough to cause stresses at the connector and produce cable damage. The 45-deg mounting arrangement eliminates this problem.

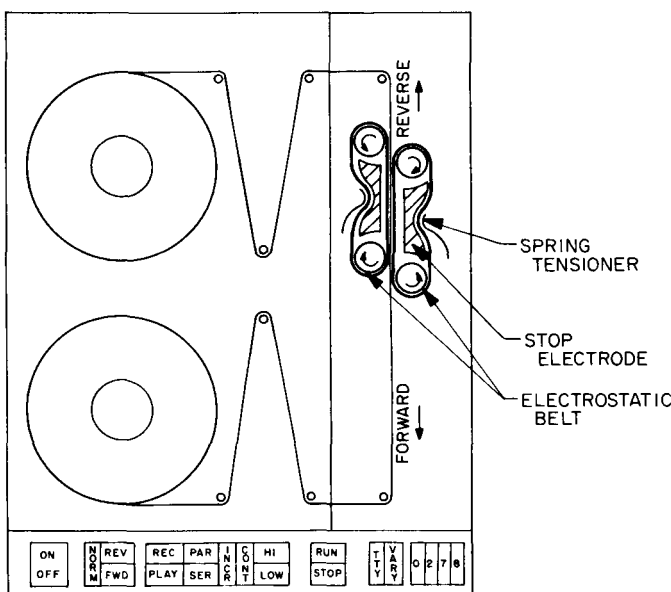


Fig. 19. Tape recorder and electrostatic drive system

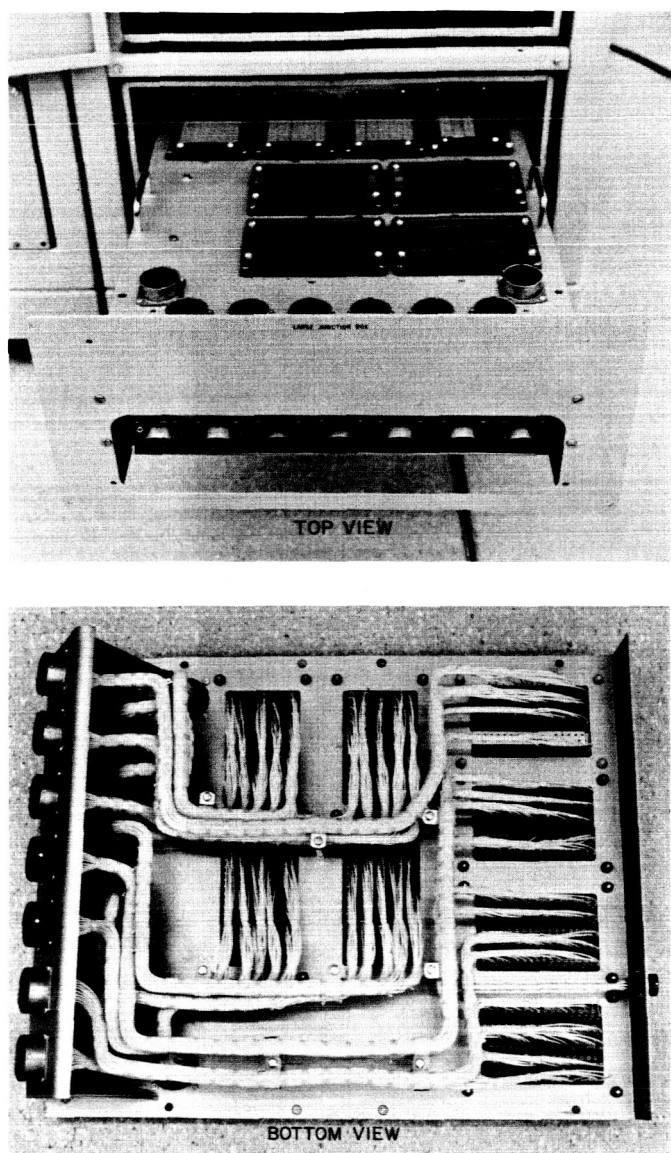


Fig. 20. Operational support equipment junction box

The *Mariner C* scientific OSE equipment has been designed for independent assembly. All the elements of the OSE such as the chassis, consoles, cables, and junction box can be assembled into a system in a very short period of time. The junction box is considered a standard item and the *Mariner C* units will be used over again on future programs.

At the present time there are two junction boxes in the *Mariner C* OSE. A significant reduction in the time required for the assembly and checkout of the scientific instruments has been accomplished through the use of this device.

7. A Computer-Controlled Checkout System for Scientific Instruments

On past spacecraft programs checkout equipment has been designed to provide manual testing facilities for the science subsystems, i.e., the scientific instruments and the data automation system (DAS). With each new spacecraft design, it has been necessary to disassemble the old equipment and to design and fabricate new equipment. The *Mariner C* operational support equipment (OSE) is designed for both manual OSE operation and computer-controlled testing. The computer system is illustrated in Fig. 21. This system consists of a Digital Equipment Corporation (DEC) PDP-4B computer and a peripheral console.

The PDP-4B is a single-address, parallel, binary machine operating with an 18-bit word length. Standard features include stored program operation, a random access magnetic-core memory, a complete order code, and indirect addressing. The machine used in the checkout system contains an 8096-word memory capacity. A tape reader is used to insert the PDP-4B program into the computer and a teletype unit displays the spacecraft data. If a malfunction is discovered, an error message is printed. A block diagram of the checkout system is shown in Fig. 22.

The peripheral console (Fig. 23) provides the interface between the computer and the spacecraft. It performs all of the signal distribution and gathering functions necessary to simulate and monitor the scientific instruments and the data automation system.

This checkout system is essentially general purpose in that only one unit of peripheral console is mission sensitive. As a result, this system can be employed to check out subsequent spacecraft by merely redesigning an adapter unit, writing a new test program, and devising a new patch board scheme for the peripheral console.

For any spacecraft, a variety of test configurations are available. During checkout operations the computer system can: (1) simulate the instruments, exercise the DAS, monitor the output data; (2) simulate the DAS, exercise the instruments, monitor the output data; (3) simulate other spacecraft functions, exercise and monitor both the instruments and the DAS. The computer system can also be patched and programmed to perform a self-check.

The *Mariner C* project presents an opportunity to evaluate this new checkout approach. It is expected that certain manual checkout equipment can be discontinued

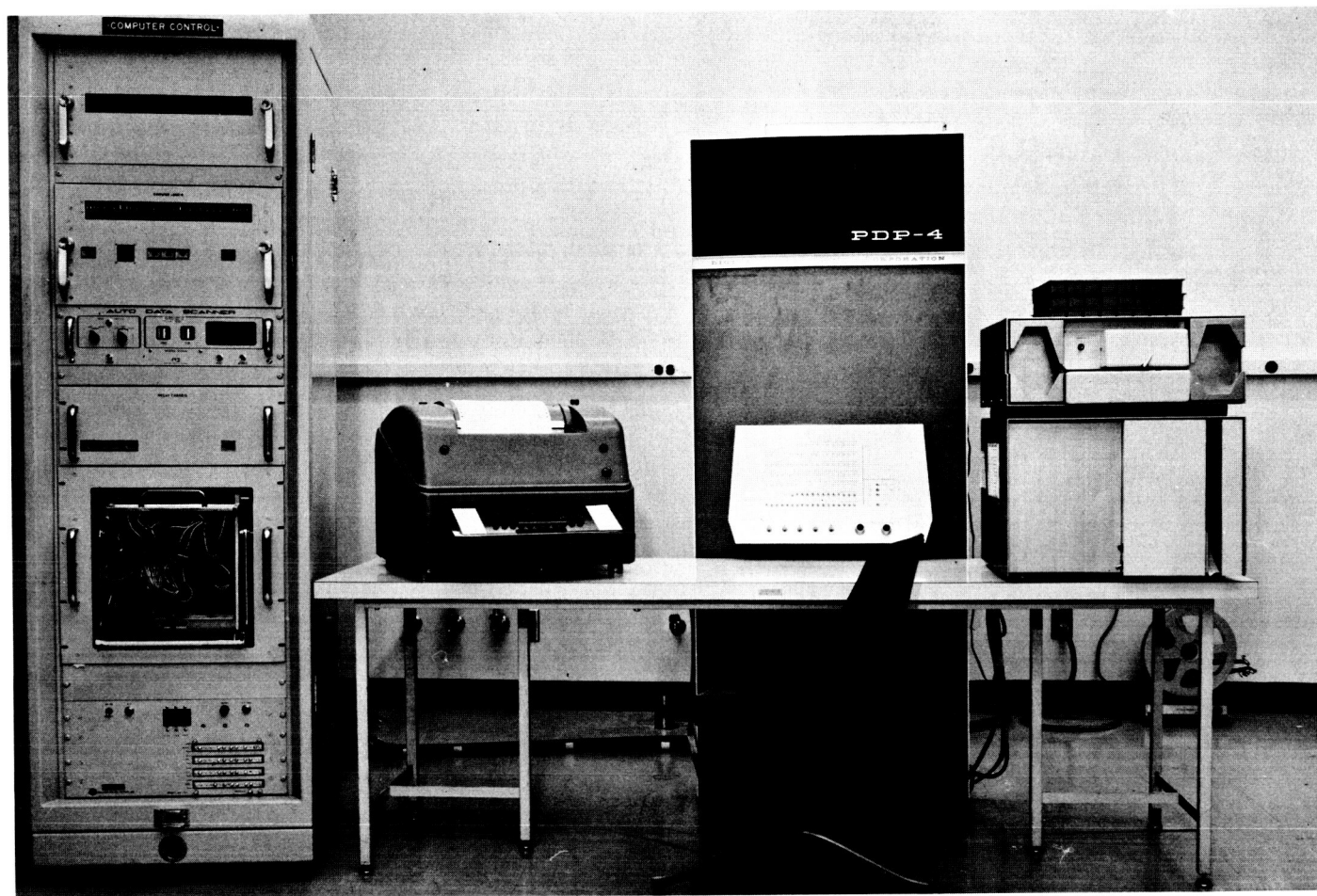


Fig. 21. Scientific instruments computer-controlled checkout system

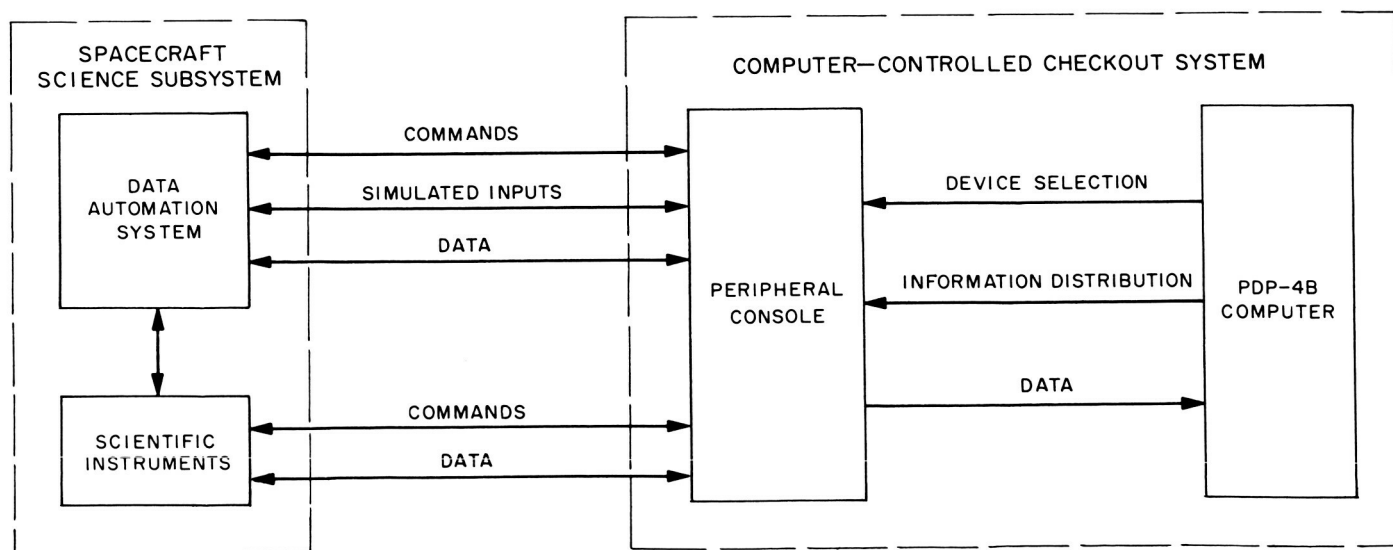


Fig. 22. Computer-controlled checkout system block diagram

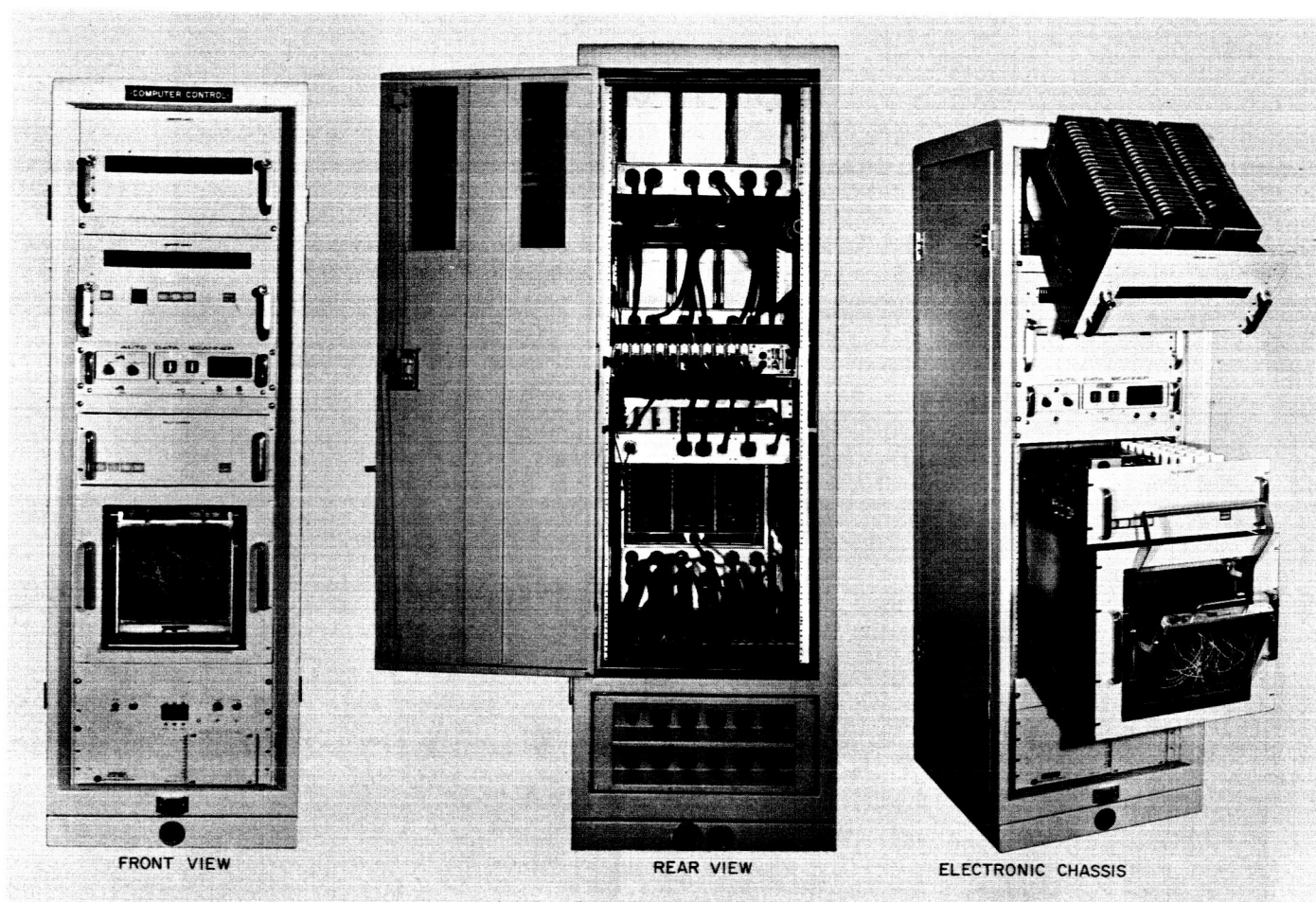


Fig. 23. Peripheral console

in the future and replaced by a computer system. This would result in lower checkout costs and a reduction in the time required to assemble the checkout equipment. Furthermore, the programmable feature offers a versatility which, when used with specific programs to meet particular objectives, can significantly enhance the testing of scientific subsystems.

This computerized testing provides extremely thorough and comprehensive testing. The probability of discovering interactions and malfunctions is greatly increased while the amount of time required for post testing data reduction is substantially reduced. The peripheral con-

sole for *Mariner C* has been developed to the same standards as conventional OSE equipment and utilizes much of the standardization being incorporated in the scientific OSE. Although the peripheral console is presently being used in conjunction with the PDP-4B it is compatible with the *Mariner C* systems test computer system. It is anticipated that after a thorough evaluation an OSE system using a computer will prove to be a highly desirable method for testing spacecraft systems.

At the present time the *Mariner C* DAS breadboard has been mated with this equipment and initially checked out. Incompatibilities have been detected and corrected.

SPACE SCIENCES

VIII. Space Instruments Development

A. A Capacitor Storage Scheme for Gas Chromatograph Detector Quiescent Current Compensation

1. Introduction

Because the quiescent current of an ionization detector used in a gas chromatograph does not remain constant for long periods of time, some form of automatic baseline stabilization¹ is required for spacecraft applications. This report describes a system in which current from a capacitor storage cancels the detector quiescent current at the electrometer input. This technique is applicable to chromatograms lasting as long as 30 min with peaks as small as 10^{-12} amp superimposed on baseline shifts of 10^{-9} amp.

2. General Description

A functional block diagram of a proposed electrometer system for a spacecraft gas chromatograph is shown in

¹J. H. Marshall, "Gas Chromatograph Detector Quiescent Current Drift Compensation," JPL interoffice Technical Memorandum, December 5, 1962; SPS 37-20, Vol. IV, p. 169; SPS 37-22, Vol. IV, p. 213.

Fig. 1. The system consists of an ionization detector; a dynamic capacitor electrometer (Ref. 1) with automatic scale switching (SPS 37-23, Vol. IV, p. 245); fixed and variable quiescent current bucking supplies; and control logic.

For a spacecraft mission, the fixed-current bucking supply is adjusted on the Earth to null out the then present detector quiescent current. When the spacecraft reaches its destination, and while only carrier gas flows in the detector, the reed switches labelled "loop" are closed, and the electrometer is placed on its most sensitive scale (feedback resistor = $10^{10} \Omega$). The comparator amplifier then adjusts the variable bucking current so that the electrometer output approaches zero according to

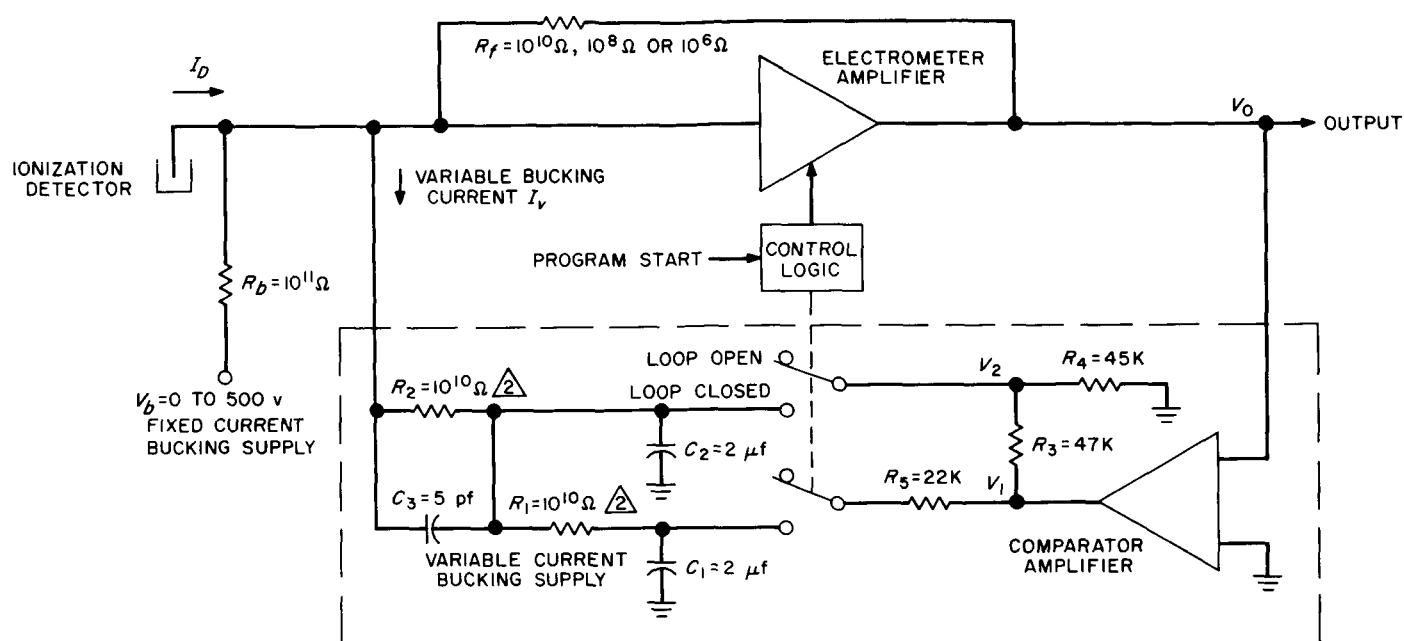
$$V_{00} = -\frac{R_2 I_D}{M_0} + V_{os} \quad (1)$$

where

V_{00} = electrometer output voltage with the loop switches closed

I_D = detector current minus the fixed bucking current

$$M_0 = \frac{R_4 M_2}{R_3 + R_4} = 1000$$



1. ALL CAPACITORS MUST HAVE LEAKAGE RESISTANCES IN EXCESS OF $10^{12} \Omega$
 2. RESISTORS SELECTED SUCH THAT THE TEMPERATURE COEFFICIENT OF THE RATIO OF THEIR RESISTANCES IS LESS THAN 20 ppm/°C

Fig. 1. Electrometer with baseline stabilization

$$M_2 = \text{comparator amplifier gain} = \frac{V_1}{V_o - V_{os}} = 2000$$

V_{os} = offset voltage of the comparator amplifier
 electrometer feedback factor $\gg 1$

$$M_0 \gg 1$$

As soon as the voltages on the storage capacitors (C_1 and C_2) have reached equilibrium, the loop is opened, and the sample to be analyzed is injected into the column. During the chromatographic analysis, the voltages on the storage capacitors decay toward zero, resulting in a decay of the variable bucking current and the following approximate change of the electrometer output voltage with time².

$$V_o = -\frac{R_2 I_D}{M_0} + V_{os} - I_D R_f \left[\frac{t}{\tau_L} - \frac{1}{2} \left(\frac{t}{\tau_Q} \right)^2 \right] \quad (2)$$

where

V_o = electrometer output voltage with the loop switches open

²For a derivation of the decay of the variable bucking current, see the double resistance-capacitor storage discussed in SPS 37-22, Vol. IV, p. 213.

t = time after the loop was last opened (small compared to τ_Q)

$$\tau_L = 40,600 \text{ sec}$$

$$\tau_Q = 18,200 \text{ sec}$$

R_f = electrometer feedback resistor

For $I_D \leq 10^{-9}$ amp, $R_f = 10^{10} \Omega$, and $V_{os} = 0$, and $V_o = 0 \pm 20$ mv for 1970 sec after the loop was last opened.

The electrometer output can also be expressed in terms of the initial output voltage (V_{10}) of the comparator amplifier by

$$V_o = -\frac{V_{10}}{M_2} - \frac{R_f}{R_2} [V_{10} + M_2 V_{os}] \left[\frac{t}{\tau_L} - \frac{1}{2} \left(\frac{t}{\tau_Q} \right)^2 \right] \quad (3)$$

If the above quantities are sufficiently stable, and if I_D does not change during the chromatogram, then peaks of the same order as the decay of the variable bucking current can be measured by recording V_{10} and correcting for the initial value and decay of the baseline. As an additional check on the proper operation of the system,

the electrometer output voltage with the loop closed could also be recorded.

3. Circuit Details

A complete schematic of the baseline compensating circuits used in a laboratory gas chromatograph is shown in Fig. 2. The comparator amplifier and the resistance-capacitor storage are designed for spacecraft application. However, for the laboratory instrument the reed switches are controlled by toggle switches, and a meter indicates the comparator output voltage. Also, the electrometer can be used without baseline compensation by opening a reed switch between the capacitor storage and the electrometer input.

The comparator is a feedback dc amplifier with a gain of 2000 and a balanced, matched differential input stage. A pole of 100 sec and a zero of 100 msec are placed in the comparator feedback loop to stabilize the over-all system against oscillation. The calculated asymptotic frequency dependence of the comparator feedback factor (Fig. 3) shows that the comparator is safe from oscillation. A complimentary emitter-follower output stage allows the load to be driven rapidly positive or negative without large standing currents in the output

emitter-follower. The ammeter in the collector circuit of Q_2 is used to ensure that the comparator amplifier is operating within its linear range when the loop is closed.

The decay shape adjustment, which determines the initial voltages V_{10} and V_{20} on the storage capacitors C_1 and C_2 , controls the time dependence of the variable bucking current after the loop is opened. The nominal value for the ratio of V_{20} to V_{10} is 0.486. An adjustment compensates for deviations of resistors and capacitors from their nominal values.

The loop toggle switch, which closes the reed switches connecting the output of the comparator amplifier to the storage capacitors, also holds cutoff transistors Q_{12} and Q_{13} in the automatic scale switching circuits (SPS 37-23, Vol. IV, p. 245). The electrometer feedback resistor then remains $10^{10} \Omega$ regardless of the electrometer output voltage. The electrometer output will be zeroed to ± 10 mv in about 2 sec after the loop is closed.

The power supply voltages are identical with those used by the automatic scale switching circuits. The power to operate the circuits is 31.3 mw, with an additional 35 mw being required to close the loop reed switches (Table 1).

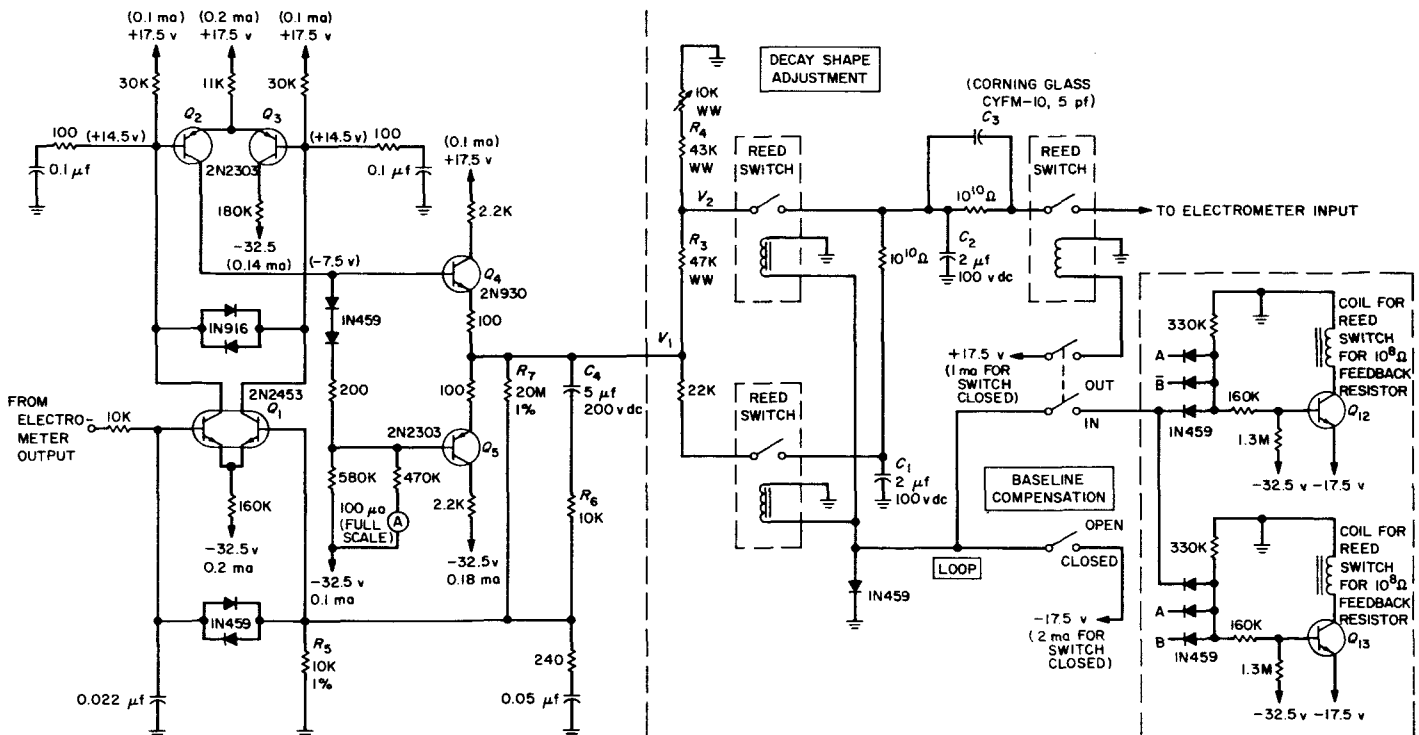


Fig. 2. Baseline compensation circuits

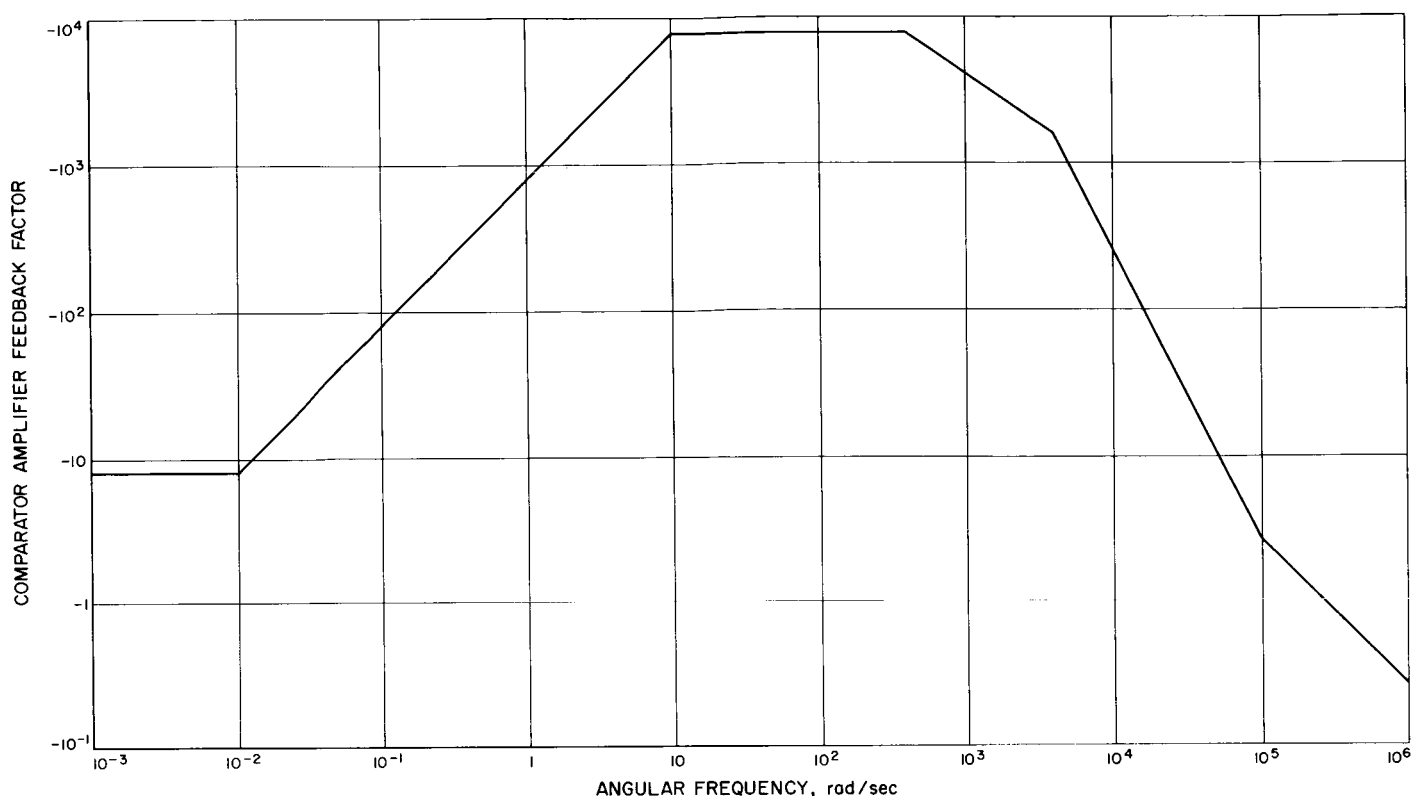


Fig. 3. Asymptotic frequency response of the comparator amplifier feedback factor

Table 1. Power requirements

Voltage, v	Current, ma	Power, -mw
+17.5 ^a	0.54	9.5
-17.5 ^b	0 or 2	0 or 35
-32.5	0.62	21.8
Total power:		31.3 or 66.3 mw
^a The current (1 ma) to operate the reed switch which connects the baseline compensation to the electrometer input was not included, because this switch probably would not be present in a spacecraft version. ^b The -17.5 v current flows only when the loop switches are closed, during which time no -17.5 v current would be required for reed switches by the automatic scale switching circuits.		

4. Feedback Factor

The feedback factor of the electrometer with the loop switches closed was calculated with the aid of Fig. 4 and is given approximately by

where

$$R_f = R_2$$

$$\frac{R_3 R_4 C_2}{R_3 + R_4} = R_2 C_3$$

$$R_7 \gg R_5 + R_6$$

$$C_2 \gg C_3$$

$$C_{in} = \text{electrometer input capacity}$$

$$C_{in} \gg C_3$$

$$C_{in} \gg C_f = \text{stray capacity across the electrometer feedback resistor}$$

$$A_1 = V_0/V_3$$

$$M_0 \gg 1$$

$$F = \frac{M_0 A_1}{2} \left\{ \frac{\left[1 + p \left(R_5 + R_6 + \frac{R_7}{M_0} \right) C_4 \right] \left[1 + p R_f C_f \left(\frac{R_7}{R_7 + M_0 (R_5 + R_6)} \right) \right]}{\left[1 + p \frac{R_f C_{in}}{2} \right] [1 + p R_7 C_4]} \right\} \quad (4)$$

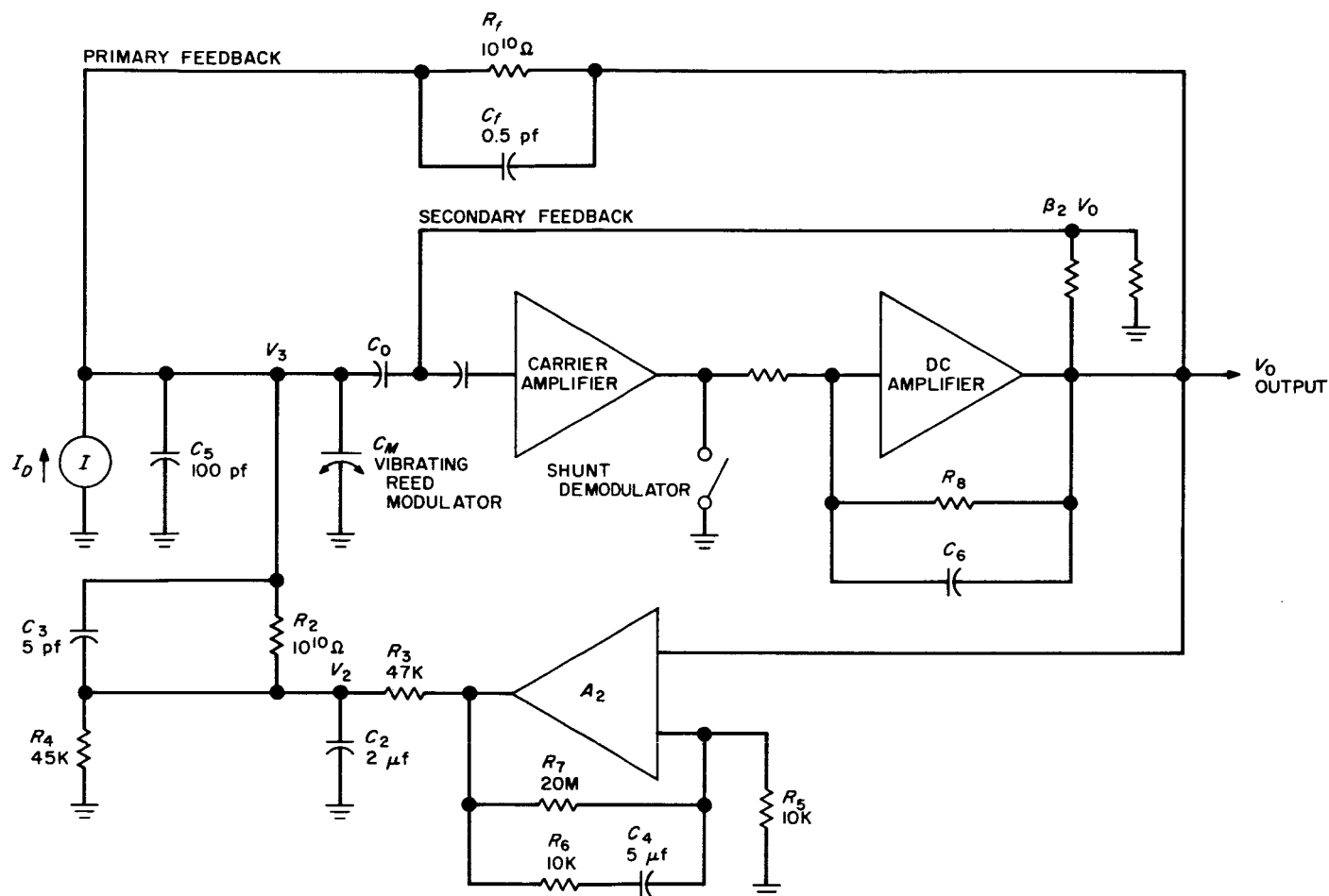


Fig. 4. Simplified schematic, closed loop configuration

Comparator amplifier feedback factor $\gg 1$ for times longer than 1 msec

p = Laplace transform variable

The electrometer input capacity is almost entirely determined by the secondary feedback loop³ and can be approximated by

$$C_{in} = \beta_2 A_0 C_0 + C_5 + C_M \quad (5)$$

where

β_2 = secondary feedback attenuation

A_0 = dc open-loop gain of the electrometer amplifier
 $= |A_1|$

C_M = rest capacity of the vibrating reed modulator

Neglecting poles and zeroes smaller than about 3 msec, the electrometer amplifier gain (A_1) is given by

$$A_1 = \frac{-A_0}{1 + \frac{pR_6 C_6}{A_0 \beta_2} \left(\frac{C_0 + C_M + C_5}{C_0} \right)} \quad (6)$$

The following values of A_1 and C_{in} were determined from the measured open-loop gain of the electrometer (without baseline compensation) versus frequency⁴ (Fig. 5) and were found to agree reasonably well with Eqs. (5) and (6):

$$\begin{aligned} C_{in} &= 2300 \text{ pf} \\ A_0 &= -1000 \\ A_1 &= \frac{-1000}{1 + p25 \text{ msec}} \end{aligned} \quad (7)$$

³J. H. Marshall, "Electrometer Open Loop Frequency Response," JPL interoffice Technical Memorandum, August 1962.

⁴J. L. Lawrence, "Electrometer Open Loop Response Versus Frequency for $10^{10}\Omega$ Feedback Resistor," private communication.

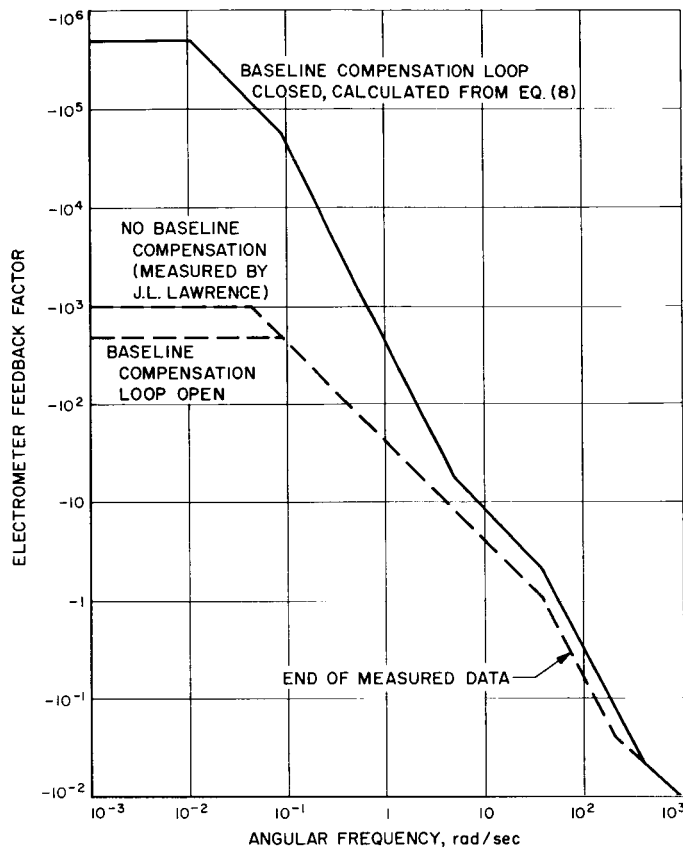


Fig. 5. Asymptotic frequency response of the electrometer feedback factor

The feedback factor is then given by

$$F = \frac{-5 \times 10^5 (1 + p200 \text{ msec}) (1 + p2.5 \text{ msec})}{(1 + p100 \text{ sec}) (1 + p11.5 \text{ sec}) (1 + p25 \text{ msec})} \quad (8)$$

The asymptotic frequency dependence of F is shown in Fig. 5 and compared with the frequency response for the electrometer without baseline compensation. Near gain crossover the feedback factor with the compensating loop is twice that without the compensating loop. Because the electrometer alone has more than 15 db gain margin, oscillation with the compensating loop appears safely prevented. If $R_2 C_3$ were made equal to $R_3 R_4 C_2 / 2 (R_3 + R_4)$, then near gain crossover the two feedback factors would be identical.

The loading of the electrometer input with an additional $10^{10} \Omega$ resistor for the baseline compensation reduces the feedback factor with the baseline compensating loop open by 6 db. If the electrometer feedback factor is then too small, the gain of the carrier amplifier could be increased by 6 db. Because C_{IN} is proportional to the

carrier amplifier gain, the feedback factor near gain crossover would not be changed, and the same gain margin should result.

5. Response to the Closing of the "Loop" Switches

The time required for V_2 to reach its equilibrium value after the loop switches are closed determines the minimum time that these switches must remain closed.

For C_1 and C_2 initially uncharged and for times long compared to the gain crossover time (30 msec) of the electrometer amplifier, the Laplace transform of V_2 is

$$V_2 = \frac{V_{10} p C_4 R_5 - I_D R_f [1 + p C_4 (R_5 + R_6)]}{\left[1 + \frac{p R_3 R_4 C_2}{R_3 + R_4}\right] [1 + p (3R_5 + R_6) C_4] p} \quad (9)$$

where

V_{10} = initial value of the comparator output voltage

$V_{os} = 0$

$$\text{For } I_D > \frac{V_s R_5}{R_f R_7} = 10^{-12} \text{ amp} \quad (10)$$

where

V_s = saturation voltage of the comparator amplifier
= 20 v

then

$$V_{10} = -V_s$$

and

$$V_2 = -\frac{V_s p 50 \text{ msec} + I_D \times 10^{10} \Omega (1 + p100 \text{ msec})}{(1 + p45 \text{ msec}) (1 + p200 \text{ msec}) p} \quad (11)$$

For $I_D = 10^{-9}$ amp, then

$$V_2 = \frac{-10 \text{ v}}{(1 + p45 \text{ msec}) p} \quad (12)$$

and the time required for V_2 to reach 0.01% of its final value is 0.42 sec.

For $I_D = 10^{-12}$ amp, then

$$V_2 = \frac{-0.01 \text{ v}}{p} \left\{ \frac{(1 + p100 \text{ sec})}{(1 + p45 \text{ msec}) (1 + p200 \text{ msec})} \right\} \quad (13)$$

and the time required for V_2 to fall to within 1 mv of its final value is 1.8 sec. Therefore, the loop switches should

be held closed for at least 1.8 sec to ensure that the electrometer is properly zeroed.

Because the 100-sec pole is placed in the comparator amplifier rather than later in the system, a large dynamic range is not required to prevent rate limiting. If, for example, C_2 were used to produce the 100-sec pole, and if the dynamic range of the comparator amplifier were not changed, over 100 sec could be needed to charge C_2 to its final value. When the 100-sec pole is early in the system, linear analysis is applicable, and 1.8 sec is sufficient to charge C_2 .

Also, if the electrometer feedback resistor were less than $10^{10} \Omega$, the resulting decrease in the feedback factor would slow the charging of C_2 . Therefore, when the loop switches are closed, the automatic scale switching circuits are bypassed, and the feedback resistor is fixed at $10^{10} \Omega$.

6. Performance

The comparator amplifier gain, offset voltage, and dynamic range were determined by measuring⁵ the amplifier output voltage versus input voltage at several temperatures from -55 to $+125^\circ\text{C}$. The $5\text{-}\mu\text{F}$ capacitor in the feedback loop was disconnected so that the amplifier output would quickly reach equilibrium. The data for -55 , $+20$, and $+125^\circ\text{C}$ are shown in Fig. 6. The gain, which was 1850 at room temperature, varied by $\pm 3.3\%$ over the temperature range. The temperature coefficient of the offset voltage, which had a room temperature value of 1.6 mv, was $+10 \mu\text{V}/^\circ\text{C}$, yielding a ± 0.9 mv change over the temperature range. These temperature variations cause less than ± 1.2 mv change in the closed loop electrometer output. The comparator amplifier dynamic range extending from $+14$ to -30 v provides variable bucking currents from -0.7×10^{-9} to $+1.5 \times 10^{-9}$ amp.

The small-signal comparator amplifier rise time, measured by applying a square-wave voltage to the amplifier input, agreed with the feedback factor calculations illustrated in Fig. 3. All rise-time effects in the comparator amplifier, except the 100-sec pole and 100-msec zero in the feedback loop, were negligible compared to the rise time of the electrometer alone.

In order to test the entire baseline compensating system, the detector was simulated by a stable power

supply connected to the electrometer input by a $10^{11} \Omega$ resistor (Fig. 7). With the power supply voltage set to 91 v, the loop switches were closed, and the electrometer output settled to -7 mv, in good agreement with the -8 mv predicted by Eq. (1) and by the measured comparator amplifier gain and offset voltage. Then the loop switches were opened, and the electrometer output volt-

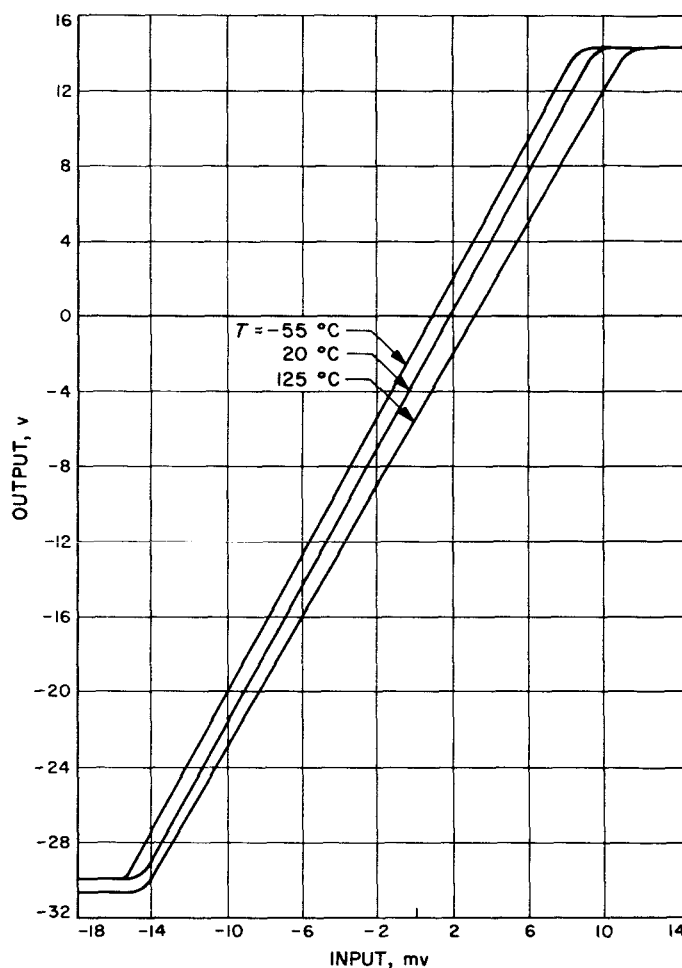


Fig. 6. Comparator amplifier input-output characteristics

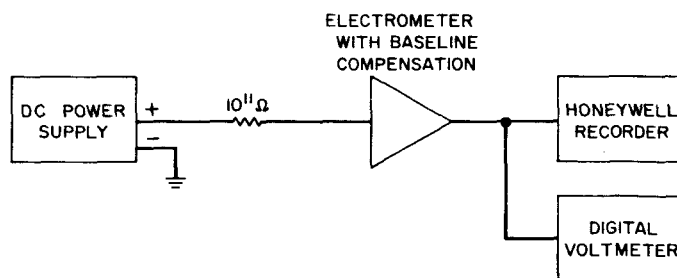


Fig. 7. Test setup

⁵H. Richeson, "Comparator Amplifier Test Results," JPL inter-office Technical Memorandum, October 1963.

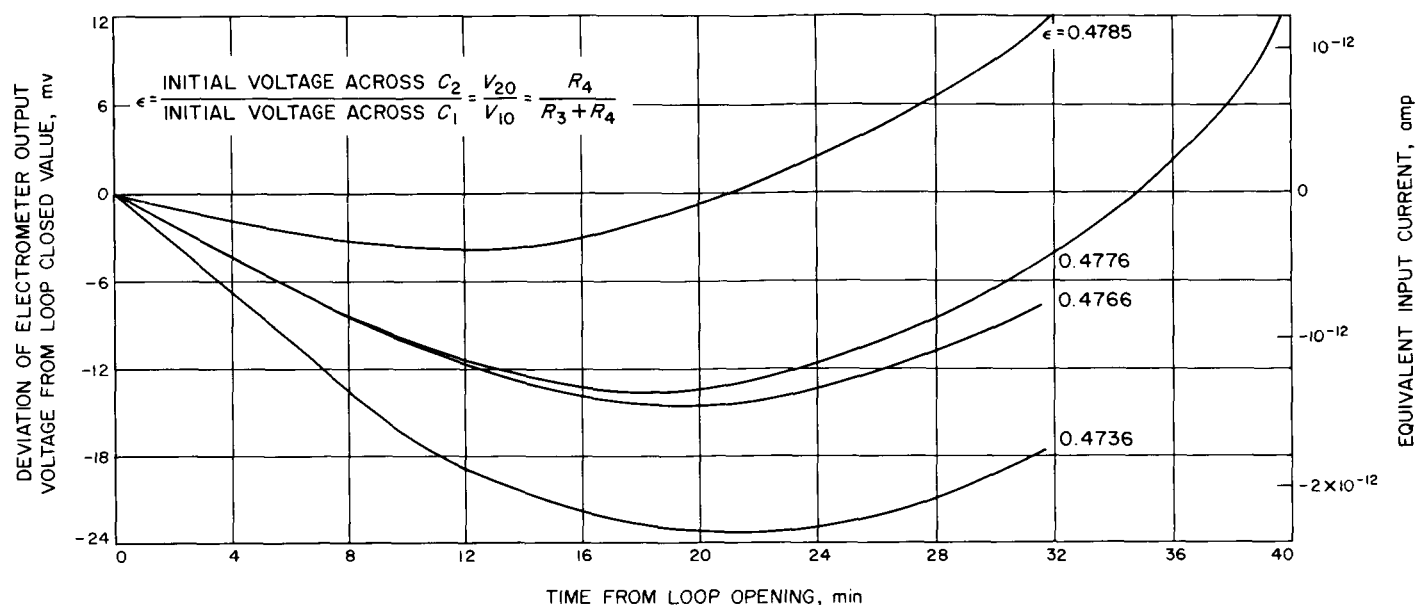


Fig. 8. Decay of the variable bucking current

age as a function of time was recorded (Fig. 8). The ratio of the initial voltages across the two storage capacitors was varied and is a parameter on the curves of Fig. 8. As predicted by Eq. (2), the electrometer output drifts no more than ± 10 mv for 30 min, if the rather critical ratio of the initial capacitor voltages is correct. If the shape of the decay of the variable bucking current is to be predictable, then this ratio must be more stable than 0.05% and the ratio of R_1 to R_2 must stay constant to better than 0.2%.

In order to measure the rise time of the voltage across C_2 when the loop switch was closed, C_2 was initially discharged by the 10 M Ω oscilloscope probe impedance, and 9×10^{-10} and 2×10^{-12} amp currents were injected at the electrometer input. For times longer than 100 msec, the waveforms predicted by Eqs. (12) and (13) were confirmed.

Presently the electrometer with baseline compensation is being used for detector tests. The only difficulty anticipated in applying this technique to a spacecraft gas chromatograph is matching the temperature coefficients of R_1 and R_2 .

B. Lightweight Sample Collector for Exobiology Experiments

S. B. Tuttle

An aerosol method of particulate sample collection has been developed, and it is currently considered feasible

for exobiology experiments. The equipment has not been optimized for material or weight, but there are no obvious problem areas.

This technique is capable of handling particles between 5 and 100 μ at a density of 2 or less. The rate of sample collection is roughly 0.02 g/min at a gas consumption 0.14 ft³/min, standard temperature and pressure. At these rates, a 0.5-g sample would require a storage volume for gas at 1800 psig equal to a sphere 4.5-in. D.

The aerosol system consists of an aspirator at ground level with suitable hoses connecting with the separator and instruments located on the spacecraft. The particulate matter is separated from entrainment and delivered to the experiments as a highly enriched aerosol mixture. Final separation at the experiments is by gravity.

A miniature aspirator has been developed for this specific application. It consists of a choked sonic jet in a constant area mixing chamber. This aspirator can be ejected from stowed position and will fall to ground due to gravity. It is discriminatory regarding size and density and will not pick up particles over approximately 100 μ . If several aspirators are ejected over a wide area, adequate sample volume is assured plus redundancy against component failure. The general scheme of multiple aspirators is depicted in Fig. 9.

The particulate matter is separated from the sterile gas with a cyclone separator. This device utilizes centrifugal and vortex action to enrich the mixture. The efficiency with which a cyclone separator will retain small-diameter

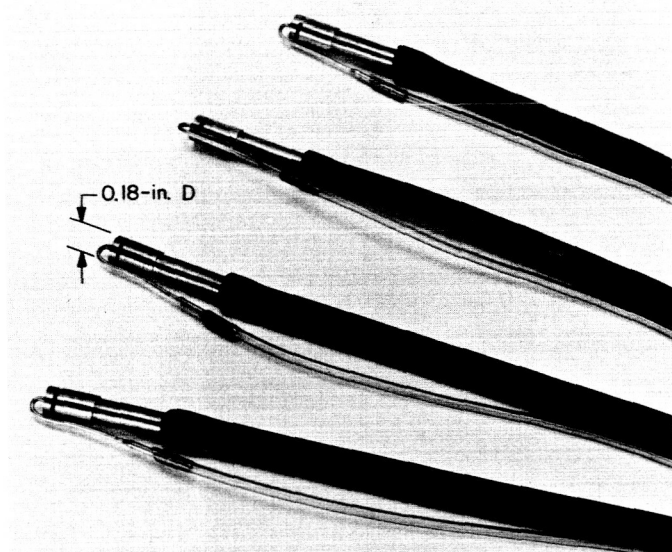


Fig. 9. Multiple aspirator system for sample collection

particles is important. Tests have been conducted using Fine Arizona Road Dust prepared by AC Spark Plug Company and having a size distribution of 40% under $5\ \mu$. This miniature cyclone captures nearly all particles above $5\ \mu$ and roughly half of the particles under $5\ \mu$. These tests are approximate, but such performance is considered acceptable. Submicron particles are vented from the cyclone separator.

The transparent model (Lucite) shown in Fig. 10 is $1\frac{1}{4}$ -in. at the largest diameter and it discharges to eight test chambers arranged in a circle.

A recent field test was made in the Salton Sea desert concurrent with a test of the Gulliver experiment. When operated over the identical area over which the "sticky strings" of this experiment had been pulled, the aerosol sample collector yielded an average of 180 mg per run. The sample included particles from 5 to $100\ \mu$. Further tests indicated that a realistic quantity of particulate matter can be collected from a hard, dry, and windswept area.

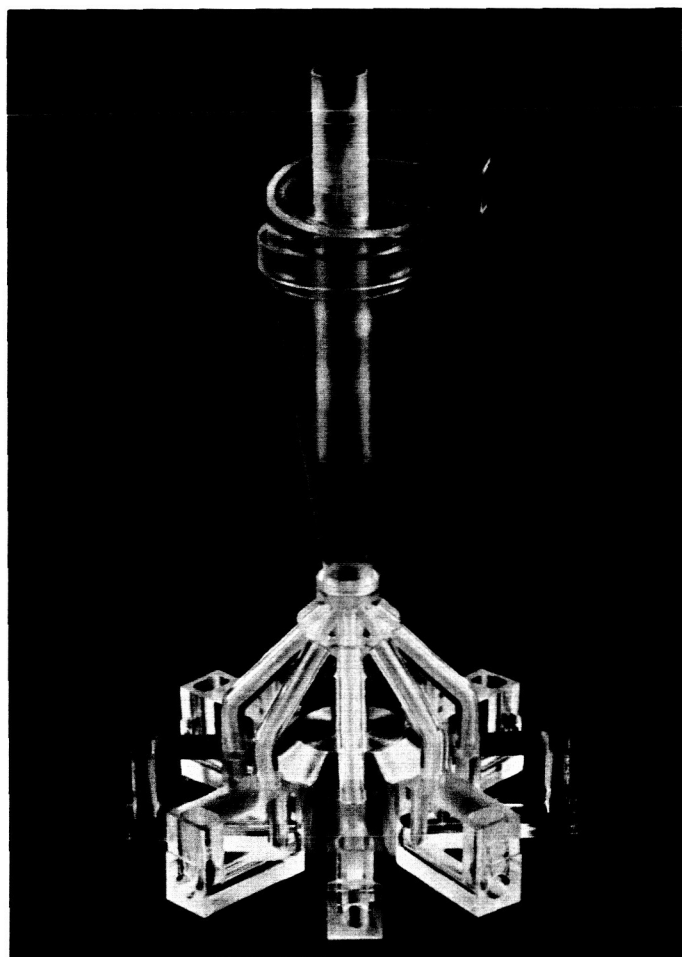


Fig. 10. Cyclone separator

Tests indicate that the aerosol sample collection technique is satisfactory providing either (1) the aspirator is moved along the ground, or (2) multiple aspirators are used. Further development tests are necessary to optimize the equipment for weight and size. Likewise, suitable materials capable of sterilization and long-time storage must be found. These considerations are largely influenced by constraints of the spacecraft and cannot be fully evaluated at this time.

Reference

1. Josias, C. S., and Lawrence, J., *An Instrument for the Measurement of Interplanetary Solar Plasma*, Technical Report No. 32-492, Jet Propulsion Laboratory, Pasadena (in preparation).

IX. Space Instruments Systems

A. An Intermittent Motion Digital Tape Recorder-Reproducer

The use of tape transport mechanisms in both satellite and space probe vehicles has been well established. Such devices have taken a wide variety of forms, and techniques for implementation of specific functions have been developed for each individual satellite or space probe. For the particular requirements of a digital, bit and word synchronous telecommunications system, several forms of recorder-reproducer systems have been developed to provide the necessary synchronous readout capability. However, such systems have concentrated on storing large quantities of data, and require either that the input data be in synchronous form, or require an additional element to moderate the asynchronous character of the input data. In addition, the typical interplanetary instruments in the particle area involve the use of devices such as ion chambers, G. M. tubes, etc., which are characterized by: (a) a very large dynamic range (1 count/hr-100,000 counts/sec), (b) asynchronous operation both in time and in data output characteristics, and (c) a relatively low instantaneous digital output rate (maximum = 20 bits/sec).

These requirements suggest the desirability of a device capable of recording, uniquely, one bit at a time, placing such recorded bits on magnetic tape in a regular fashion, and having the capability of synchronous readout. Further, the capability exists of fabricating such a device in a small enough package so that this device could be supplied to the individual experiment. Such a device would obviate the necessity for synchronous motor control or additional buffer elements, since it would be interrogated, on demand, and in the desired synchronous manner, at and by the telecommunication system basic transmission clock. To achieve these ends, the following basic system considerations were established:

- (1) The recorder-reproducer is to record and play back only upon receipt of a command pulse.
- (2) The maximum stepping rate is to be 200 steps/sec or greater.
- (3) Size and physical configuration shall be such as to store 10^5 bits.
- (4) No standby power shall be supplied to the recorder-reproducer.

- (5) Ultimate life expectancy of the recorder-reproducer is to be about 10^8 steps.

A contract was entered into by JPL with the Raymond Engineering Laboratory to develop this recorder-reproducer. The results of this development are described.

1. Implementation

a. General description. The completed feasibility model of the recorder-reproducer developed is shown in Fig. 1. A closer view of the actuator mechanism, which provides the intermittent motion, is shown in Fig. 2. This model is a stacked-reel design, powered by a 50-turn negator spring with a storage capacity of 60 ft of tape. The function of the actuator is to release a precise amount of tape, nominally 0.005 in., which results in a bit packing density of 200 bits/in., in a repetitive manner, past the record-playback head, at a rate up to 200 steps/sec, only upon receipt of an externally derived command pulse. When the sprocket wheel in the actuator is released, the initial tape motion is provided by the flexure of the flat springs seen in Fig. 1. This spring motion balances the negator which takes up the resultant slack and restores the system to its original position. A pulse of information is supplied to the recording head at the point of maximum tape velocity by the head.

b. Tape reels and negator spring. The recorder-reproducer employs a stacked-reel mechanism (Fig. 1), a simple and compact method for storing tape.

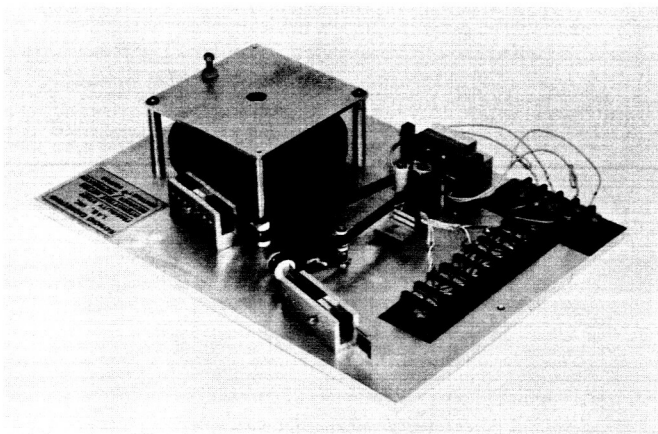


Fig 1. Completed intermittent motion digital tape recorder-reproducer

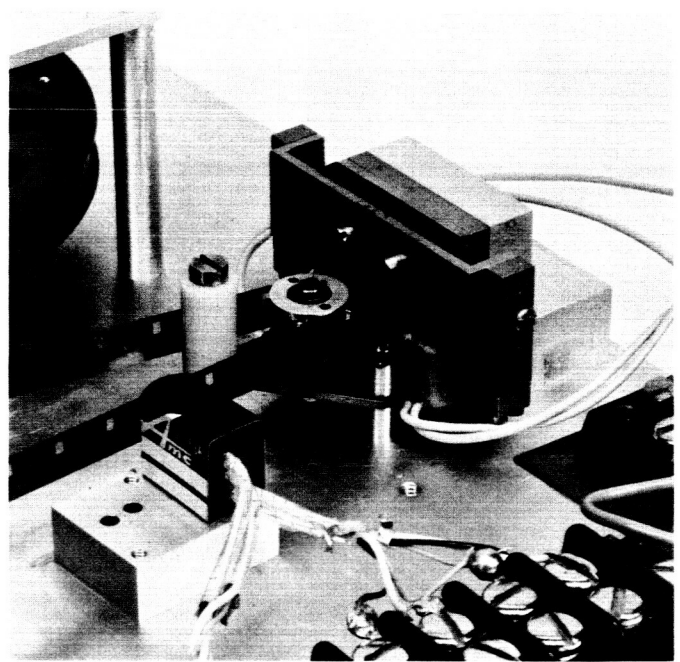


Fig. 2. Actuator—head area

Several systems were studied before choosing the final stacked-reel design. In each case, calculations were made of the reel diameters that would be required to satisfy two conditions:

- (1) The ratio of initial static tape tension (full storage reel) to final static tape tension (empty storage reel) should be less than 3:1. This ratio was established in order to maintain the minimum tape tension necessary to operate the recorder at the required stepping rate and yet not produce a tension high enough to produce sprocket hole distortion. The maximum load imposed on the tape sprocket hole edge, with a static tape tension of 3 oz, is 4000 psi, well below the yield point of 12000 psi of the tape backing material.
- (2) The number of negator spring turns must be less than 50. This is a practical limit set by the spring manufacturer.

In each case, the simplicity of the transport and its total inertia was evaluated. An estimate was made of the breadboard size and the possibilities of smaller flight models were considered. For the final configuration selected, the following calculations were performed:

Assume a $3\frac{1}{2}$ -in. storage reel outside diameter (OD) and a $2\frac{7}{16}$ take-up reel OD.

The area for 60 feet of 2-mil tape is:

$$(60) \times (12) \times (0.002) = 0.459 \text{ in.}^2$$

$$\text{Storage reel hub radius} = (1.750)^2 + 0.459 = 1.615 \text{ in.}$$

$$\text{Take-up reel hub radius} = (1.219)^2 - 0.459 = 1.01 \text{ in.}$$

The following tension formulas are obtained:

(1) With a full storage reel

$$T = M [0.992 - 0.572] = -0.42 M. \quad \text{Eq. (1)}$$

where

T = torque; M = torque output from negator

(2) With empty storage reel

$$T = M [0.821 - 0.62] = 0.201 M. \quad \text{Eq. (2)}$$

$$\text{Ratio} = \frac{420}{201} = 2.1$$

Number of tape wraps on storage reel

$$= \frac{\text{outside radius} - \text{hub radius}}{\text{tape thickness}}$$

$$= \frac{1.750 - 1.615}{0.002} = 67.5$$

(3) On tape-up reel

$$= \frac{1.219 - 1.010}{0.002} = 105$$

Required number of negator turns

$$= 105 - 67.5 = 37.$$

c. Tape tension springs. The functions of the tape tension spring in the take-up reel are: (1) to accelerate the tape and the escapement parts through a finite number of steps while the tape reels are accelerating, and (2) to provide a means for changing the tape level. The function of the tape tension spring in the storage reel area is to allow the tape to move a finite number of steps before the storage reel achieves steady-state velocity. The springs allow instantaneous stopping and starting of recorder. It will be noted that these springs are of a flat, cantilever type (Fig. 1). Such a spring is relatively flexible; its rate can be adjusted simply by moving the support point, and it will not rotate about its horizontal axis under the application of nonplanar torques. The following analysis was employed in the spring design.

The design equations for flat cantilever springs are

$$S = \frac{6 PL}{bh^2} \quad F = \frac{4 PL^3}{E bh^3}$$

where

S = stress in psi

P = load, lb

L = distance from load to support, in.

b = spring width, in.

h = spring thickness, in.

F = deflection, in.

E = Young modulus

These values were used in the typical analysis which follows:

$$E = 30 \times 10^6 \quad b = 0.500 \text{ in.}$$

$$L = 1.500 \text{ in.} \quad h = 0.015 \text{ in.}$$

Condition No. 1 (supply reel fully loaded): $P = 12.8 \text{ oz}$

$$F = \frac{(4) (12.8) (1.5)^3}{(30 \times 10^6) (0.500) (0.015)^3 (16)} = 0.200 \text{ in.} \quad \text{Eq. (3)}$$

Condition No. 2: sudden stop with a full take-up reel after moving at 500 steps/sec, constant deceleration.

It is assumed that the negator torque exerted on the storage reel will cause it to stop after the actuator has stopped the sprocket. The tape tension spring in this area will experience a sudden decrease in load. The deceleration time and the amount of tape unwound during this time are calculated in order to determine the spring travel. The equations used in the calculations are

$$F_{ISR} = \frac{ISR (\omega - \omega_0)}{t (R_{SR} + r_{SR})} \quad \text{Eq. (4)}$$

$$F_{ISR} = \frac{M}{R} = \frac{0.0404}{1.750} = 0.231 \text{ lb} \quad \text{Eq. (5)}$$

$$I_{SR} = 5.66 \times 10^{-5} \quad \text{Eq. (6)}$$

$$\omega_0 = \frac{v}{R} \frac{2.5}{1.750} = 1.43 \text{ rad} \quad \text{Eq. (7)}$$

$$t = \frac{I_{SR} (\omega - \omega_0)}{F_{ISR} (R_{SR} + r_{SR})} = \frac{(5.66 \times 10^{-5}) (1.43)}{(0.231) (1.750/12)} = 0.0024 \text{ sec} \quad \text{Eq. (8)}$$

$$\omega = \omega_0 t + t \quad 0 = 1.43 + (0.0024) \quad \text{Eq. (9a,b)}$$

$$= -\frac{1.43}{0.0024} = -596 \text{ rad/sec} \quad \text{Eq. (10)}$$

$$\theta = \omega_0 t + \frac{1}{2} \omega t^2 = (1.43)(0.0024) - \frac{1}{2}(596)(0.0024)^2$$

$$\theta = 0.000172 \text{ rad} \quad \text{Eq. (11)}$$

$$S = r\theta = (1.750)(0.000172) = 0.003 \text{ in.}$$

$$\quad \text{Eq. (12)}$$

where

I = mass moment of inertia

SR = storage reel

ω = angular velocity

t = time to move one step

v = velocity

θ = angle

Therefore, spring travel is negligible.

d. Electromagnetic actuator. The actuator element is the key to the proper functioning of this recorder-reproducer. The consistency of tape travel between steps over the total range of stepping speeds, the maximum stepping rate capability, the power consumption of the entire system, the lifetime in terms of number of steps to failure, all center upon this element.

The electromagnetic actuator (Fig. 2) consists of an armature, fabricated by sandwiching a pallet between laminations and pivoting the pallet on a shaft with a conical point on each end. The shaft is supported at each end by a pivot bearing consisting of four balls in a cup. The armature swings through a 6-deg arc between two pole pieces made from Allegheny Ludlum 4750 metal. A bobbin wound coil is located next to each pole face. The coils are connected in series and driven by a square wave pulse. An Indox permanent magnet is sandwiched between the middle and outer legs of the E-shaped actuator. The permanent magnet is magnetized across its faces rather than at its ends. The permanent magnet flux makes a closed loop path between the middle leg and one side of the "E," thus holding the armature against one pole face. To actuate this element, a positive pulse is applied to both coils (series-connected). This pulse produces a polarity in the left pole face which is opposite to the original permanent magnet polarity, and the armature and pole piece face repel each other. The coil on the right pole face creates an opposite polarity; therefore, the armature is attracted to it. After the coil pulses have been removed, there is a new permanent magnet circuit on the opposite portion of the E-shaped actuator. To move the armature back to its original position, a negative pulse is applied to the coils.

The required torque output of the electromagnetic actuator was calculated based upon a given distance and given travel time. A review of the preliminary design and magnetic circuit calculations were performed under contract to the Herbert C. Roters Company of New York. A sample calculation follows:

Calculation of torque required to accelerate

$$T = I\alpha,$$

$$T = 1.27 \times 10^{-6} \times 0.0525 \times 10^6 = 0.067 \text{ oz-in.}$$

The torque required to overcome friction (estimated as bearing friction) was given = 0.100 oz-in. Therefore, the total torque required to move the pallet 6 deg in 2 msec = 0.067 + 0.100 = 0.167 oz-in.

2. Testing Program

a. General. The testing program of the intermittent-motion recorder-reproducer was quite extensive. This testing program was necessary in order to obtain sufficient experimental data to determine the feasibility of such a device.

b. Friction forces. Probably the major unpredicted, and unpredictable element, involved in transporting the tape, are the friction forces encountered. Due to the several twists in the tape and the absence of precision bearing assemblies, for cost reasons, in the small rollers (Fig. 1) over which the tape passes, measurements of friction forces in the transport were greater than originally calculated. Since the tape tension established by the negator spring has to be within the elastic limits of the tape material, this tension, coupled with the high-friction forces, was not sufficient to unload the reels fully. Consequently, only one half of the total tape on the reels could be used. The measured friction forces are tabulated below:

Component	F, oz
Storage reel spring roller	0.19
Escapement and sprocket mechanism, top post roller heads	0.64
Take-up spring roller	0.18
Bottom post roller	0.36
Reels (2)	0.03
Total	1.4

c. Recording and playback measurements. The original goal of this program included a criterion for the recording and playback of a single pulse, or train of pulses, upon receipt of a command pulse and (suitably delayed) information pulse. Initial measurements of the playback system only with a prerecorded, constant frequency demonstrated that the existing actuator mechanism could step at a rate in excess of 200 steps/sec before successive steps melded into each other. Thus, one of the goals was achieved immediately. The next test was to record digital signals on the intermittent transport itself. Fig. 3 shows signals recorded and played back at 50 steps/sec and both demonstrates the stepping action and illustrates graphically several of the problems which were encountered. The following facts are evident:

- (1) A playback signal indeed exists for every step command pulse.
- (2) Each playback signal pulse corresponds exactly, plus the delay time, to each step command pulse.
- (3) Severe amplitude variations in the playback pulse exist.

- (4) The detailed form of each playback pulse does not correspond to that normally expected from such a signal.
- (5) The step command pulse radiates through the actuator to the playback head and severely corrupts the playback signal.
- (6) Baseline noise in the playback pulse train is evident.

Conditions 1-6 were noted at all stepping rates, up to and including the goal of 200 steps/sec. However, the mechanism operated at all rates up to and including 200 steps/sec.

d. Actuator and escapement mechanism life test. The life test was performed with a simple loop of tape engaging the mechanism. The actuator was operated at a rate of 200 steps/sec, for a continuous period of five days, before failure. This amounted to over 90,000,000 accumulated steps. Failure was due to the actuator armature pivot shaft becoming worn on both ends. The armature is held by an F-shaped bracket which contains the armature pivot shaft bearings. As the pivot shaft wore, the

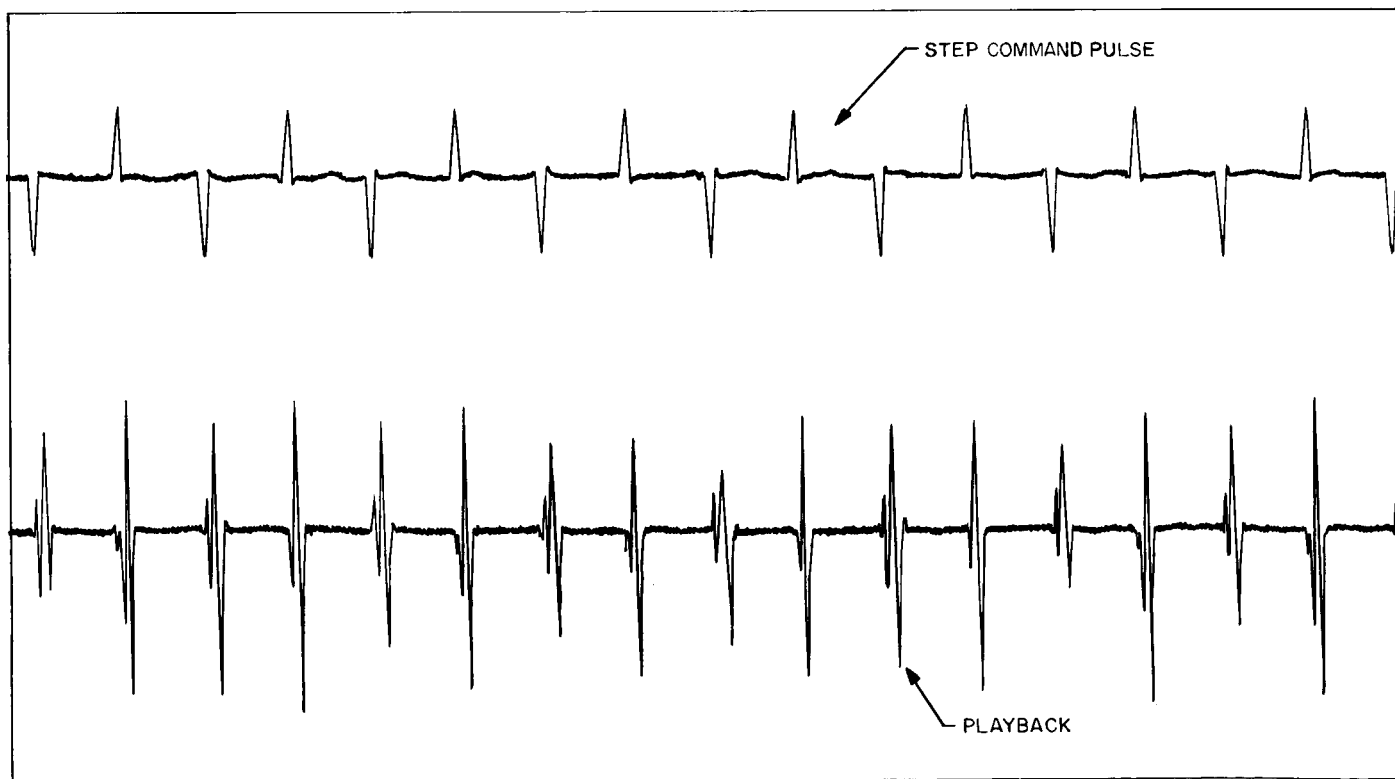


Fig. 3. Visicorder record of playback output at a rate of 50 steps/sec

clearance between the bottom lamination of the armature and the inside faces of the F-shaped bracket gradually decreased. Finally, the bracket face and the pallet face bottom (lamination) came into direct contact and the actuator magnetic force could no longer overcome the increased friction. The two worn ends of the armature pivot shaft, the worn wheel teeth, and the worn pole face are shown in Fig. 4.

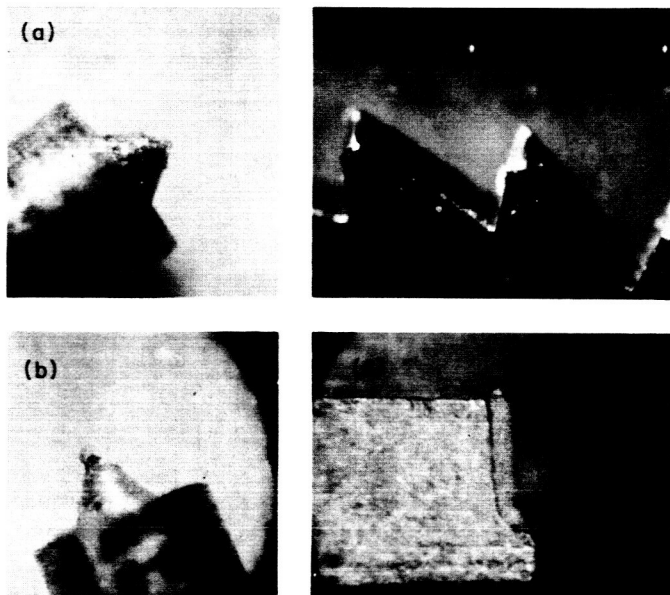


Fig. 4. Worn parts of actuator assembly: (a) armature pivot, point a, (b) armature pivot, point b, (c) wheel teeth, (d) pole face

3. High-Speed Photographic Analysis

A series of high-speed motion pictures were taken of important action to aid in the evaluation process. Pictures were taken of the escape wheel, the tape moving across the recording heads, upstream hair spring, and the downstream hair spring.

The motion pictures were made with the tape moving at 50 steps/sec and at 200 steps/sec. The camera was running at a rate of 3000 frames/sec. The motion pictures were analyzed in two different ways: (1) dynamically projected and studied visually; and (2) statically projected (frame by frame), and measurements of the displacement of moving parts of the mechanism were taken. Due to the relatively slow frame rate compared with the actuator speed ($1/3$ msec), accuracies are low in this measurement area. Errors in registration, projection and measurement of angular displacement of the rotary elements amount to a maximum of 15% in the relevant

curves. Analysis of these motion pictures revealed the following:

- (1) The action of the escape wheel was regular and consistent at 50 and 200 steps/sec, with some slight hesitation and bounce.
- (2) In the head area no ripples or liftoff of tape occurred.
- (3) In the hair springs, tape motion on rollers was readily detectable, but only an extremely small motion was noted in the springs.

Fig. 5 is a typical displacement curve, compiled by performing three separate measurements of each point of each picture and averaging the three points thus obtained to form the points through which the final curve was drawn. Figs. 6 and 7, respectively, are a typical velocity and an acceleration curve. The acceleration curve is de-

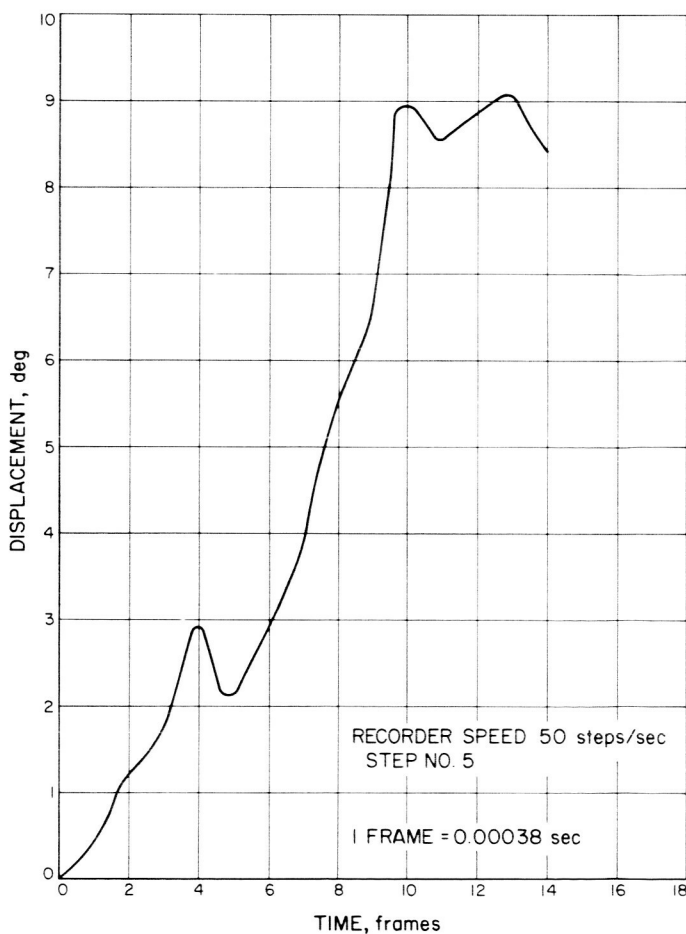


Fig. 5. Escape wheel displacement versus time

rived by differentiating the displacement curve. Examination of these curves indicates the nonuniform motion of the elements comprising the actuator, which indicates the presence of significant friction in the mechanism, bouncing due to improper damping of the pallet, nonuniformity of torque application to the escape wheel, and the presence of considerable backlash in the mechanism. The dimple in Fig. 8 between frame numbers 4 and 5 is direct evidence of backlash. The following summarized conclusions were drawn from these and visicorder measurements performed simultaneously:

- (1) Each step was consistent with all other steps photographed.

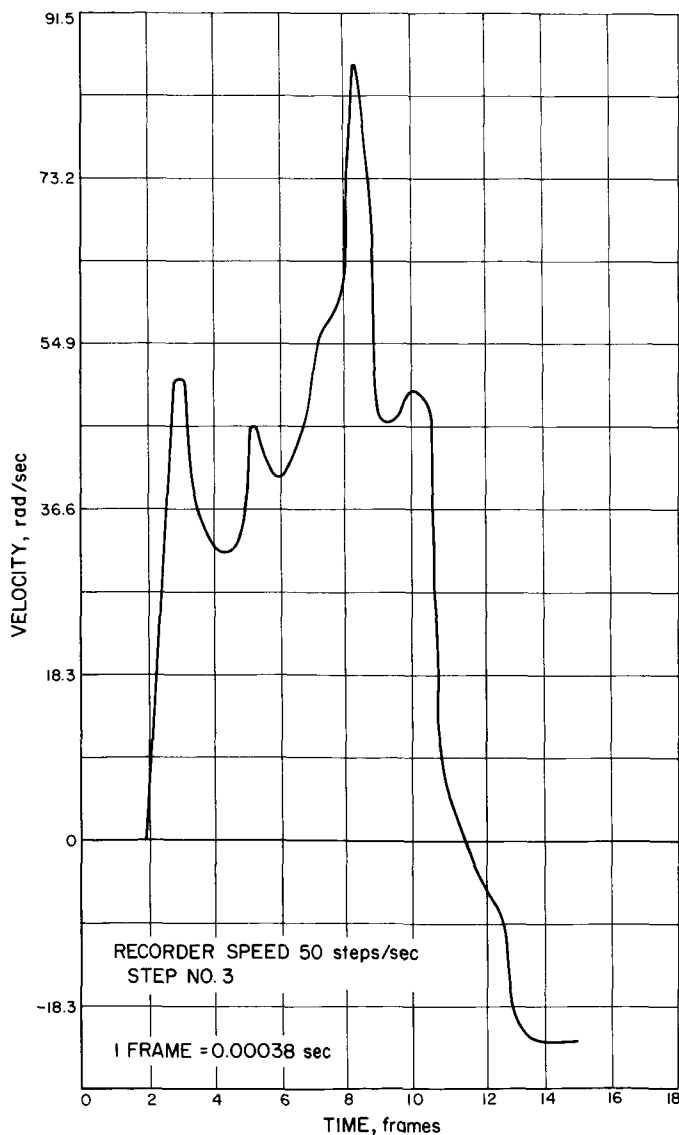


Fig. 6. Escapement velocity versus time

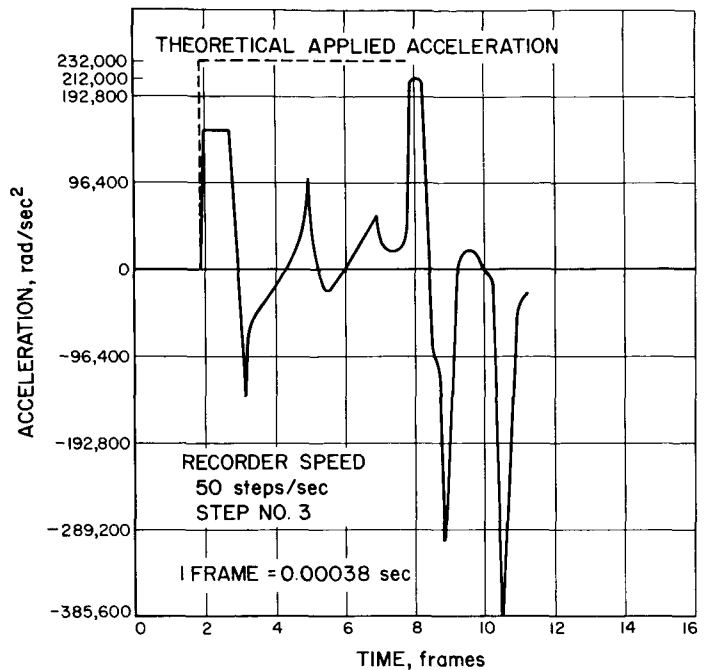


Fig. 7. Escapement acceleration versus time

- (2) The maximum stepping rate is 200 steps/sec.
- (3) If the system resonances and friction forces were to be changed, a significant increase in maximum stepping rate could be effected. Similarly, reducing or eliminating the pallet bounce would increase the stepping rate.
- (4) The severe variations in playback amplitude are caused by the high and varying friction forces encountered.
- (5) Careful orientation of the playback head with respect to the actuator windings, the addition of magnetic shielding, and the use of lower actuator currents are required to prevent the radiation of the step command into the playback head.

4. Conclusions

This study program has demonstrated the feasibility of an intermittent-motion tape recorder with stepping capability of zero to 200 steps/sec, with adequate storage and lifetime capabilities. Additionally, and most importantly, this study has shown the necessity for the development of such a device to be governed by very careful application of sound engineering techniques to reduce the friction forces and the nonuniform motions evidenced in the

important actuator element area. Care must be taken to use high-quality miniature bearings throughout the system. Additionally, a technique for tape handling must be developed to simplify the torturous path presently followed by the tape. It is further necessary, before continuing such a project, to develop measurement techniques several orders of magnitude more sensitive and accurate than those employed here for measuring: (a) the very small displacements of the hair springs; and (b) the motion of the pallet/escape wheel area.

B. Development of a Hysteresis-Induction Motor

1. Introduction

In SPS 37-23, Vol. VI, pp. 71-76 the general requirements of a motor for spacecraft tape recorder applications were listed with the advantages and shortcomings of both ac hysteresis-synchronous and dc motors. It was shown that the hysteresis-synchronous motor is the best suited (and most commonly used) for such applications. However, its low efficiency and low acceleration torque per unit of weight clearly indicate the desirability of a motor without these shortcomings. A modified hysteresis-synchronous motor, herein referred to as a hysteresis-induction motor, is currently under development. Preliminary test results indicate considerable improvement in acceleration properties and efficiency.

2. Basic Design Considerations

All ac motors embody the same basic stator design for generating a rotating magnetic field along the air gap by means of a one-, two-, or three-phase winding. Various rotor concepts can be combined into one unit, the performance of which can then reflect certain qualities of each concept. In the development presented here, characteristics of the hysteresis motor and the induction motor have been combined. The induction motor develops a high acceleration torque but loses its effectiveness at synchronous speed. Therefore, it is the logical complement of the hysteresis motor which has low acceleration torque but excellent performance at synchronous speed.

There are, however, certain obstacles to the effective merging of these two concepts:

- (1) The hysteresis and induction fields associated with the common rotor interfere, and it is impossible to calculate these fields for the various performance phases.
- (2) The high damping torque of an induction cage tends to cause its rotation to follow very closely the rotating magnetic field established by the stator winding. Ordinarily this may be considered an asset. However, in the case of squarewave excitation of the stator field, which is a significant convenience in spacecraft applications, this characteristic may lead to speed variations, e.g., a "cogging" effect. Calculations indicate that this effect may be of minor significance. Tests will be performed to confirm the calculations.

3. Rotor Design Considerations

One of the more important considerations in the design of a miniature motor is simplicity, not only for ease of construction, but also for providing reasonably good performance under a variety of operating conditions. Figs. 8 and 9 illustrate a rotor consisting of G.E. P-6 magnetic alloy laminations. These laminations have high hysteresis losses and therefore reflect the hysteresis motor concept. Embedded in the laminar structure is the induction cage. In order to provide reasonably smooth operation of the motor, as controlled by the hysteresis characteristics, the induction cage must be assembled into completely closed slots so that a smooth rotor surface results. However, closed slots produce a magnetic shunt to the stator field, thus tending to reduce the cage current. It is desirable, therefore, to minimize the thickness of magnetic material between the slots and the outside diameter of the rotor. In order to achieve this, the rotor laminations are punched slightly oversize and the cage holes are then bored. After assembly of the rotor the outside diameter is ground to the correct size.

Since the stator design is quite routine, it is not discussed. Its design parameters are, however, included in subsequent rotor calculations.

In order to reflect the desired hysteresis motor characteristics, the rotor yoke must have the same cross-section as the hysteresis ring of a conventional hysteresis motor.

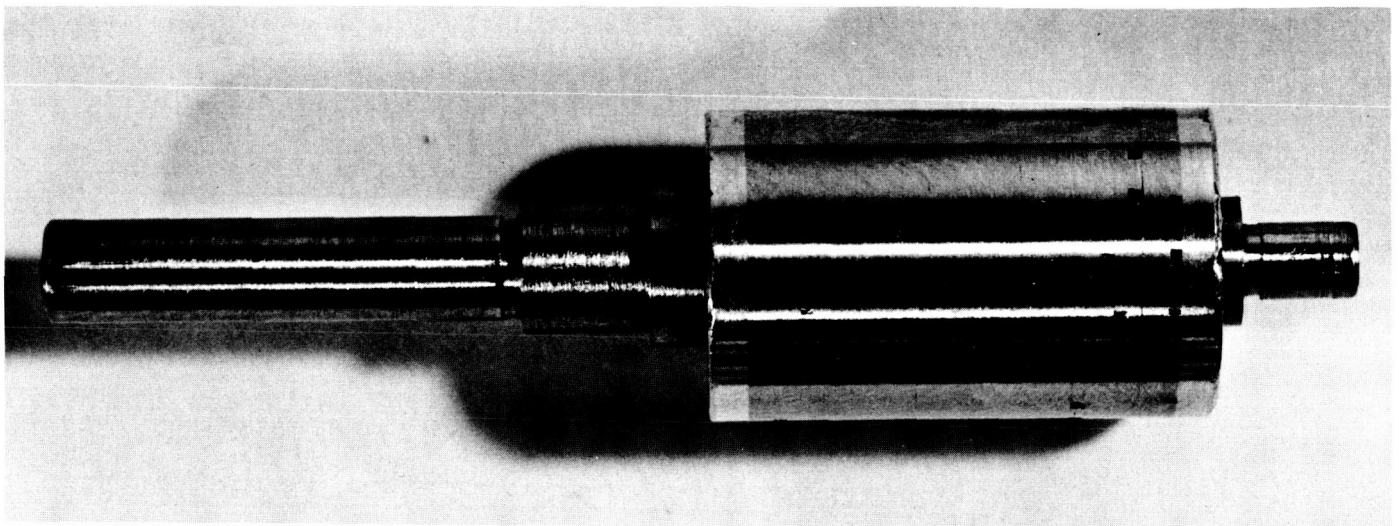


Fig. 8. Rotor of a hysteresis induction motor

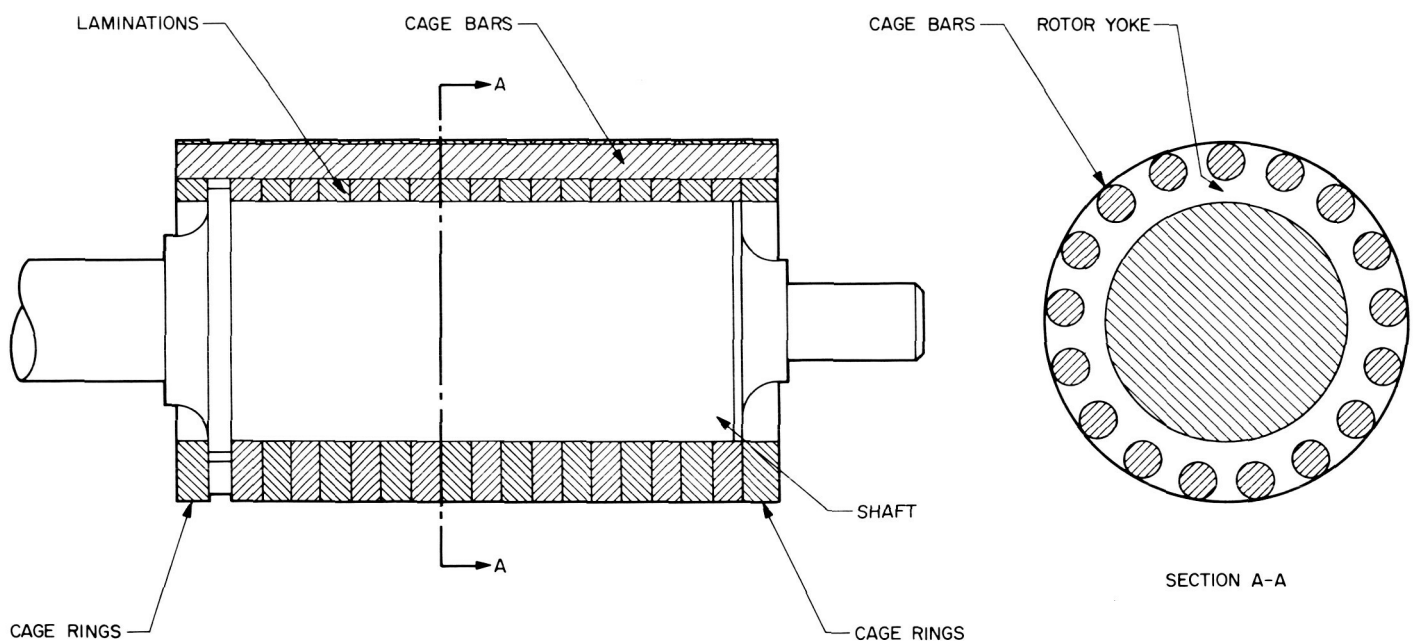


Fig. 9. Cross-section of a rotor of a hysteresis induction motor

This value is calculated on the basis of the amount of magnetic flux developed by the stator. Moreover, sufficient cross-section of hysteresis material must be provided between the cage bars in order to encourage the flow of flux into the rotor yoke. Considering only the hysteresis motor function, it is desirable to make both cross-sections of equal size.

During acceleration the magnetic fields generated by the cage currents will suppress most of the hysteresis fields. Therefore, for purposes of calculating acceleration

torque, it is assumed that the device is an induction motor. The torque is given by

$$T = \frac{M}{2\pi N} \frac{E_{20}^2}{\left[\frac{R_1'}{(1+\sigma)^2} + \frac{R_2}{S} \right]^2 + (\sigma X_2)^2} \frac{R_2}{S} \quad (1)$$

where

M = number of phases = 2

N = speed in rpm = 8000

E_{20} = voltage induced in cage at zero speed

R_2 = resistance of cage per phase

R'_1 = resistance of stator winding transformed to the rotor

σ = leakage coefficient for magnetic field $\simeq 0.2$

X_2 = rotor reactance

S = slip of the rotor ($0 \leq S \leq 1$)

The transformed stator resistance is given by

$$R'_1 = R_1 \frac{N_2}{\frac{4MP}{(W_1 \xi_1)^2}} \quad (2)$$

where

R_1 = resistance of stator winding = 46.4 Ω

N_2 = number of cage bars

W_1 = number of stator windings = 146

ξ_1 = phase-factor of stator windings = 1.0

P = number of pole pairs = 3

The number of bars of the cage is determined mainly by the field harmonics in the air gap. It can be shown theoretically that the number of cage bars N_2 , suitable for proper performance, must be 13, 17, 19, 23, etc. A number, $N_2 = 17$, was chosen for these calculations and on this basis the transformed stator resistance is

$$R'_1 = 1.54 \text{ m}\Omega$$

The rotor reactance is given by

$$X_2 = 0.79 \frac{f}{P} (\lambda_{N_2} + \lambda_{S_2} + \lambda_{02}) \cdot 10^{-7} \Omega \quad (3)$$

where

f = frequency = 400 cps

$$\lambda_{N_2} \simeq 0.66 + \mu_r \frac{d_B}{0.3 d_c} \quad (3a)$$

$$\lambda_{S_2} = \frac{0.0344 N_2 \tau_{pc}}{P L_2} \log_{10} \left(\frac{\tau_{pc}}{m + n} \right) \quad (3b)$$

$$\tau_{pc} = \frac{\pi}{2P} (D_r - n)$$

$$\lambda_{02} = \frac{0.1266 k_c \tau_p N_2}{28 P} \sum_{v=1}^{\infty} \left(\frac{1}{\frac{N_2}{P} [v \pm 1]} \right)^2 \quad (3c)$$

μ_r = relative permeability of iron in the bridge between the cage and the air gap $\simeq 50$ for P6 alloy.

d_B = bridge thickness

d_c = diameter of the rotor slots

L_2 = length of the rotor lamination stack about equal to that of the stator lamination stack
 $L_1 = 0.55$ in.

m = axial width of cage rings

n = radial width of cage rings

D_r = outside diameter of rotor = 0.374 in.

k_c = Carter's factor = 1.0

τ_p = length of a pole on the air gap = 0.196 in.

δ = length of air gap = 0.004 in.

From Eqs. 1 to 3, several conclusions can be drawn without further calculations. As σ is a constant and the torque T is to be as large as possible, X_2 must be as small as possible [Eq. (1)]. Examination of Eq. (3) reveals the following requirements:

d_B = as small as possible.

d_c = as large as possible.

Other design parameters are fixed or have rather minor effects on the torque. Both the above requirements conform very well to previously derived requirements, and the diameter of the cage bars can thus be adjusted so as to achieve equal cross-sections for the main flux throughout the rotor. In order to keep d_B as small as possible, the induction cage will be placed as closely as possible to the outside diameter. This placement results in the following dimensions:

$$d_B = 0.001 \text{ in.}$$

$$d_c = 0.0375 \text{ in.}$$

$$m = 0.032 \text{ in.}$$

$$n = 0.07 \text{ in.}$$

With these values the rotor reactance becomes

$$X_2 = 0.074 \text{ m}\Omega$$

$$\sigma X_2 = 0.0148 \text{ m}\Omega$$

It can be seen that for all values of R_2 and S

$$\left[\frac{R_1'}{(1+\sigma)^2} + \frac{R_2}{S} \right]^2 \gg (\sigma X_2)^2$$

This condition is only true for very small motors. Eq. (1) can be simplified by omitting the rotor reactance

$$T \simeq \frac{M E_{20}^2}{2\pi N} \times \frac{\frac{R_2}{S}}{\left[\frac{R_1'}{(1+\sigma)^2} + \frac{R_2}{S} \right]^2} \quad (4)$$

or

$$T \simeq C \frac{R_2 S}{\left[\frac{R_1' S}{(1+\sigma)^2} + R_2 \right]^2} = C f(S) \quad (4a)$$

Fig. 10 shows the acceleration torque versus speed characteristics for different values of R_2 , depending on whether the cage is made of copper, brass, or bronze. The maximum values are independent of the cage resistance but occur at different speeds. The bronze cage produces the highest stall torque, while the copper cage develops best torque near synchronous speed. The brass cage develops high torque during most of the acceleration phase, thus achieving minimum motor start time.

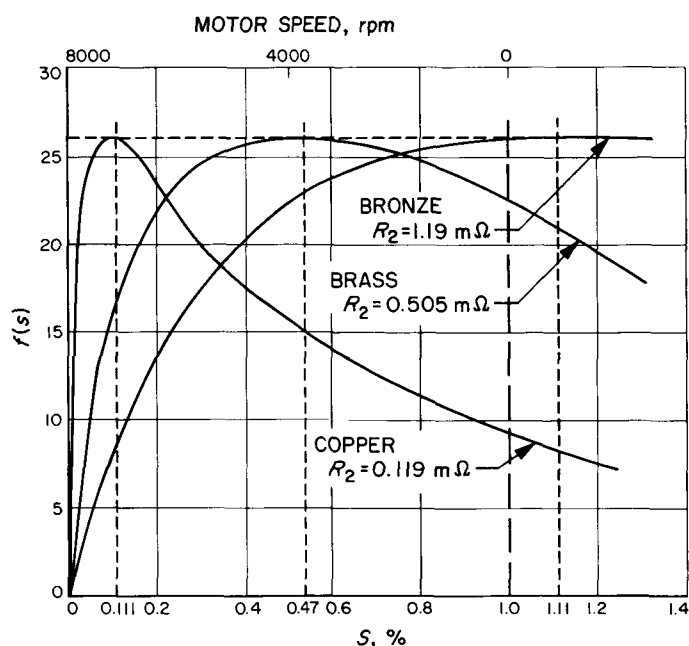


Fig. 10. Calculated torque versus motor speed of the induction motor for various cage materials

Another important property can be derived from Fig. 10. The copper cage will develop significant synchronous torque at such low values of slip as may be developed by variations in the angular velocity of the rotating field. Utilizing square wave power, the copper cage motor can thus be expected to have much more jitter than the bronze cage motor. For this reason the bronze cage is the most logical choice for our application.

4. Performance

The design of the rotor is such as to allow its installation into the stator of an available hysteresis-synchronous motor. In this way a performance comparison can be easily made between a hysteresis-synchronous and a hysteresis-induction motor.

In grinding the rotor diameter for optimum air gap, the first test point revealed typical performance of an induction motor running with large slip and negligible hysteresis torque. With further increase in air gap the hysteresis torque appeared and the performance approximated that anticipated.

Fig. 11 illustrates, for the same voltage, maximum pull-out torque and 5% slip-torque versus air gap. The pull-out torque is a function of the hysteresis effect only, whereas the 5% slip-torque is a function of both the hysteresis and induction effects. It can be concluded that with an air gap of less than 0.0043 in. the motor performs as an induction motor. The acceleration torque is equal to, or greater than, the pull-out torque. The motor will start quickly but may be unable to pull heavy loads into synchronism. With an air gap in excess of 0.0043 in. the

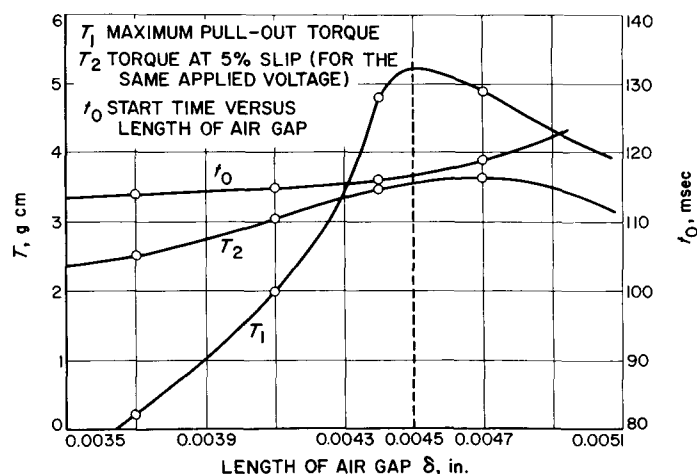


Fig. 11. Torque and start time versus length of air gap

motor acquires the characteristics of a synchronous motor having a pull-out torque in excess of its 5% slip torque. A distinct pull-into-synchronism action occurs, and subsequent rotation is free of hunting. Optimum performance is achieved with an air gap of 0.0045 in. As input power is only slightly affected by increasing the air gap within the considered range, the curve T_1 also represents the efficiency of the motor at pull-out torque, and curve T_2 the efficiency at 5% slip.

The start time is increased with the increased air gap; however, it is still much shorter than that of the original motor.

5. Comparison of the Hysteresis-Induction Motor with a Conventional Hysteresis-Synchronous Motor

The hysteresis-induction motor has about the same pull-out torque as the original hysteresis-synchronous motor, but has a somewhat greater acceleration torque. The hysteresis-induction motor draws less current, and consumes less power during synchronous operation. This is attributable to the influence of the induction cage on the hysteresis material during acceleration. Table 1 compares some characteristic properties of both motors. All

measurements were performed with 400-cps, 2-phase, squarewave power.

6. Further Work Anticipated or in Progress

In an attempt to separate the acceleration torques of hysteresis and induction motors, an additional rotor lacking the induction-cage was built. It was, however, impossible to separate the two torques because of the interaction of the two magnetic fields. The motor constructed without a cage showed some improvements over the original hysteresis motor, indicating that a laminated hysteresis rotor seems to be superior to a rotor using a solid ring. This fact cannot be explained satisfactorily, but in this respect the effect of harmonics seems significant. This problem is being investigated.

A complete motor reflecting the design considerations herein presented is being manufactured by the Gaylord Rives Company as a flight-prototype unit. The new motor will be considerably smaller in size and consume less power than those currently used in miniature tape recorders. Improvements in start-time or efficiency or both over currently used flight units are anticipated. Cogging effects occurring with low frequency drive signals will be evaluated by measuring signals actually recorded on the tape under these conditions.

Table 1. Comparison of the hysteresis-induction motor with a conventional hysteresis motor

Parameter	Hysteresis motor	Hysteresis induction motor (0.0045-in. air gap)
Maximum pull-out torque	5.27 g cm	5.2 g cm
Voltage resulting in maximum pull-out torque	30 v rms	32 v rms
Stall torque at same voltage	5.8 g cm	7.1 g cm
Input power at pull-out torque	2.33 w	1.79 w
Efficiency	28 %	36 %
Current per phase at maximum pull-out torque	70.5/77.5 mA	58/64.5 mA
Start time without load, using the same bearings	129 ms	117 ms

C. Mariner C Scientific Instrumentation

1. Science Subsystem

The *Mariner C* (Mars mission, 1964) science subsystem is composed of instruments and ancillaries selected to meet the mission objectives, namely, to make planetary observations and perform field and particle measurements in interplanetary space during the trip and in the vicinity of Mars. These observations and measurements are intended to investigate the topography of Mars, its possible magnetic field and trapped radiation belts, the atomic oxygen and hydrogen content of its outer atmosphere, and the dust particles that may be trapped in close proximity to the planet. The instruments and their ancillaries designed to accomplish these purposes are listed and briefly described in Table 2 and Fig. 12. All instru-

Table 2. Mariner C instruments and ancillaries

Description	Spacecraft unit number	Weight, lb	Power, w	Look angle	Instrument		
					Purpose	Number of sensors	Output data
Cosmic ray telescope	21	2.7 ^a	0.300 ^a	30 deg 1/2 \ominus along + z axis	To detect and measure trapped corpuscular radiation in the vicinity of Mars. To measure the flux and energy of alpha particles and protons as a function of position and time in interplanetary space.	1 sensor, 3 detectors in telescope	Digital (4)
Cosmic dust detector	24	2.3 ^a	0.215 ^a	Into plane of ecliptic in direct and retrograde motion	To make direct measurements of the dust particle momentum and mass distribution in the Earth-Moon, Mars-Deimos-Phobos, and interplanetary regions.	2 sensors	Digital (1)
Trapped radiation detectors	25	2.1 ^a	0.36 ^a	3 sensors 70 deg to probe-Sun line, 30 deg 1/2 \ominus 1 sensor 135 deg to probe -Sun line, -30 deg 1/2 \ominus	To search for magnetically trapped particles in the vicinity of Mars and, if found, make a preliminary estimate of their distribution, energy spectra, and identity. To monitor solar cosmic rays and energetic electrons in interplanetary space, to determine their angular distribution, energy spectra, and time history.	4 sensors	Digital (5)
Ionization chamber	26	2.6 ^a	0.5 ^a	Omnidirectional	To detect and measure the average omnidirectional flux of corpuscular radiation in regions between the Earth and Mars. To measure the average specific ionization attributable to this flux. To measure the omnidirectional flux and specific ionization of charged particles which may be trapped in the vicinity of Mars.	2 sensors	Digital (2)
Plasma probe	32	6.0	2.6 ^a average, 2.9 ^a peak	30 deg 1/2 \ominus , 10 deg from probe-Sun line	To measure the spectral distribution, flux density and time history of the positively charged solar plasma traveling outward from the Sun and to correlate these measurements with those from the magnetometer.	1 sensor (3 sections)	Pulse width (1)

Magnetometer	33	5.2	5.5	1 sensor along z axis, 1 sensor along y axis, 1 sensor along x axis	To investigate the existence of a Martian planetary field and determine its characteristics as a function of direction, magnitude, multipolarity, and orientation with respect to the planetary rotational axis. To investigate the interaction between planetary and interplanetary magnetic fields. To measure the magnitude and direction of the steady and slowly varying components of the interplanetary magnetic field and to determine its variation with heliographic altitude and longitude.	3 sensors	Pulse width (3)
Ultraviolet photometer	34	5.5	3.5 average, 4.5 peak	1.25 deg 1/2 ▽	Measurement of atomic hydrogen (1216 Å) and atomic oxygen (1300 Å) radiation in the outer atmosphere of Mars during the encounter period.	3 sensors	Pulse width (2)
Television	36	11.73 ^a	9.0	1.05 deg × 1.05 deg	To make preliminary topographic reconnaissance of portions of the surface of Mars. To attain an improved knowledge of areas of possible living matter. To obtain additional data on the Martian surface reflectivities so that the design of future systems will be enhanced.	1 sensor, 2 alternate color filters	Digital (3), pulse width (1) sequenced
Ancillary							
Data automation system	20	10.66 ^a	2.10 average during cruise, 4.26 average during encounter, 8.0 peak during encounter		The DAS provides the sequencing, processing, storage, buffering, and encoding necessary to realize the optimum scientific value of each instrument. The DAS also performs certain engineering measurements in addition to those made by the spacecraft data encoder.	None	See Fig. 13
Scan system	31	5.65 ^a	3.0 (2400 cps) 3.5 (400 cps)		The scan system is used to point the television and ultraviolet photometer sensors at a point on the planet that is dependent upon the bisector of radiation and the trajectory of the spacecraft.	1 sensor	Pulse width (1)
Narrow angle Mars gate	7MG1	0.20 ^a	Included in DAS power requirement (~0)	2.5 deg × 1.5 deg	Serves to trigger the DAS into the television sequencing mode. In this sense it serves as a backup to the TV.	1 sensor	None
^a Measured values, no cabling harnesses included.							

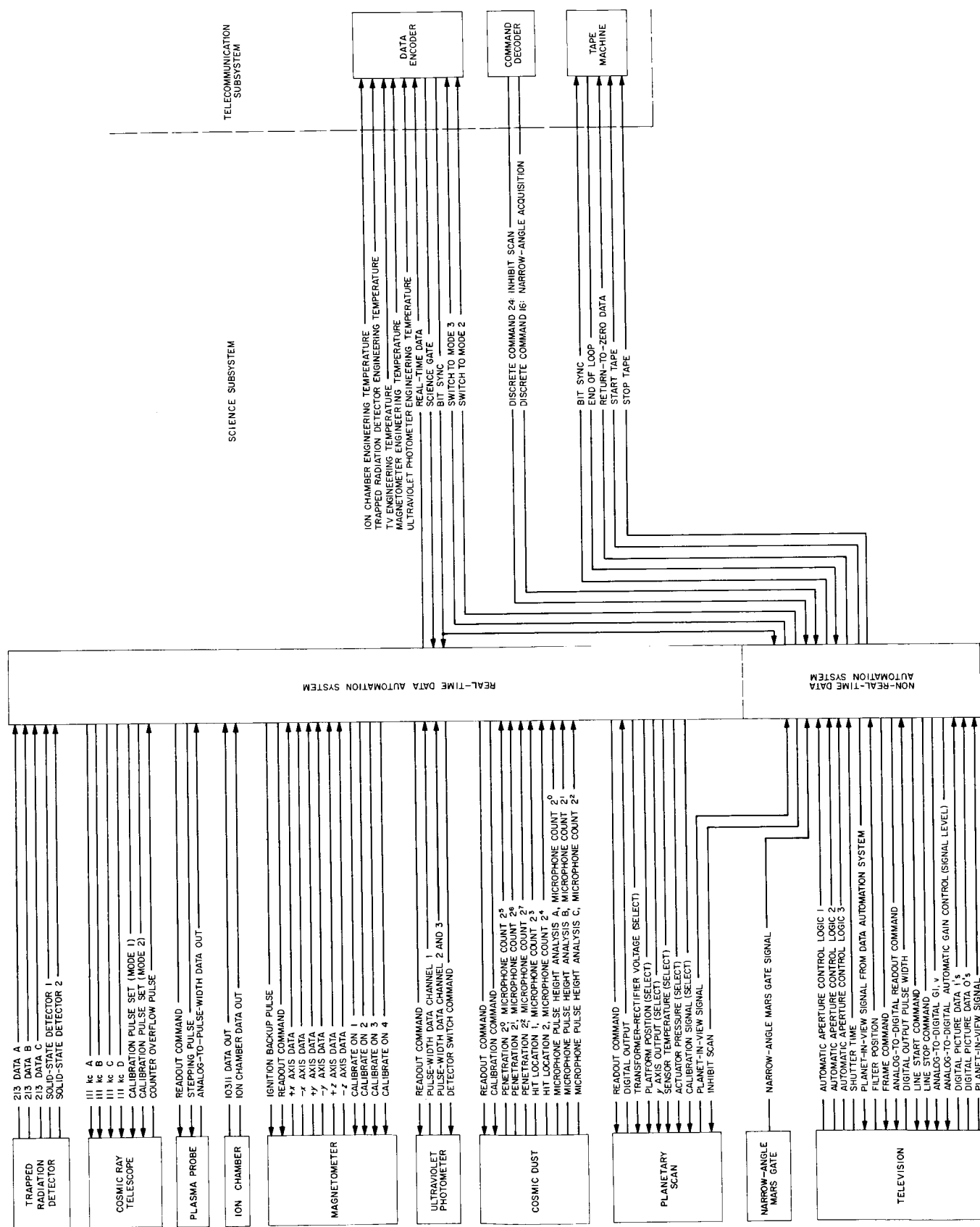


Fig. 12. Mariner C science subsystem functional block diagram

ments, except the television and ultraviolet photometers, are capable of making measurements during the cruise portion of the flight; they will be programmed to take interplanetary data concerning solar plasma, micrometeorite, magnetic field, and energetic particle distribution in space. The experiments to be conducted with the instruments in Table 2 are under the direction of the principal investigators shown in Table 3.

a. Project and subsystem requirements. In order to communicate the project requirements, in terms of documentation, instrument quality, testing, delivery schedule, etc., a JPL document entitled "Procedures and Requirements for Scientific Instruments, *Mariner Mars '64*," (EPD-59) was written. The requirements stated therein, except as specifically waived, are binding on all equipment, flight or OSE, produced or contracted for by the Space Sciences Division.

Some of the ground rules established for this project were generated by the Project Office and others are required by the Space Sciences Division in order to control the design and development of the science subsystem. The more significant of these ground rules are listed below.

- (1) Redundancy shall be included so that a failure of the scan system to start wide angle scanning or to stop scanning after acquisition cannot abort the mission.
- (2) The science subsystem must be capable of an operating test on the launch pad prior to liftoff.

Table 3. Mariner C principal investigators

Instrument	Principal investigator	Affiliation
Cosmic ray telescope	J. Simpson	University of Chicago
Cosmic dust detector	M. Alexander	Goddard Space Flight Center
Trapped radiation detector	J. Van Allen	State University of Iowa
Ionization chamber	H. Neher	California Institute of Technology
Plasma probe	H. Bridge	Massachusetts Institute of Technology
Helium magnetometer	E. Smith	Jet Propulsion Laboratory
Ultraviolet photometer	C. Barth	Jet Propulsion Laboratory
Television	R. Leighton	California Institute of Technology

- (3) All scientific data taken during the encounter period shall be stored and played back to Earth as many times as practicable after encounter. In addition, selected measurements required for engineering evaluation of the instruments or data interpretation shall be added to the encounter mode data and sent back in real-time by the telemetry system.
- (4) A components parts screening program for all science subsystems is a project requirement.
- (5) The helium magnetometer is to be located as far as possible from possible sources of permanent or slowly varying (< 10 cps) magnetic fields.
- (6) Complete spare units are required for the planetary scan system, data automation system (DAS), and television system. Selected spares are optional for the remainder of the science subsystem.
- (7) A complete science subsystem test must be accomplished prior to delivery of that subsystem to the Spacecraft Assembly Facility.

b. Functional operation of the subsystem. The spacecraft is launched in Data Mode 2 with the science subsystem turned off. When the shroud is separated, the cruise or real-time data automation system (RT-DAS) and the interplanetary instruments are energized. The data from these instruments are handled as shown in Fig. 13a.

In Data Mode 1 no science data will be transmitted, although the RT-DAS will continue to sample the instruments.

The initiation of the encounter mode by the central computer and sequencer (CC&S) accomplishes the following:

- (1) The television (TV), ultraviolet photometers (UV), non-real-time data automation system (NRT-DAS), planetary scan system (PSS), and tape recorder (TR) are energized and the DAS sequences the TV in a normal operating mode without issuing start/stop commands to the tape recorder.
- (2) The protective cover is removed from the TV, UV, and PSS sensors.
- (3) The science subsystem data format changes so as to incorporate the UV data in the 280 bits allotted

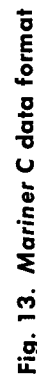


Fig. 13. Mariner C data format

to science measurements in Data Mode 2. This is shown in Fig. 13b.

The PSS then scans plus and minus 90 deg from its normal or stowed position. When the planet is acquired, the following events occur:

- (1) The PSS tracks the planet to insure that the platform continues to point at the bisector of brightness defining the location of Mars.
- (2) An output from the PSS through the DAS to the data encoder initiates Data Mode 3.

When the edge of the lighted disk comes into view of either the television or narrow angle Mars gate, the DAS is triggered into the science encounter mode. The DAS waits until the beginning of the next standard sequence and then starts the recording cycle. This sequence is illustrated in Fig. 13c. Note that all science data taken during encounter are stored on magnetic tape. The measurements made by the RT-DAS are sent back via the telemetry channel and also transferred to the NRT-DAS for storage. Scan motion is inhibited during this mode.

The science encounter mode and spacecraft Data Mode 3 are terminated when the second end of tape marker occurs. The DAS also contains a stop record circuit. This provides sufficient redundancy to insure that the recording sequence will be terminated.

The spacecraft then returns to Data Mode 2, but the science subsystem stays in the modified encounter mode so that adequate coverage of the outer atmosphere of Mars may be obtained by the UV photometers. A preset time later, nominally 6½ hr, the encounter instruments and NRT-DAS are de-energized and the science subsystem reverts to the standard cruise mode.

The playback of stored science data is initiated by CC&S command or discrete command (Ground Command). The science instruments and RT-DAS are switched off, Data Mode 4 is initiated, and stored data are transmitted to Earth.

The pictures are transmitted individually and between each picture the data encoder switches to Data Mode 1 so that engineering telemetry can be received and the condition of the spacecraft evaluated.

2. Science Data Automation System

The science data automation system (DAS) has the following general constraints and requirements:

- (1) To control and synchronize the science instruments within the DAS timing and format structure so that the instrument internal sequencing is known, and to send such commands to the instruments as are required.
- (2) To provide the necessary instrument sampling rates—both simultaneous and variously sequential.
- (3) To perform the necessary conversions and encoding of the several forms of science data and place them in a suitable format.
- (4) To buffer the science data, which occur at different and sporadic rates, and send them to the telemetry data encoder at several, constant specified rates.
- (5) To issue to and receive commands from other subsystems aboard the spacecraft which pertain to the operation of the science subsystem.

The DAS is divided into two electrically and physically separable units: the real-time (RT) DAS and the non-real-time (NRT) DAS. The entire DAS subsystem consists of: (1) the RT DAS, packaged in two 1½ × 6 × 7 in. chassis; (2) the NRT DAS, packaged in one 1½ × 6 × 7 in. chassis; (3) two identical 1320-bit core buffer memories which are used in conjunction with the NRT DAS and are housed in one 1 × 6 × 6 in. chassis; and (4) electrically separate ac to dc power converters for the RT DAS, and the buffers and NRT DAS, which are both packaged in one 1½ × 6 × 6 in. chassis.

The complete subsystem weighs approximately 10 lb and consumes about 4 w of spacecraft power in Mode 2 and about 9 w in Mode 3.

The RT DAS is mechanized primarily for the cruise or interplanetary instruments, whereas the NRT DAS is mechanized primarily for the planetary instruments. However, the RT DAS handles the ultraviolet photometers, which are planetary instruments, and does encode some television performance data; and the NRT DAS stores all of the RT data on the *Mariner C* tape machine during encounter to preclude the loss of real-time data in the event of loss of real-time transmissions at that time. A block diagram of the DAS is shown in Fig. 14.

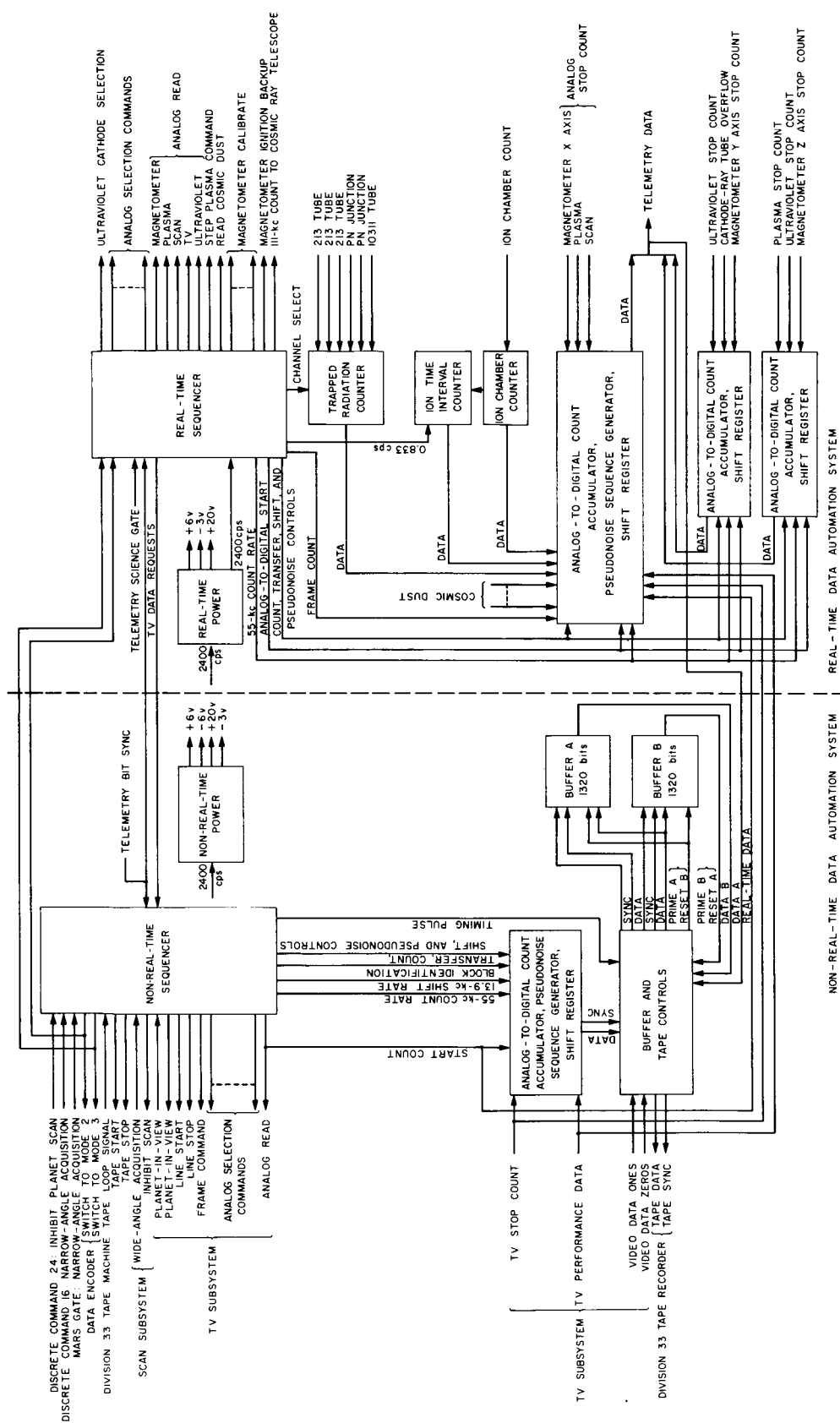


Fig. 14. Mariner C DAS block diagram

The DAS handles data from nine science instruments and communicates with five other subsystems aboard the spacecraft. All signals to and from the DAS are transformer-coupled, with two exceptions, to eliminate ground loop or common mode noise problems. Only the digital status data from the television subsystem and the channel selection signal to the ultraviolet photometers are directly coupled to the DAS.

a. Real-time format. The RT format is shown in Fig. 15. Although the science data words are of various lengths, from 1 to 20 bits, the DAS word length is 10 bits. There are, therefore, 28 words (280 bits) in the Mode 2 (cruise) format and 42 words in the Mode 3 format, of which 14 are encounter-oriented. The RT DAS is mechanized in such a fashion that it always operates as though it were in Mode 3. Thus, the dormant encounter instruments are sampled throughout Mode 2 even though the telemetry data encoder does not accept these 14 words. In this manner the DAS format is not changed for Mode 3; it is merely expanded by appending the 14 encounter-oriented words.

However, the DAS format is modified when the NRT power is on; this event gates ultraviolet data into Words 24 through 27 in place of one magnetometer and one plasma readout. The displaced magnetometer and plasma readings are regained during Mode 3 when they appear in Words 32 through 35.

The RT DAS contains three output counter-shift registers. These registers enable the DAS to make analog conversions of the three axes in the magnetometer simultaneously, thereby eliminating the correlation ambiguities inherent in making successive samples of the three axes. A magnetometer reading is thus taken at essentially one point in space instead of being spread out over several kilometers. In addition, three output registers provide an element of redundancy to the system.

Since the RT DAS is synchronized to the telemetry bit rate, a change in the bit rate will only compress or expand the time scale of the DAS format.

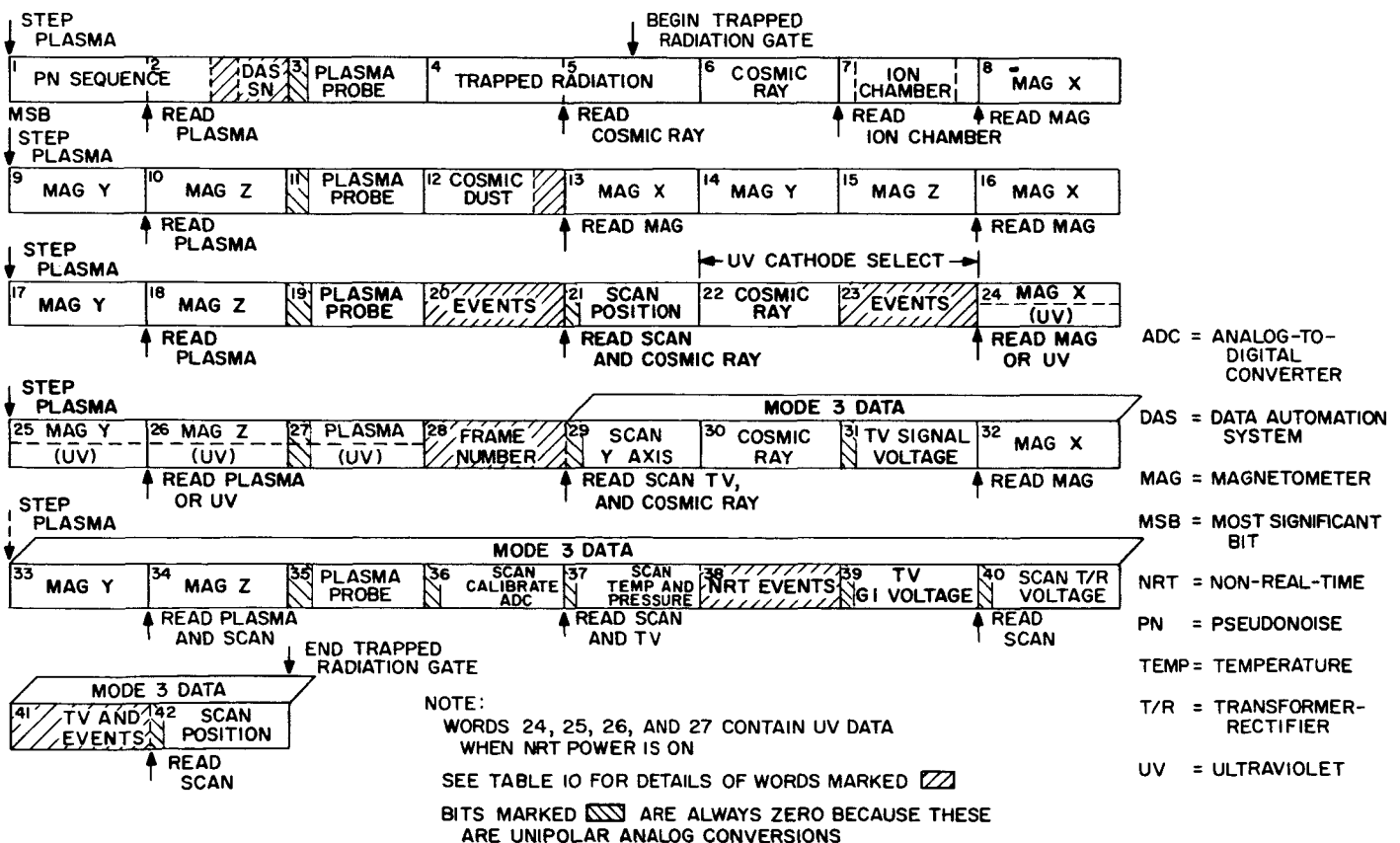


Fig. 15. Mariner C DAS real-time format

Parity is omitted in the DAS format for several reasons. It would consume 10 to 20% of the available channel capacity; it would emasculate the format. Past experience has shown that any parity error received from the spacecraft would be ignored in favor of the performance of the data in the context of its day-to-day and month-to-month behavior; and any data which appear to be anomalous would be disregarded even if there were no parity error.

Every word and bit which could otherwise be spare, is used as indicated in Table 4 to give as much information about the operation of the science subsystem as pos-

sible. Each frame of RT science data will contain approximately 42 bits, which are known or are predictable a priori in Mode 2; an additional 27 bits are added in Mode 3. The known bits include: (1) 15 bits of pseudo-noise (PN) sequence for the identification of science data; (2) 3 bits of DAS serial number to preclude any ambiguity when more than one spacecraft is being tracked at one time, and to furnish each system with a distinguishable mark for the purpose of test history; (3) 11 bits of time and frame number to uniquely identify each frame for recurring periods of 28 $\frac{1}{2}$ hr; (4) 13 sign bits which are always zero because of unipolar analog conversions; and

Table 4. *Mariner C* DAS real-time format details

Bit	Data	Bit	Data
Word 2		Word 23	
1 ^a	PN sequence	Reserved for DAS power voltage	
2	PN sequence		
3	PN sequence		
4	PN sequence		
5	PN sequence		
6	Wide-angle acquisition	Word 28	
7	Narrow-angle acquisition	1 ^a	Calibrate clock
8	DAS serial number	2	Calibrate clock
9	DAS serial number	3	Calibrate clock
10	DAS serial number	4	Calibrate clock
Word 12		5	Calibrate clock
1 ^a	Cosmic dust	6	Calibrate clock
2	Cosmic dust	7	Calibrate clock
3	Cosmic dust	8	DAS frame number
4	Cosmic dust	9	DAS frame number
5	Cosmic dust	10	DAS frame number
6	Cosmic dust	Word 38	
7	Cosmic dust	10 bits of NRT PN sequence from buffer output	
8	Cosmic dust		
9	Calibrate		
10	Calibrate clock		
Word 20		Word 41	
1 ^a	Magnetometer calibrate 1	1 ^a	TV shutter time
2	Magnetometer calibrate 2	2	TV automatic aperture control 3
3	Magnetometer calibrate 3	3	TV automatic aperture control 2
4	Magnetometer calibrate 4	4	TV automatic aperture control 1
5	Planet-in-view (Mars gate)	5	TV planet-in-view
6	Planet-in-view (scan)	6	TV filter position
7	NRT power on	7	Inhibit scan
8	Cosmic ray calibrate	8	End of tape marker/TV frame start
9	Cosmic dust calibrate	9	Tape start/stop
10	Cosmic dust read/ultraviolet channel select	10	Ultraviolet channel select/cosmic dust read
^a Most significant bit.			

(5) 43 bits for continually monitoring the internal status of DAS functions and events and for measuring predictable events in science instruments.

b. Encounter sequence. The following description deals briefly with those events which are germane to the DAS in the context of its over-all operation.

Approximately 6½ hr prior to planet encounter, the power to the NRT DAS, scan subsystem, and TV subsystem is turned on. The scan subsystem then begins moving the platform back and forth through an angle of approximately 180 deg.

The DAS begins sequencing the TV subsystem but does not record any data on the tape machine. The NRT DAS frame count is inhibited until narrow-angle acquisition (Fig. 16).

A wide-angle planet sensor with an approximate field of view of 50 deg is mounted on the platform, along with two narrow-angle sensors which have approximate fields of view of 1½ deg.

When the wide-angle sensor detects the planet, an hour or so before encounter, the DAS sends a command to the data encoder to switch to Mode 3. Having received a wide-angle planet-in-view signal the scan subsystem begins to track the center of the planet.

When either or both narrow-angle sensors detect the planet, the DAS sends an inhibit command to the scan subsystem which locks the platform, enables the previously inhibited NRT frame count, and begins recording TV data on the tape machine. The recording sequence continues until an end-of-tape signal has been received from the tape recorder following the 18 TV pictures or until 11 NRT frames have been recorded, whichever occurs first. Upon receipt of either of these signals, the DAS stops the NRT sequence and sends a command to the data encoder to return to Mode 2. The spacecraft then remains in Mode 2 for about 6½ hr before going to Mode 4, the playback mode.

c. The NRT format. The NRT frame is 144 sec long and is divided into six 24-sec intervals. Fig. 16 shows the gross DAS format and timing functions. During each NRT frame 3 TV pictures are taken, but only 2 are recorded on the tape machine; the tape machine has storage capacity for 20 pictures.

The digital TV picture data are read into the 1320-bit DAS buffers one line at a time. The 200 lines comprising a picture are alternately read into the two DAS buffers.

The NRT frame contains three formats which are designated: (1) TV (two 24-sec blocks); (2) RT1 (one 24-sec block); and (3) RT2 (three 24-sec blocks).

During the 24 sec of each TV block, the buffers A and B will be alternately loaded and dumped into the tape machine. Every 120 msec the following data will be loaded into one of the buffers:

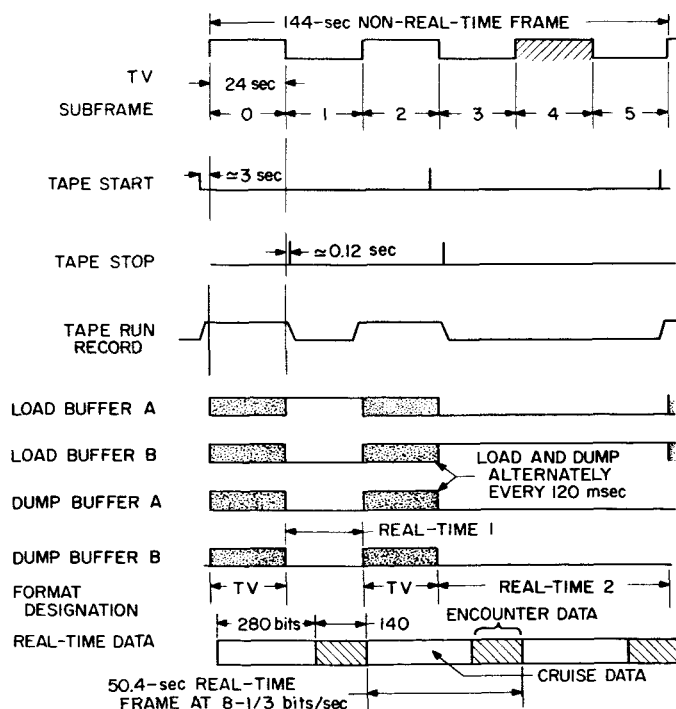


Fig. 16. DAS encounter timing

Data	Number of bits
PN sequence	31
NRT frame count	4
Subframe count	3
Line number	9
TV automatic aperture control 1, 2, 3 or filter position, shutter time, and "0" (subcommutated every other line)	3
Real-time data	1
TV performance data; signal level and target voltage (subcommutated every other line)	10
TV picture data—200 elements	1200
Total	1261

Total number of bits for 24 sec = $1261 \times 200 = 252,200$ bits/block or 504,400 bits/NRT frame.

During the 24 sec of the RT1 block, Buffer A only will be loaded as follows:

Data	Number of bits
Tape servo bits	80
PN sequence	31
NRT frame count	4
Subframe count	3
Line number	9
Spare	3
Real-time data	200
Total	330 for each NRT frame

During the 72 sec of the RT2 block, Buffer B only will be loaded as follows:

Data	Number of bits
Tape servo bits	80
PN sequence	31
NRT frame count	4
Subframe count	3
Line number	9
Spare	3
Real-time data	600
Total	730 for each NRT frame

The total number of bits recorded on the tape machine will vary depending upon the accuracy and stability of the 10.7-kc bit sync clock; at 10.7-kc, 1284 bits will be recorded on the tape machine each time a buffer is read out. The nominal total number of bits recorded on the tape machine during each 144-sec frame is then:

Blocks	Number of bits
2 TV	513,600, of which 504,400 are significant
RT1	1,284, of which 330 are significant
RT2	1,284, of which 730 are significant
Total	516,168

d. Operational description.

Analog conversions. All analog conversions are made in conjunction with an analog-to-pulse-width converter located in the instrument. A "begin conversion" pulse is sent to the converter by the DAS; at the same time the DAS begins counting a 55-kc clock in a 10-bit accumulator. The pulse-width converter sends the DAS a "stop count" pulse, which is delayed from the "begin conversion" pulse by a time proportional to the amplitude of the analog voltage. By sending only pulses between the instrument and the DAS, noise interference is greatly reduced, and the analog voltage is not degraded by the noise coupling and attenuation in the spacecraft cabling. All conversions are 9-bits plus sign for a plus or minus 6-v signal.

Complementary count. In an instrument containing its own count accumulator, the complement of the binary number in the accumulator is read out by the DAS. This is done in a manner quite similar to the way the DAS handles analog signals through the analog-to-pulse-width converters. The DAS sends a burst of 111-kc pulses to the instrument for a maximum interval of 11.5 msec. These pulses enter the instrument count accumulator in parallel with the data input, and at the same time will be counted by the DAS. When the counter in the instrument overflows, a signal is sent to the DAS; the DAS in turn stops counting and stops sending pulses to the experiment. The binary number in the DAS register will be one plus the one's complement of the original number in the instrument accumulator.

Count rates. If an instrument having one or more random count-rate outputs does not have its own count accumulators, this function is performed by the DAS. There are six such inputs to the *Mariner C* DAS. These count rate inputs, from particle detectors, are commutated so that four inputs are read once every eight frames and two of the inputs read once every four frames. The inputs are sampled for approximately 45 sec at $8\frac{1}{2}$ bits/sec and for one-fourth of this period at the $33\frac{1}{2}$ bits/sec telemetry rate. A single, 20-stage counter is available for these inputs. When a "1" appears in the twentieth stage, two stages of pre-scaling are added to the count, although they are not read out since their use is indicated by the twentieth bit. Twenty bits are read out each frame for the count-rate data inputs. The maximum count capacity for any reading is slightly more than 2.62×10^6 counts.

Ionization chamber. The ionization chamber data are encoded in a manner different from any other instru-

ment; the ion chamber pulses are counted continuously by the DAS and are encoded in two different ways. At a known point in each frame the 10-stage ion-pulse register is reset and 6 stages of the register begin counting time pulses having a 1.2-sec period. (At the $33\frac{1}{3}$ bits/sec telemetry rate the time interval is 0.3 sec.) When the first ion pulse occurs, it inhibits the 6-bit time count for the remainder of that frame; it is also counted in a 3-stage counter, thereby giving the time from a known reference point to the first ion pulse and also the number of ion pulses in that frame. When 7 ion pulses have been received in one frame, the 6-bit time portion of the register will be reset to zero. When 8 pulses are received the tenth stage is set to indicate that the remaining 9 bits now represent a straight binary count of accumulated ion pulses; the tenth stage remains a "1" for the remainder of the frame. A maximum of 511 ion pulses can be counted in a frame.

Parallel data. When it is required that registers in an instrument not be cleared upon readout, or when only a few bits are to be read, the DAS then performs a parallel transfer. This is done for the cosmic dust detector and for the TV subsystem. The cosmic dust detector has two 8-bit registers which are commutated every other frame. The TV subsystem has 5 bits of status information, shutter time, and filter position which are read once each frame during encounter, or Mode 3, in the RT DAS and once each TV line in the NRT DAS.

e. DAS buffer memory. The two, identical 1320-bit buffers used in the DAS are bit-serial, sequentially-addressed core memories. A photograph of the first flight model memory is shown in Fig. 17. A block diagram of the memory is shown in Fig. 18.

The coincident current bit selection is accomplished by three ring counters which provide both address selection and drive currents to the memory. The ring counter-address registers consist of tape-wound switch cores arranged in an $8 \times 11 \times 15$ array, thus requiring only 34 stages of address selection.

Each buffer requires four external signals: clear-to-write, clear-to-read, shift, and data. Both clear-to-write and clear-to-read signals clear the address registers and set a "1" into the first stage; clear-to-write also clears the memory cores of all data.

Every memory core is threaded with five wires: X, Y, and Z select, a sense line, and a C line. The C line is connected between the Z line and the positive power

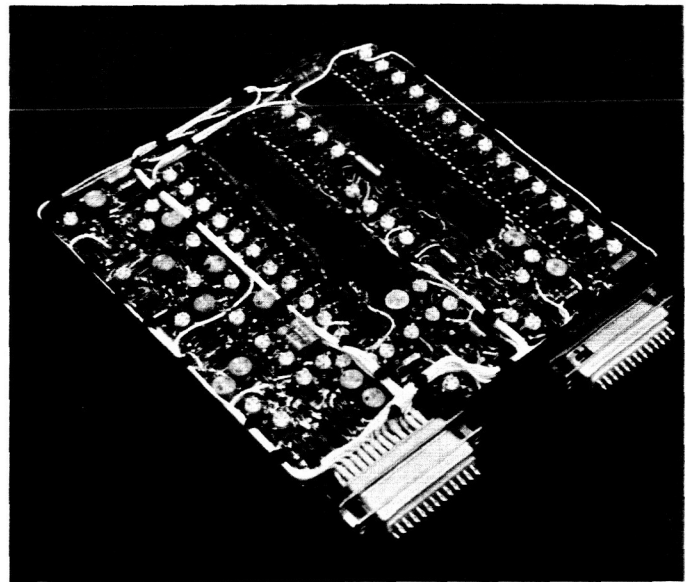


Fig. 17. DAS buffer memory

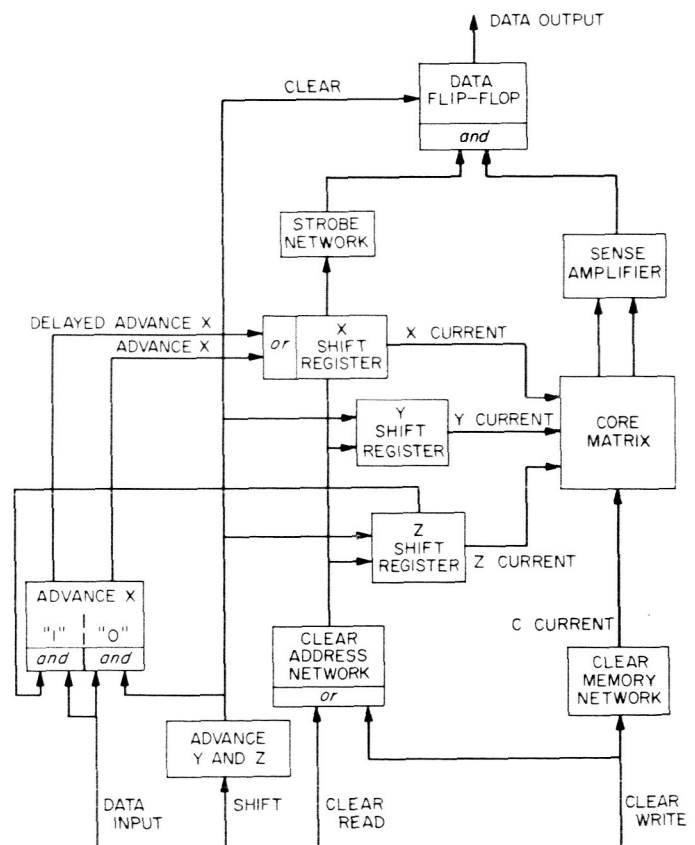


Fig. 18. Block diagram of Mariner C memory

supply as shown in Fig. 19. A drive current in the Z line produces a magnetic field in each memory core which cancels the field produced by the same current when it is

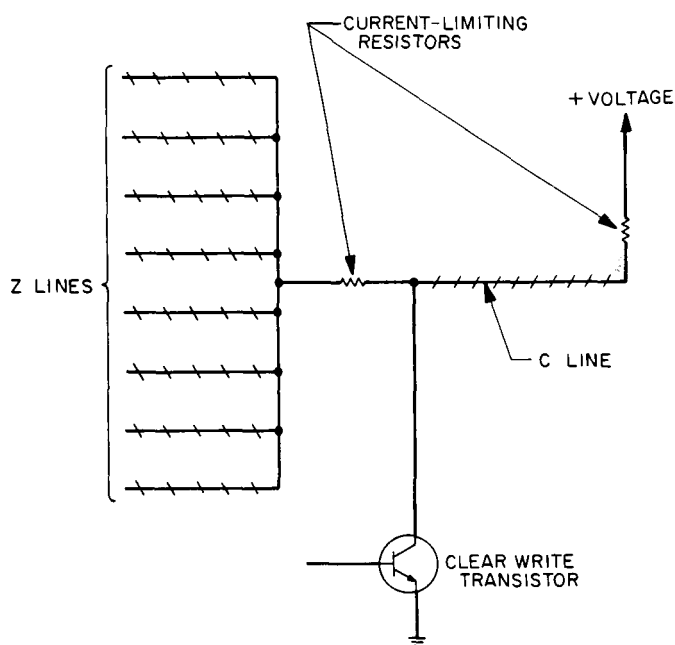


Fig. 19. C-Line connection

in the C line, and drive currents in the X, Y, and Z lines produce aiding magnetic fields. Thus, the current applied to a selected core is the X current plus the Y current plus the Z current minus the C current.

Each drive current is one-half the current required to switch a core; thus, a selected core will have the switching current I and an unselected core will have a current of either $+I/2$, zero, or $-I/2$ passing through it. When the memory is cleared to write, a full-select current is applied to the C line while no currents are applied to the other drive lines, resulting in a "1" being written in each core.

If the input data is a "1", the X drive current is delayed until after the occurrence of the Y and Z drive currents, thereby preventing the core from switching and leaving a "1" in the memory.

The pair of buffers comprising the DAS buffer memory consume about $\frac{1}{3}$ w of power and weigh 20 oz. The Univac Division of Sperry-Rand Corporation is responsible for the design and fabrication of the buffer memory.

f. Status. In the previous period, the flight prototype DAS was delivered to JPL by the Computer Control Company. It is presently undergoing bench tests. A Digital Equipment Corporation PDP-4 computer is being utilized to check out a breadboard model of the DAS, prior to checking out the prototype and flight models.

Operating in conjunction with a JPL-designed marriage unit, the computer simulates all DAS inputs, including the scientific instruments, and checks all data outputs against the inputs.

3. Analog Data Conditioning of the Scientific Instruments

The use of an analog-to-pulse-width (A/PW) converter can improve analog-to-digital (A/D) conversions in systems where physical separation of the analog source and the digital converter is a necessity. In such systems, the transmission of analog signals from one part of the system to the other may result in errors in measurement due to noise interference. An A/PW converter module has been developed for use in the *Mariner C* science subsystem. It is described here with emphasis on system applications as well as the converter's operational characteristics.

a. System considerations. The science subsystem for *Mariner C* is composed of several scientific instruments whose data is conditioned and formatted by the data automation system (DAS). A portion of a simplified science subsystem is illustrated in Fig. 20. This system is typical of those used on previous spacecraft in that analog data signals are carried across the interface between the instruments and the DAS. A system of this type will be inherently plagued with measurement errors due to the various types of system noises affecting the analog signals. The two most common errors in measurement across an analog interface occur as a result of: (1) high-frequency noise that is magnetically or electrostatically coupled into the analog lines, and (2) dc potentials on ground returns. Noise of these two types can reduce the accuracy of low-level measurements and limit the resolution of the system.

Individual A/D converters, complete with a digital accumulator and/or shift register at each sensor or instrument are not feasible on the *Mariner C* because of power consumption, size, and weight. Differential to single-ended conversion also is not desirable.

Fig. 21 illustrates a system which overcomes some of the problems associated with the transmission of analog signals across the spacecraft interfaces as shown in Fig. 20. The system of Fig. 21 utilizes an A/PW conversion at the source of the analog signal and thereby implements the A/D conversion entirely by the use of transformer-coupled pulses between the DAS and the instruments.

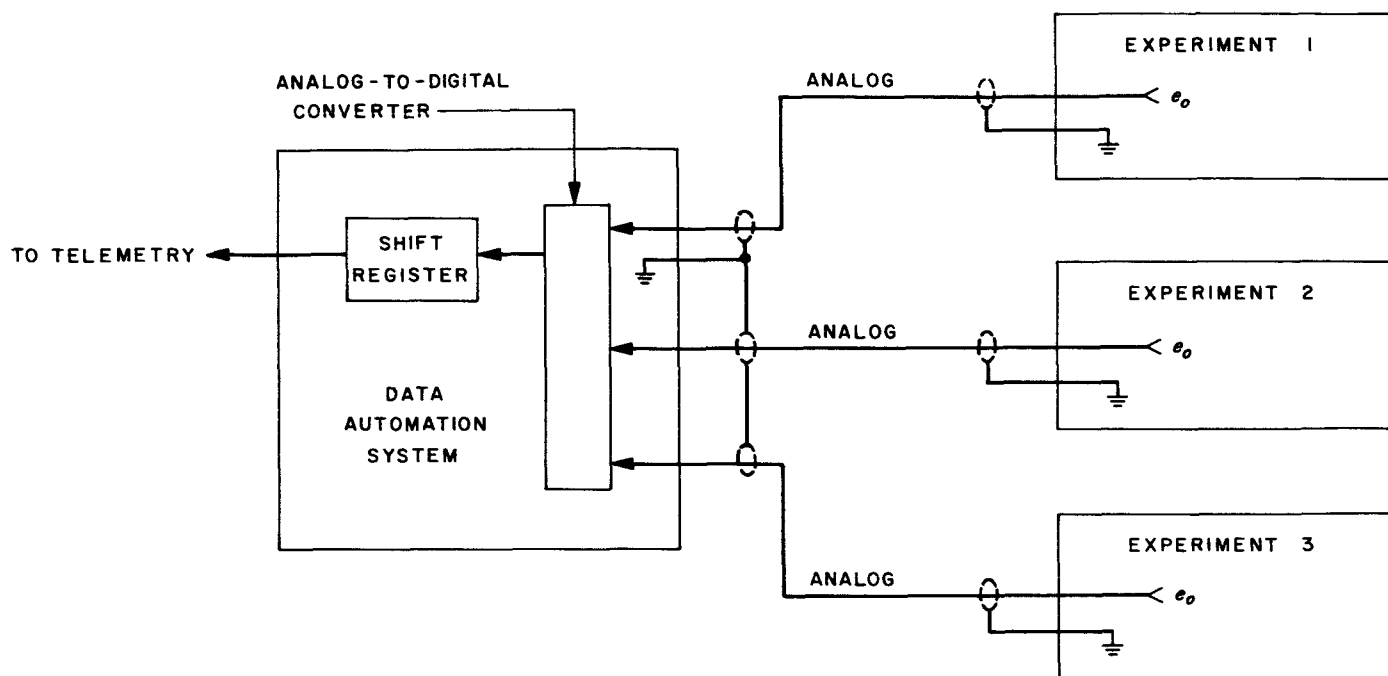


Fig. 20. Typical science subsystem performing the analog-to-digital conversion in the data automation system

The analog information in this system is contained in the time duration of the pulse from the instruments. Errors due to noise coupled into the system via the interface lines are minimized since the DAS has a threshold level which must be exceeded for operation of its logic and since the analog information is contained only in the leading and trailing edges of the pulse. The use of pulse transformers at the input to the DAS maintains dc isolation between the DAS and the instrument and thereby circumvents many of the signal ground-return problems previously encountered in spacecraft science subsystems.

The *Mariner C* science subsystem is similar to the system illustrated in Fig. 21. All analog signals are converted at the instrument to a pulse whose duration is directly proportional to the analog signal amplitude. This pulse is transformer-coupled to the DAS where it is used to gate 55.55-kc clock pulses into a nine-bit counter-shift register. The nine-bit conversion by the DAS is necessary in order to satisfy the requirements of some experiments for a high resolution. Contrary to the high-resolution requirement, the system requirements for accuracy are modest, with primary interest in resolution and accuracy near zero. Thus, the A/PW converter is required to provide a fine resolution and accuracy near zero with modest accuracy near full scale. An eight-bit conversion accuracy at full scale is adequate for most experiments.

b. The A/PW converter. A standard A/PW converter module was developed for use in the *Mariner C* science subsystem. The converter was designed to satisfy the requirements previously outlined, as well as requirements for simplicity and small modular size. The need for simplicity and small size is necessitated by the fact that the converter is used in differing electronic assemblies.

Fig. 22 illustrates the functional operation of the *Mariner C* A/PW converter. Upon command by the DAS, the flip-flop is set and a comparison is made between the analog signal and the voltage ramp. The comparator detects the crossover point and resets the flip-flop through the dc amplifier. The period of time the flip-flop remains in the set condition is the data output of the A/PW converter. This time is directly proportional to the analog input and is the time required for the ramp generator to change from 0 to a voltage equivalent to the analog input. It is not feasible to transformer-couple a wide output pulse into the DAS. Since the start is known at the DAS side of the interface, it is merely necessary to return the trailing edge of the output pulse in order for the DAS to reconstruct the pulse width.

The converter illustrated in Fig. 22 will convert analog signals of only one polarity. A bipolar conversion can be implemented with two converters of complementary de-

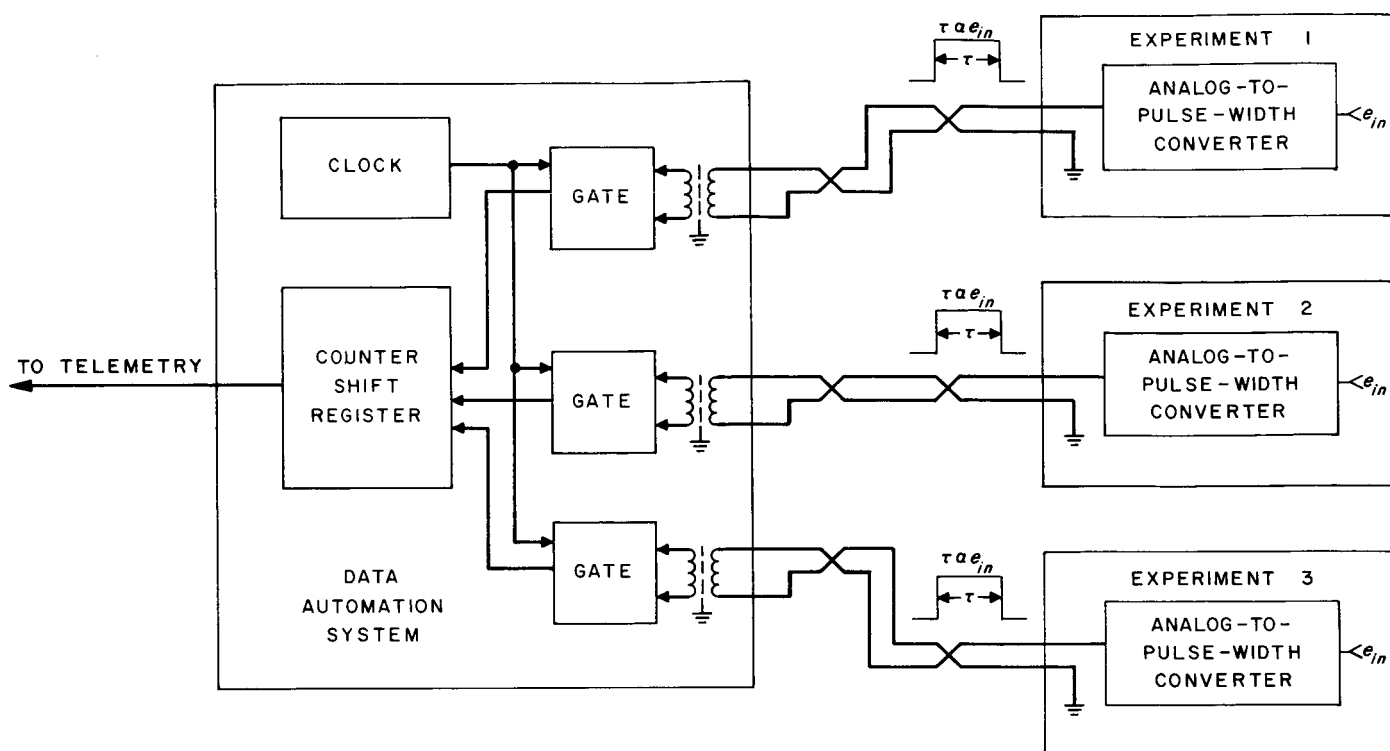


Fig. 21. Typical science subsystem utilizing analog-to-pulse-width converters

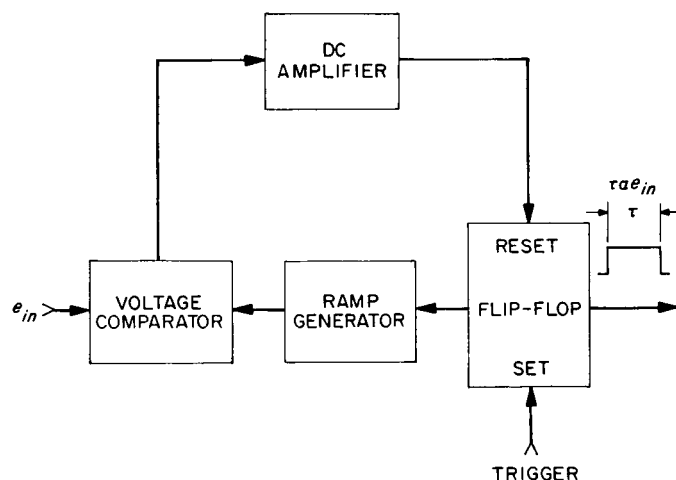


Fig. 22. Block diagram of analog-to-pulse-width converter

sign with their inputs connected in parallel and the proper operations made on the output pulses.

Errors of two types are predominant with the A/PW converter shown in Fig. 22. These are: (1) offset errors in the comparator stage, and (2) errors in the generation of the ramp voltage. Offset errors are, generally speaking,

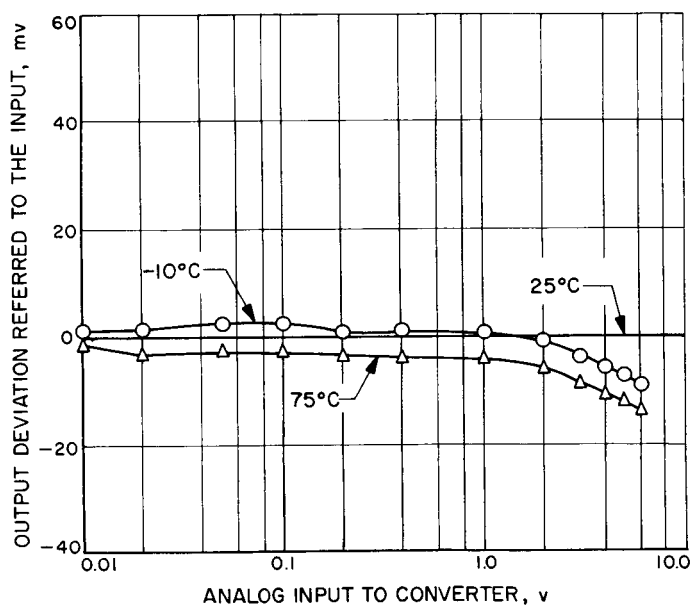


Fig. 23. Typical deviation in analog-to-pulse-width converter output with temperature

not a function of input voltage and can be held to a few millivolts over a reasonable temperature range. The magnitude of error incurred in the generation of the ramp

voltage is a direct function of the analog input voltage and is the primary source of error in the converter. This error in the generation of the ramp voltage is compatible with the accuracy requirements of the system, i.e., maximum accuracy near zero, minimum accuracy near full-scale. The smooth ramp is compatible with the resolution requirement.

The A/PW converter developed for *Mariner C* uses some fifty components, including eleven transistors, and is encapsulated in a module measuring $1.5 \times 1 \times 0.65$ in. The input-output specifications, as well as the stability and linearity of the output under environmental conditions of temperature ranging from -10 to $+85^{\circ}\text{C}$ are as follows:

Input	0 to 6 v
Output	10- μsec pulse delayed 10 to 9216 μsec from the application of the trigger
Stability	± 3.25 mv $\pm 0.5\%$ of the analog input (deviation from 25°C referred to the input)
Linearity	Same as stability

Fig. 23 shows deviations in the data output of a typical A/PW converter module with variations in temperature. Changes in the converter output with temperature, due to the two types of errors discussed previously, are readily apparent.

For those applications where an absolute accuracy of eight bits is not required, a pre-flight calibration of the A/PW converter transfer characteristics will be sufficient to interpret the received data from the spacecraft. For those instruments that require at least an eight-bit accuracy over the entire range of input voltages, an in-flight calibration sequence will be performed periodically. Thus, any changes in the A/PW converter output during flight will be detected and a corresponding change will be made in the instrument calibration.

c. Summary. The *Mariner C* science subsystem utilizes an A/PW conversion at the instruments to implement the ultimate analog-to-digital conversion performed by the DAS. This technique eliminates the coupling of analog signals directly between the DAS and the various users and thereby circumvents many of the potential sources of error that may occur due to noise or dc potentials on signal lines and ground returns.

The nine-bit digitization by the DAS and the A/PW conversion combine to provide excellent resolution with modest accuracy. An 11.7-mv resolution is realized in the system with an accuracy up to eight bits or better, depending upon whether or not in-flight calibration is used.

The A/PW converters are standard throughout the science subsystem. The modules (Fig. 24) are fabricated with standard components in a welded encapsulated module which occupies a volume of less than 1 in³.

d. Status. A total of ten converters is required per spacecraft, and are located in 4 different instruments. Prototype and *Mariner C-1* deliveries have been completed by the contractor, Alphatronics Corporation, Monrovia, California.

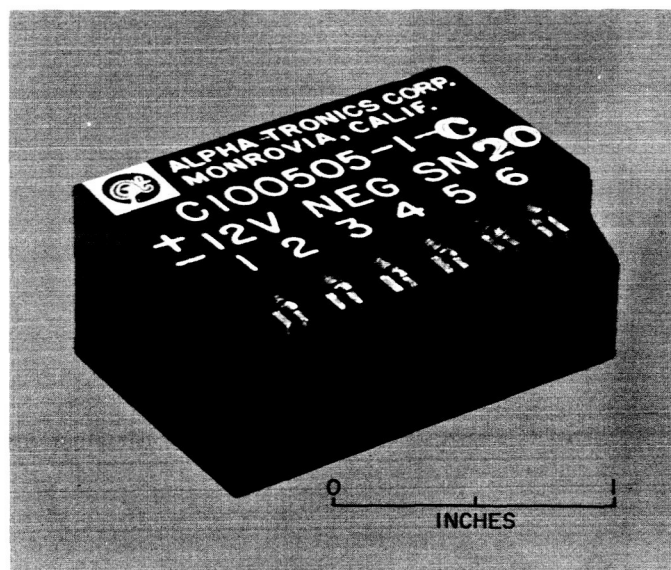


Fig. 24. Analog-to-pulse-width module